The Hong Kong Polytechnic University

Department of Civil and Structural Engineering

DEVELOPMENT OF TITANIA NANOTUBE FILMS FOR DEGRADATION OF THE RECALCITRANT ORGANIC POLLUTANTS IN WATER

LIANG Hai Chao

A thesis submitted in partial fulfilment of

the requirements for the Degree of Doctor of Philosophy

November 2008

CERTIFICATE OF ORIGINALITY

I hereby declare that this thesis is my own work and that, to the best of my knowledge and belief, it reproduces no material previously published or written, nor material that has been accepted for the award of any other degree or diploma, except where due acknowledgement has been made in the text.

________________________________(Signed)

________Liang Haichao________(Name of student)

ABSTRACT

This research work was designed to develop titania nanotube (TNT) films as photocatalysts for the destruction of recalcitrant organic pollutants in water and wastewater. In this study different TNT films were prepared by an anodic oxidation process under various experimental conditions. The morphology and structure of the prepared TNT films were examined by field emission scanning electron microscopy (FESEM), X-ray diffraction (XRD), and X-ray photoelectron spectroscopy (XPS). The effects of nanotubular structures including tube length, tube wall thickness, and crystallinity on their photocatalytic activities were investigated with details. Photocatalytic activities of the TNT films were evaluated in terms of the degradation of 2,3-dichlorophenol (2,3-DCP) in aqueous solution under UV light irradiation. The experimental results showed that the large specific surface area and high pore volume, the thin tube wall, and the optimal tube length would be three important factors to achieve good performances. Moreover, the TNT films calcined at 500 ^{o}C for 1 h with the higher degree of crystallinity exhibited the higher photocatalytic activities than other TNT films calcined at 300 and 800 ^{o}C. These results indicate that the optimization of TiO_2 nanotube structures is critical to achieve the high performance of photocatalytic reaction.

Research efforts were further focused on the effects of reaction factors including dissolved oxygen (DO), pH and anions on the photocatalytic activities of TNT films for the degradation of 2,3-DCP in aqueous solution. The results showed that the rate of 2,3-DCP degradation is a function of DO concentration, since DO acts as an effective electron acceptor to extend the hole's lifetime and to form the oxidizing species of •OH radicals, affecting the photocatalytic activities of the TNT film. The effect of solution pH demonstrated that an alkaline condition is favourable to 2,3-DCP degradation and dechlorination but an acidic condition is more conducive to further mineralization. The effects of individual anions (NO_3^-, Cl^-, SO_4^{2-}, and $H_2PO_4^-$) indicated that the inhibition degree of photocatalytic degradation of 2,3-DCP caused by these anions can be ranked from high to low as $SO_4^{2-} > Cl^- > H_2PO_4^- > NO_3^-$.

A comparison study to evaluate the photolytic and photocatalytic degradation of herbicide diphenamid (DPA) in aqueous solution was then investigated. It was found that at pH 7.2 the photolysis system with UVC (254 nm) irradiation alone was quite efficient in degrading DPA with 100% removal after 360 min, but poor in removal of dissolved organic carbon (DOC) only 8%. In contrast, the photocatalysis system with TNT/UVA (350 nm) showed 51% of DPA removal and

11% of DOC removal after 360 min, respectively. These results indicate that although the DPA degradation by the TNT/UVA photocatalysis was much slower than that by the UVC photolysis, the DOC removal was higher than that by photolysis. In the meantime, more than 20 intermediates from DPA degradation were identified by LC-MS and ^{1}H-NMR analyses, and the possible pathways of DPA degradation by direct photolysis and photocatalysis were proposed based on the identified intermediate products and the main reaction mechanism.

Furthermore, a new type of TNT film, polythiophene sensitized-TNT (PTh/TNT) photocatalyst, responsive to visible light, was successfully synthesized by a two-step electrochemical method. The obtained composite PTh/TNT films were characterized by SEM, XRD, XPS and UV-Vis absorbance. UV-Vis absorbance analysis showed that these composites have a strong photoresponse in the visible region at 500 nm. The prepared PTh/TNT films revealed significant activities for 2,3-DCP degradation under visible light irradiation and also sunlight irradiation. The experiments also confirmed that the side-chains of polythiophene could influence its photocatalytic activities significantly.

In summary, this research synthesized the highly ordered TNT films successfully and detailed the effects of nanotube structures on their photocatalytic activities.

After the optimization of the TNT structures, effects of DO, pH and anions in aqueous solution on their photoactivities were investigated with details. Furthermore, a new type of polymer-sensitized TNT photocatalyst responsive to visible light was successfully developed. Based on the results obtained in this study, there is better understanding of the photochemical reactions using TNT films as a photocatalyst for the degradation of organic pollutants in water.

LIST OF PUBLICATIONS

Journal Papers

1. **Liang, H.C.**, Li, X.Z., Yang, Y.H., Sze, K.H., 2008. “Effects of dissolved oxygen, pH, and anions on the 2,3-dichlorophenol degradation by photocatalytic reaction with anodic TiO_2 nanotube films”. *Chemosphere.* 73, 805-812.
2. **Liang, H.C.**, Li, X.Z., 2009. “Effects of structure of anodic TiO_2 nanotube arrays on photocatalytic activities for the degradation of 2,3-dichlorophenol in aqueous solution”. *J. Hazard. Mater.* 162, 1415-1422.
3. **Liang, H.C.**, Li, X.Z., 2009. “Visible-induced photocatalytic reactivity of polymer-sensitized titania nanotube films”. *Appl. Catal. B-Environ.* 86, 8-17.
4. **Liang, H.C.**, Li, X.Z., Yang, Y.H., Sze, K.H., 2008. “Degradation of diphenamid in aqueous solution by direct photolysis and photocatalysis with TiO_2 nanotube films: mechanism and pathway”. *In preparation.*

Conference Paper

1. **Liang, H.C.**, Li, X.Z., 2008. “Visible-induced photocatalytic reactivity of polymer-titania nanotube films”. *236th American Chemical Society National Meeting & Exposition.* August 17 - 21, 2008, Philadelphia, USA.

ACKNOWLEDGEMENTS

I am very much indebted to my supervisor, Professor X. Z. Li, for his generous support, excellent guidance and valuable discussions throughout the course of this work. I deeply appreciate Professor Li's contribution to providing me with the unique opportunity to pursue my PhD, a significant personal achievement. Also, I would like to express my sincere thanks to technicians, Mrs K. H. Ng, W. S. Lam and C.W. Lau, in the Water and Wastes Laboratory for their kind of help in instrumental usage and chemicals provision. I am very grateful to Drs. K.H. Sze, Y. Shi, B.L. Yuan, T.X. Liu and other friends for their constant encouragement and valuable advice over the past few years.

I am especially grateful to my parents and my wife for their unwavering and immense support, encouragement and understanding throughout my doctoral studies. Finally, I would like to express my gratitude to the Research Committee of The Hong Kong Polytechnic University for providing me a PhD scholarship.

TABLE OF CONTENTS

CHAPTER 1 INTRODUCTION

CHAPTER 2 LITERATURE REVIEW

CHAPTER 3 MATERIALS AND METHODOLOGY

CHAPTER 4 CHARACTERIZATION AND PHOTOCATALYTIC ACTIVITIES OF TiO_2 NANOTUBE FILMS

CHAPTER 5 PHOTOCATALYTIC DEGRADATION OF 2,3-DCP WITH TiO_2 NANOTUBE FILMS AND EFFECTS OF DISSOLVED OXYGEN, pH AND ANIONS

CHAPTER 8 CONCLUSION AND RECOMMENDATION

LIST OF FIGURES

LIST OF SCHEMES

LIST OF TABLES

GLOSSARY

ACN	Acetonitrile
AOPs	Advanced oxidation processes
BFEE	Boron fluoride-ethyl ether
COSY	Correlation spectroscopy
2-CR	2-Chlororesorcinol
2,3-DCP	2,3-Dichlorophenol
DDW	Deionized distilled water
DO	Dissolved oxygen
DOC	Dissolved organic carbon
DPA	Diphenamid
EDX	Energy dispersive X-ray spectroscopy
FESEM	Field-emission scanning electron microscopy
HOMO	Highest occupied molecular orbital
HPLC	High performance liquid chromatography
LUMO	Lowest unoccupied molecular orbital
NMR	Nuclear magnetic resonance
PTh	Polythiophene

TNT	Titania nanotube
XPS	X-ray photoelectron spectroscopy
k	The reaction rate constant
ζ	Photonic efficiency
ζ_r	Relative photonic efficiency

Chapter 1 – Introduction

1.1 Background

New advances in environmental health reveal that organic chemicals are present as pollutants in industrial wastewater and landfill leachates, and diffused into groundwater and surface water. These pollutants pose a serious health threat to humans and aquatic life due to their high toxicity, carcinogenicity, mutagenicity and/or endocrine-disruptivity (Pocchiari and Silano, 1983; Fry, 1995; Folmar et al., 1996; Johnson and Sumpter, 2001). To protect water resources and achieve drinking water quality, these pollutants must be removed. Many physical and chemical processes have been proposed and are currently employed to destroy them (Peterson et al., 1994; Kang et al., 2000). Conventional biological treatment method consists of a combination of physical and biological processes, in which parts of organic pollutants are degraded by bacteria in activated sludge with/without oxygen to make the water non-toxic (Peterson et al., 1994; Shiny et al., 2005; Tallec et al., 2006; Foladori et al., 2007). Nowadays, however, many persistent and recalcitrant pollutants that are present in wastewater, particularly those discharged from the chemical, textile and pharmaceutical industries, can hardly be detoxified biologically (Katsoyiannis et al., 2004; Auriol et al., 2006; Yoon et al., 2007). In addition, most pollutants are only adsorbed by the sludge and are not degraded (Pagga and Taeger, 1994). Biological treatment has therefore proven ineffective in destroying such pollutants, giving way to a growth in advanced oxidation processes (AOPs) over the past decades. AOPs are based on the generation of very reactive species such as hydroxyl radicals (•OH) that oxidize a broad range of pollutants quickly and nonselectively. The most attractive feature of this oxidation technology is that complete mineralization of organic pollutants can be achieved at ambient temperature and pressure.

AOPs such as Fenton and photo-Fenton catalytic reactions (Kuo, 1992; Kang et al., 2000; Goi and Trapido, 2002), H_2O_2/UV processes (Costa et al., 2004; Goldstein et al., 2007) and semiconductor mediated photocatalysis (Barbier et al., 2002; Mars et al., 2004; Choi et al., 2007) have been studied under a broad range of experimental conditions. Among AOPs, semiconductor photocatalysis using titanium dioxide (TiO_2) as photocatalyst appears to be the most emerging destructive technology (Crittenden et al., 1997; Ilisz et al., 1999). Since TiO_2 is largely available, inexpensive, non-toxic, chemically stable and can lead to complete mineralization of organic pollutants into CO_2, the photocatalytic process with TiO_2 has been receiving increasing attention. Moreover, the TiO_2 photocatalysis in conjunction with solar technologies may be developed into an effective measure to reduce water pollution.

However, there are some issues for the practical application of TiO_2, which need to be overcome. For example, (1) the inherently low quantum efficiency in TiO_2 (in bulk or large particles more than 90% of the photo-generated carriers can undergo recombination), (2) the requirement of separation of suspended powder and (3) the requirement of near ultraviolet light energy ($\lambda < 380$ nm) for activation.

Utilizing the available visible light spectrum and not merely the scarcely available UV spectrum is a relatively recent objective that has been intensively researched in the past decade. It is also one of the major challenges for the scientific community involved in photochemistry research. Visible light is typically described as the portion of the electromagnetic spectrum with wavelengths between 400 and 700 nm. However, in its unmodified form, TiO_2 is rendered highly inefficient for visible light applications due to its wide bandgap. In general, at room temperature, anatase has a band gap of 3.2 eV and rutile has one of 3.05 eV (Tang et al., 1994). To utilize the visible light for TiO_2 photocatalysis, several different approaches have been proposed:

(1) Combination of other semiconductors, such as CdS, Cu_2O, Fe_2O_3, WO_3, etc., which can absorb visible light (Hoffmann et al., 1995). However, this attempt failed as no semiconductors thus far have been able to meet the requirements of band gap, chemical stability and photocatalytic activity together. The recently reported $InTaO_4$ photocatalyst was able to photo-split water with visible light but its efficiency was lower than 1% (Zou et al., 2001).

(2) Doping of photocatalysts with metal ions (for example Cr^{3+}, Fe^{3+}, V^{5+}), which creates local energy levels within the band gap of the photocatalysts (Serpone et al., 1994; Takeuchi et al., 2000). It was assumed that the photoexcitation of such impurities should lead to the generation of free charge carriers to initiate surface chemical processes. However, the efficiency of such systems under visible light significantly depended on the preparation methods used, the dopant amount and the calcination temperature. By optimizing these experimental conditions, the doped species can act as separation centres of electron-hole pairs to achieve the photocatalysis under visible light irradiation. In many cases, however, such doped photocatalysts might show no activities under visible light and decrease the activities in the UV spectral range compared to the non-doped

photocatalysts because of the occurrence of carrier recombination through the metal ion levels.

(3) Doping of photocatalysts with non-metal atoms, such as N, F, S and C. Asahi et al. (2001) reported significant red shifts (up to 540 nm) of the spectral limit of the photoactivities of TiO_2 photocatalysts doped with N. They interpreted such results in terms of band gap narrowing due to mixing of the p states of the dopants with O 2p states forming the valence band of TiO_2. A similar conclusion has also been reached by Lin et al. (2005) for the spectral changes observed for P-doped TiO_2. However, the present problem for the anion-doped TiO_2 photocatalysts is that their photocatalytic activities under visible light are much lower than those under ultraviolet light.

Among the three approaches, the third one tends to be best for the development of photocatalysts utilizing visible light (Fujishima and Zhang, 2006). However, the present problem for the anion-doped TiO_2 photocatalysts is that their photocatalytic activities under visible light irradiation are not high enough for practical applications. Therefore, more effort must be made to overcome this obstacle or develop visible-induced photocatalysts. However, it is still a considerable challenge to develop a new generation of photocatalysts that can overcome the three drawbacks of TiO_2 for water treatment. Hence, this becomes one of objectives of this study.

Degussa P25, a commercial TiO_2 powder, has been used frequently as a benchmark in TiO_2 photocatalysis studies. It has a surface area of ~53.2 $m^2\ g^{-1}$ and an average crystallite size of ~25 nm. This powder consists of a mixture of anatase and rutile, with a ratio of 3–4:1 (Datye et al., 1995; Trejo-Tzab et al., 2008). Past research shows that TiO_2 P25 suspension has a relatively high photocatalytic activity for exposing different organic compounds in aqueous solutions. In the case of dispersed TiO_2, an increase of photocatalytical degradation efficiency by at least a factor of 10 has been reported when compared to TiO_2 applied in fixed-bed configurations (Guillard et al., 2003). This is because the suspended TiO_2 particles have large surface areas in contact with the substrates, which allows more number of photons hit the catalyst and large adsorption capacity results. However, it is generally not easily separated from treated water and further undergoes agglomeration. This dramatically decreases the utilization efficiency. In order to overcome the disadvantages of the commercial TiO_2 fine powder, coating TiO_2 on carriers such as glass beads or plates (Yu et al., 2000; McMurraya et al., 2004), stainless steel or other metal foil (Byrne et al., 1998; Zhang et al., 2003a), carbon (Nagaoka et al., 2002; Guo et al., 2008), polystyrene beads (Fabiyi and Skelton, 2000) and reactor walls etc. has been frequently studied. Sol-gel and particulate-film techniques are two of the most commonly used methods for the preparation of thin-film TiO_2. Both the techniques generally consist of three steps: the preparation of TiO_2 suspension or gel, dipping or spreading, and sintering (Kim and Francis, 1993). In the sol-gel technique, a solution containing titanium-alkoxide is first prepared. The solution is then hydrolyzed to produce crystalline TiO_2 colloids. A solid plate is then dipped and removed from the sol gel to create a liquid film on the carrier surface. The gel-coated plate is air-dried and sintered at 500 ^oC for around 1 h to produce chemical banding between the film and the solid. The resulting film consists of a single layer of TiO_2 at a thickness of 0.2 to 0.5 μm (Aegerter et al., 1989). The procedure can be repeated to increase the number of TiO_2 layer and its thickness. The procedure of preparing thin-film TiO_2 using a particulate technique is similar to that of sol-gel. The only difference is that the starting material is TiO_2 powder (Mmurraya et al., 2004). The solution containing powder TiO_2 is usually sonicated to eliminate any aggregates or clumps and to ensure the dispersion of TiO_2 particulate. The sonicated solution is spread uniformly onto the surface of a solid plate. The TiO_2-coated plate is then heated at 400 ^oC to obtain a thin film of TiO_2

particulate. The two techniques have been used equally well in the preparation of thin film TiO_2 in photocatalytic studies.

Even though the immobilization of TiO_2 seems to provide an alternative to overcoming the drawback of suspended TiO_2 in water where post-treatment is necessary, many new questions have been raised. For example, does the immobilization affect the quantum efficiency of TiO_2 particles? Will the transport of contaminant molecules in the composite TiO_2-carrier become a limiting factor in the destruction of contaminants? And if it does, how will the configuration of the coating (including thickness and porosity) affect the reaction rate? Does the carrier material affect the photocatalytic reaction? Most of these questions have only been posed recently and remain unanswered. When compared to the TiO_2 particle suspension, the most important question of the traditional TiO_2 coating is regarding their poor photocatalytic efficiency due to the relatively low surface area and the fast recombination of electron-hole pairs.

In recent years new types of TiO_2 films with high surface area and porosity were successfully developed for the applications in solar cell, water-splitting and environmental purification. However, considering the practical application of photocatalytic films for water treatment, the developed TiO_2 films seem to still have some problems, which may limit their application in large-scale photocatalytic systems. Therefore, the development of TiO_2 films with large pore morphology and with desired characteristics, such as high mechanical robustness, good structural integrity, high surface area and porosity, is undoubtedly becoming an important topic in photocatalysis for water purification.

1.2 Aims and Objectives

This study is aimed at enhancing the photoefficiency of the immobilized TiO_2 films for water treatment with the one-dimensional TiO_2 nanotube (TNT) structures which have the larger surface area and the higher porosity than the traditional TiO_2 thin-film photocatalysts. Meanwhile, this study is also aimed at achieving the significant photocatalysis under visible light irradiation using the TNT films conjugated with polymer as a sensitizer. Some specific objectives of this study are listed below:

- To prepare the TNT films through anodic oxidation methods and to optimize the anodic TNT films with the maximized photocatalytic activities.

- To evaluate the effects of some exterior factors on the TNT photoactivities for the destruction of water contaminants, including dissolved oxygen, initial pH, inorganic anions, and so on.
- To study the reaction mechanism and pathway of pollutants (such as diphenamid) degradation by direct photolysis and photocatalysis.
- To synthesize a novel and highly effective polymer-TiO_2 nanotube photocatalyst for pollutant degradation under visible light irradiation and further understand the interaction mechanism of the functionalized polymer/TiO_2 composites.

1.3 Scopes of Study

To achieve the designated objectives, the scope of the study includes the following tasks.

- A comprehensive literature review including the theory of heterogeneous photocatalysis using TiO_2 as a photocatalyst, the development of TiO_2/UV processes for water treatment, the preparation of TiO_2 nanotube photocatalysts and their application in environmental purification.

- Preparation of different TNT films as photocatlysts by an anodic oxidation technique and evaluation of their photocatalytic activities in terms of the 2,3-dichlorophenol (2,3-DCP) in aqueous solution under UV light irradiation.
- Investigation on the photocatalytic activities of TNT films affected by their structures and calcination temperature.
- Investigation on the photocatalytic degradation of 2,3-DCP with the TNT films affected by dissolved oxygen, pH and anions in aqueous solution.
- Study on the reaction mechanism and possible pathway of 2,3-DCP degradation towards mineralization through the identification of main intermediate products by ^{1}H-NMR analysis.
- Comparison study on the degradation of herbicide diphenamid (DPA) by photolysis (UVC) and photocatalysis (TNT/UVA), including their degradation efficiency, intermediates and reaction pathways.
- Development of a novel photocatalyst, polymer-TiO_2 nanotube (PTh/TNT) composite, by a two-step electrochemical method for photocatalysis under visible light irradiation and sunlight irradiation.

Chapter 2 – Literature Review

2.1 Theory of Photocatalysis

2.1.1 Theory of TiO_2 Photocatalytic Oxidation

Since the discovery of photocatalytic water splitting on TiO_2 electrodes by Fujishima and Honda (1972), interest in applying TiO_2 as a photocatalyst for the remediation of groundwater and wastewater has grown (Hsien et al., 2001; Kositzi et al., 2004; Prieto et al., 2005), particularly due to its potential to degrade a wide range of organic and inorganic compounds (Linsebigler et al., 1995; Li et al., 1999a; Kabra et al., 2004). The effective photoexcitation of TiO_2 photocatalysts requires the application of light with energy higher than its band-gap energy of 3.05–3.2 eV (Boer, 1990; Mills and Hunte, 1997), thus resulting in the formation of electrons (e^-) in the conduction band and positive holes (h^+) in the valence band. Excited state conduction-band electrons and valence-band holes can recombine and dissipate the input energy as heat, get trapped in metastable surface states or react with electron donors and electron acceptors adsorbed on the semiconductor surface or within the surrounding electrical double layer of the charged particles (see Figure 2-1). In Figure 2-1, Red is an electron donor (i.e., reductant) and Ox is an electron acceptor (i.e., oxidant). If suitable Red or Ox is available to trap the hole or electron, recombination is prevented and subsequent redox reactions may occur. While in the absence of suitable electron and hole scavengers, the stored energy is dissipated within a few nanoseconds by recombination. The valence band holes are powerful oxidants (+1.0 to +3.5 V vs NHE depending on the semiconductor and pH), while the conduction-band electrons are good reductants (+0.5 to –1.5 V vs NHE) (Grätzel, 1989).

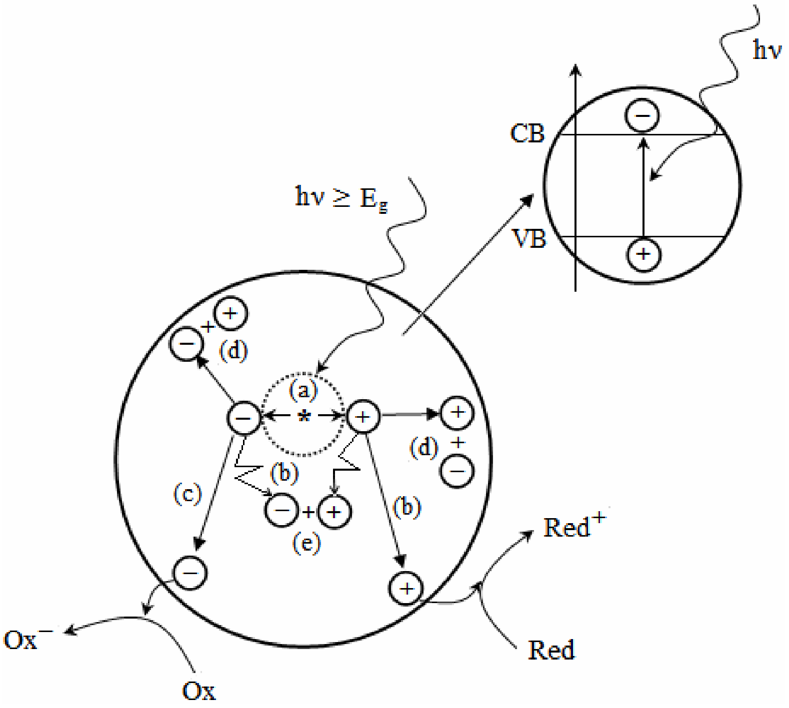

Figure 2-1. Main processes occurring on a semiconductor particle: (a) electron–hole generation; (b) oxidation of donor (Red); (c) reduction of acceptor (Ox); (d) and (e) electron–hole recombination at surface and in bulk, respectively (Mills and Hunte, 1997).

In this general mechanism, it is assumed that the substrate does not undergo direct hole transfer and that oxidative electron transfer occurs exclusively through a surface-bound hydroxyl radical (•OH) or equivalent trapped hole species. However, there exists a significant body of literature advocating that photocatalytic reactions may occur by either indirect oxidation via the surface-bound hydroxyl radicals (i.e. a trapped hole at the particle surface reacts with HO^- or H_2O to transform into •OH) or directly via the valence-band hole (Hoffmann et al., 1995). In support of hydroxyl radicals as the principal reactive oxidant in photoactivated TiO_2, it is the observation that intermediates detected during the photocatalytic degradation of halogenated aromatic compounds are typically hydroxylated structure (Turchi and Ollis, 1990; Mills and Hoffmann, 1993). The •OH radicals produced by TiO_2 are the most powerful oxidizing species after fluorine with an oxidation potential of 2.80 V (Legrini et al., 1993) as listed in Table 2-1. Unlike other radicals, hydroxyl radicals are non-selective and thus readily attack a large group of organic chemicals to be hydroxylated or partially oxidized intermediates (Li et al., 1999b; Konstantinou et al., 2001). At sufficient contact time and proper operation conditions, it is practically possible to mineralize the target pollutant to CO_2. The remarkable advantage of semiconductor photocatalysis over all chemical and biological processes is that they are totally ‘‘environmentally-friendly’’ as they neither transfer pollutants from one phase to the other (as in chemical precipitation, adsorption and volatilization) nor produce massive amounts of hazardous sludge (Ince and Apikyan, 2000).

Table 2-1. Oxidation potentials of some oxidants (Legrini et al., 1993).

Species	Oxidation potentials (V)
Fluorine (F_2)	3.03
Hydroxyl radical (•OH)	2.80
Atomic oxygen	2.42
Ozone (O_3)	2.07
Hydrogen peroxide (H_2O_2)	1.77
Potassium permanganate ($KMnO_4$)	1.67
Hypobromous acid (HBrO)	1.59
Chlorine dioxide (ClO_2)	1.50
Hypochlorous acid (HClO)	1.49
Chlorine ($C1_2$)	1.36
Bromine (Br_2)	1.09

2.1.2 Theory of Polymer-sensitized TiO_2 Photocatalysis

The conjugated polymers with extending π-conjugated electron systems, such as polyaniline, polythiophene, polypyrrole and their derivatives, have shown great promises due to their high absorption coefficients in the visible part of the spectrum, high mobility of charge carriers and excellent stability (Pron and Rannou, 2002). In general, they are also efficient electron donors and good hole transporters upon visible light excitation (Shaheen et al., 2001). Recently, conjugated polymers have been found to act as stable photosensitizers combined with wide band gap inorganic semiconductors (e.g., TiO_2, ZnO, CdSe and CdTe) is an emerging area of research for optical, electronic and photoelectric conversion applications (Roberson et al., 2004; Beek et al., 2005; Min et al., 2007). In a conjugated polymer/TiO_2 system, polymer, bound to TiO_2, can actively harvest the visible light matching the semiconductor energy levels and then inject electrons into the conduction band (CB) of TiO_2. Over the past several decades, researchers have successfully investigated and described theoretically the movement of charge across the bulk/molecular interfaces. A schematic diagram for the charge transfer processes of conjugated polymer and TiO_2 is illustrated in Figure 2-2. Here, when the conjugated polymer harvests visible light, an absorbed photon promotes an electron from the ground state of the polymer located in the semiconductor energy gap into an excited state that is in resonance with the CB. The polymer π-orbital becomes the highest occupied molecular orbital (HOMO) in the combined system. Since the lowest unoccupied molecular orbital (LUMO) levels of polymer are energetically higher than the conduction band edge of TiO_2 (Salzner et al., 1998; Snook et al., 2005), the electron transfer paths in Figure 2-2 are possible. Efficient electron injection into the edge of the CB avoids the energy loss by relaxation to the CB edge (Duncan and Prezhdo, 2007). The injected electron delocalizes from bulk to surface, simultaneously relaxing to the bottom of the CB owing to coupling to vibrations. If the electron remains trapped at the surface, it will react with the electron acceptor such as oxygen or hydrogen peroxide residing on the electrolyte mediator.

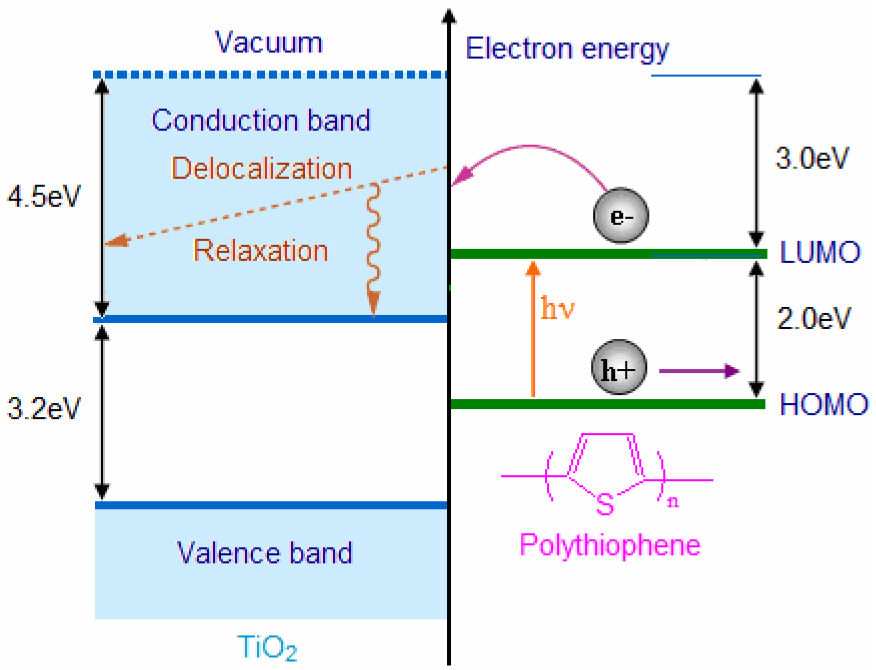

Figure 2-2. Photogeneration mechanism of conjugated polymer/TNT nanocomposites. Here, the conjugated polymer = polythiophene.

As a result, it should be a vital prerequisite for photosensitization that the interfacial charge transfer between photosensitizer and semiconductor takes place, being capable of responding to visible light. However, there are quite limited reports to gain attention to the photocatalysis of TiO_2 sensitized by such a polymer under visible light irradiation.

2.2 Application of TiO_2/UV Process in Water Treatment

2.2.1 Two Approaches of TiO_2/UV Processes

The TiO_2/UV process as photocatalytic oxidation is known to have many important advantages that a large number of organic compounds dissolved or dispersed in water can be completely mineralized; the rate of reaction is relatively high if large surface areas of the photocatalyst can be used; TiO_2 is available at a relative modest price and would be recycled on a technical scale (Legrini et al., 1993). In photocatalytic degradation using TiO_2/UV, two modes of TiO_2 applications are adopted using (1) TiO_2 suspended in aqueous medium and (2) TiO_2 immobilized on certain support materials.

The use of TiO_2 in suspension is considerably efficient due to the large surface area of catalyst available for reaction. Some researchers have developed pilot scale treatment systems employing TiO_2 in aqueous suspension. For example, Suri et al.

(1999) designed a pilot-scale system to investigate the technical feasibility of the removal and destruction of organic contaminants in water using adsorption and photocatalytic oxidation. The process consists of two consecutive operational steps: (1) removal of organic contaminants using fixed-bed adsorption; and (2) regeneration of spent adsorbent using photocatalysis or steam, followed by decontamination of steam condensate using photocatalysis. The pilot-scale study was conducted to evaluate these options at a water treatment plant in Wausau (Wisconsin) for treatment of groundwater contaminated with tetrachloroethene (TtCE), trichloroethene (TCE), cis-dichloroethene (cis-DCE), toluene, ethylbenzene (EB), and xylenes. The adsorbents used were granular activated carbon (GAC F-400 and Ambersorb 563). In the first treatment strategy, the adsorbents were impregnated with photocatalyst and used for the removal of aqueous organics. The spent adsorbents were then exposed to ultraviolet light to achieve photocatalytic regeneration. In the second treatment strategy, the spent adsorbents were regenerated using steam, followed by cleanup of steam condensate using photocatalysis. Four cycles of adsorption and three cycles of steam regeneration were performed. Ambersorb 563 adsorbent was successfully regenerated using saturated steam at 160 °C within 20 h. The steam condensate was treated using fixed-bed photocatalysis with Pt-TiO_2 photocatalyst of 1% supported on silica gel. After 35 min of empty bed contact time, more than 95% removal of TCE, cis-DCE, toluene, EB, and xylenes was achieved, and more than 75% removal of TtCE was observed.

Although TiO_2 is known to be an excellent photocatalyst for removal of organic contaminants, the separation of TiO_2 particles creates another problem in practical applications of the process. A major difficulty in the separation of TiO_2 particles from treated water arises because TiO_2 particles are too fine to be removed by gravity settling. Recently, some attempts have been made to effectively separate TiO_2 photocatalysts, for example, by coagulation (Kagaya et al., 1999; Baran et al., 2005), membrane separation (Molinari et al., 2000; Erdei et al., 2008), and magnetic separation, etc. When a coagulation technique is applied using aluminum chloride, TiO_2 particles are flocculated and settled rapidly. Kagaya et al. (1999) investigated the coagulation technique for separating TiO_2 photocatalyst from its aqueous suspensions after the photocatalytic degradation of organic contaminants. When a basic aluminium chloride was used as a coagulating agent, TiO_2 in the aqueous suspensions could be flocculated and settled rapidly; the supernatant solution after sedimentation was practically transparent at pH 8−9; the transmittance of the supernatant solution was more than 93% for 100 mg of TiO_2. Other coagulating agents, iron(II) sulphate and calcium chloride, were also examined, but their transmittance of the supernatant solution was less than that by basic aluminium chloride. Baran et al. (2005) also studied the separation of catalyst after photocatalytic reactions conducted in the presence of TiO_2/$FeCl_3$/UV. They found that the best effects of separation were obtained at the lowest examined pH 5.5 and the worst effects were at the highest pH 8.5. More than 90% of turbidity removal was obtained after bringing pH of the samples to 5.5–7.5 and at a concentration of $FeCl_3$ within the range 0.8–1.5 mM. In the samples at higher pH it was observed a yield decrease of the turbidity removal, especially at lower $FeCl_3$ concentration. Based on these results, it seems that the coagulation technique may contribute to the industrial applications of the photocatalytic degradation using a titanium dioxide-suspended reactor for the treatment of wastewater. However, the TiO_2 particles recovered from the sediment need several further treatment steps prior to reuse. For example, the obtained precipitate including TiO_2 and $Al(OH)_3$ was dissolved with concentrated hydrochloric acid. The TiO_2 was filtered by suction using a membrane filter (Nihon Millipore omini pore membrane, pore size 0.2 μm and then washed with about 2 M hydrochloric acid solution followed by distilled water (Kagaya et al., 1999). The coagulation method also has another problem related to the production of chemical sludge that must be disposed.

In the past decade a new type of photocatalytic membrane reactors (PMRs), taking advantage of combining photocatalysis and membrane technologies for water and wastewater treatment, has been received increasing attention. These reactors are designed in a promising way of solving the problems of photocatalyst separation from the reaction mixture in aqueous suspension. In such PMRs TiO_2 is either physically immobilized on the membrane or retained in its suspension by means of the membrane (Molinari et al., 2000; Xue et al., 2008). Most of the PMRs described in the literature combine photocatalysis with pressure-driven membrane processes such as microfiltration (MF), ultrafiltration (UF) or nanofiltration (NF). A typical TiO_2 slurry-membrane photoreactor is shown in Figure 2-3 (Choo et al., 2008). This work investigated the performance of a submerged hollow fiber membrane module with regard to the removal of natural organic matter (NOM) and the control of membrane fouling. Membrane permeability in PMR was also characterized at different levels of permeate flux and UV irradiation. The addition of ferrihydrite into the TiO_2-mediated PMR enhanced the removal of humic acid in synthetic water, but there was an adverse effect on lake water NOM with low specific UV absorbance and high pH values.

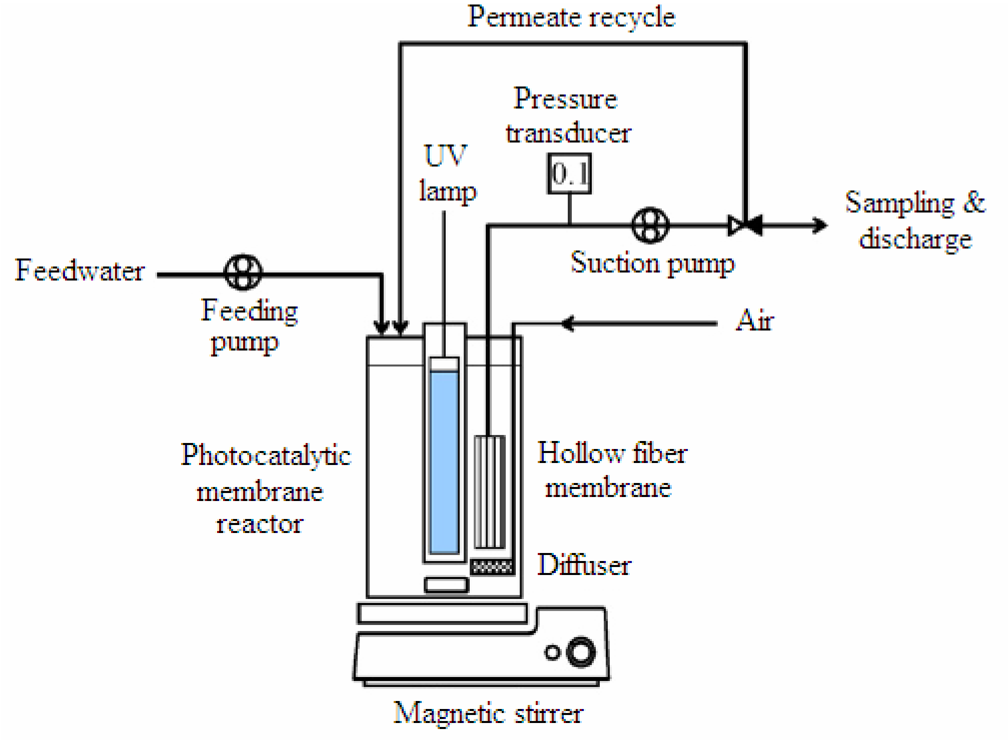

Figure 2-3. Schematic diagram of a laboratory submerged photocatalytic membrane reactor (Choo et al., 2008).

Although application of membrane processes provides an opportunity to separate the catalyst from a treated solution, in practical process, two key factors of membrane pore size and operational pressure need to be considered. For example, Molinari et al. (2000) studied the behavior of the membrane photoreactor using the suspended TiO_2 catalysts. In their report, eleven polymeric membranes (see Table 2-2) were used in the photoreactor for the photodegradation experiments. The experimental results show that a nearly complete degradation of 4-NP was observed in the presence of TiO_2 suspended in the solution and pure oxygen. The water permeation flux showed a linear trend which increased very slightly with the pressure in the range 100–180 kPa and decreased slightly by increasing the amount of TiO_2.

Table 2-2. Types of commercial membranes used in UV-Vis irradiation tests (Molinari et al., 2000).

Types of membrane	Manufacturer	Type of polymer	Cut-off/ pore size
MPPS 0000 u002	Separem	Polysulphone	15 kDa
MPPS 0000 u006	Separem	Polysulphone	40 kDa
MPCU 0000 u20	Separem	Polyamide	2.5 kDa
MPCU 0000 u25	Separem	Polyamide	2.0 kDa
P-12-10	Self-made	PEEK	--
FS 50 PP[a]	Dow	Fluoride + PP	50 kDa
PES	TechSep	Polyethersulphone	40 kDa
PVDF	Techsep	Polyvinylidenefluoride	0.1 kDa
GR 51 PP	Techsep	Polysulphone + PP	50 kDa
PAN	Techsep	Polyacrylonitrile	40 kDa
CA 600 PP	Dow	Cellulose acetate + PP	20 kDa

[a] Polypropylene.

Lee et al. (2001) reported that an UF membrane with cut-off/pore size of 30 kDa had reject higher than 97% under cross-flow velocity of 1.0 m s^{-1} and transmembrane pressure of 70 kPa. Xue et al. (2008) found that when the ultrafine TiO_2 from aqueous suspension was separated using cross-flow UF membrane with cut-off/pore size of 30 kDa, a relatively higher flux level could be obtained by setting transmembrane pressure being of in the range 100–200 kPa and the cross-flow rate being of in the range 1–2.8 m s^{-1}.

Shon et al. (2008) also investigated an integrated photocatalysis–membrane hybrid system for wastewater treatment with the main focus on improving the cross flow permeate flux. Photocatalysis with TiO_2 (Degussa P25) suspension as photocatalyst was applied both as pre-treatment and as inline treatment with MF. MF membrane used in this experiment consisted of a flat sheet polyvinyl chloride (PVC) (Pure-Envitech Co. Ltd., South Korea) with a pore size of 0.4 μm. The membranes were operated at transmembrane pressure of 30–50 kPa, cross flow rate of 0.5 m s^{-1} and room temperature of ~30 °C. As a result, the TiO_2 slurry was found to have significant effect in permeate flux for wastewater with lower dissolved organic carbon concentration.

Recently, Mozia et al. (2006) reported a new type of PMR utilizing photocatalysis with P25 catalyst and direct contact membrane distillation (MD). One of the main advantages of the new configuration is high quality of the product (distillate). MD is a process of evaporation of feed volatile components through a porous hydrophobic membrane. During the process operation, the gas phase is maintained inside the pores of the membrane. The driving force of the mass transfer through the membrane pores is a vapor pressure difference on both sides of membrane, which depends on the temperature and the solutions composition in the layers adjacent to the membrane (Gryta et al., 2001). Feed temperatures in MD usually range from 60 to 90 ^oC, although temperatures as low as 30 ^oC have been used. For example, in 2008 Mozia and co-workers investigated the application of a newly prepared TiO_2 (A-700-1h) for decomposition of azo dye Acid Red 18 (AR18) in a PMR, coupling photocatalysis and membrane distillation. The inlet temperature of the feed was 62 ^oC for the reaction temperature (in the feed tank) of 60 ^oC. Taking into account the composition of permeate, it was found that only a small amount of by-products of dye photodecomposition was transported through the MD membrane. Moreover, a complete retention of the model dye was observed.

However, when a catalyst in suspension is applied, the membrane fouling is often observed, especially in case of MF and UF membranes. Moreover, the quality of permeate is not very high, as small molecules can pass easily through the membranes used, even in case of NF. In addition, low membrane life time and high operating cost would limit the practical application of membranes in wastewater treatment.

To further encourage industrial use of photocatalytic reactors, it is necessary to find a compromise among many parameters to achieve a practical, robust, inherently safe, controllable system which is able to cope with flow variations, no fine tolerances in mechanical parts, and easy to be scaled up. For this, Bickley et al. (2005) designed a flexible modular photocatalytic reactor using a suspension of relatively large titanium dioxide catalyst particles (ca. 10 to 100 μm), which can be separated from treated wastewater using a hydrocyclone. A different lamp type (e.g., low-pressure and medium-pressure lamps) could be used if required to obtain photolysis as well as photocatalysis or to find a more economical design. A flow rate per module at an order of 1 m^3 h^{-1} was achieved. By using larger particle size catalyst it becomes possible to use robust hydrocyclones for catalyst recovery, a more acceptable solution than sedimentation or filtration. Actually, in recent years some researchers developed some new spherical photocatalysts called TiO_2 microsphere, which are at microscale with porous or nonporous structures, with the purposes of conducting an efficient photooxidation in its suspension with ease of separation from treated water (Li et al., 2003; Lee et al., 2008). However, such microspheres generally have lower catalyst reactivity than that of very fine particles and also need the post-treatment prior to reuse.

On the other hand, TiO_2-coated magnetic particles have also been proposed as a means to enhance the separation of the catalyst from treated water by the application of an external magnetic field (Gao et al., 2003; Chung et al., 2004; Kurinobu et al., 2007). The magnetic core materials mainly contain the three strongly magnetic (ferromagnetic) elements: iron, nickel, and cobalt. Among them, ferrite is the most popular because of its strong ferromagnetism and ease of preparation of the colloidal particles. Chung et al. (2004) synthesized a titania–silica layer-coated $NiFe_2O_4$ photocatalyst powder by a multi-step ultrasonic spray pyrolysis. By separating magnetic core preparation and titania–silica coating into two steps, high crystallinity of titania was achieved without phase transformation of the core magnetic particles. This enables to select a wide range of magnetic core materials such as Fe_2O_3, $MgFe_2O4$, $MnFe_2O_4$, and $NiFe_2O_4$. The experimental results show that the prepared powder had magnetic property and it was demonstrated that the powder could be separated by a magnetic material from the slurry and recycled to the reactor. The adhesion of the coated layer on the magnetic core particles was strong enough to withstand vigorous mixing in the slurry reactor. Also, Kurinobu et al. (2007) prepared the magnetic photocatalyst particles with a core-shell structure of three layers coating Fe_3O_4 core particles with SiO_2 and TiO_2. The magnetic photocatalyst particles efficiently decomposed the organic substances such as methylene blue, red basic dye, blue basic dye, nonylphenol, and octylphenol. After treatment, the magnetic photocatalyst particles were easily recovered using magnetic separation.

However, there are two major difficulties in employing titania-coated magnetic materials as a photocatalyst. The first obstacle is low photoactivities arising from the low crystallinity of titania. The second obstacle is a photodissolution phenomenon, which is an electronic interaction between titania coating and the ferrite core. It has been found that the attachment of TiO_2 powder on those free carriers is not stable enough for a long period of operation from an engineering point of view.

In terms of technical application, therefore, using immobilized TiO_2 is an alternative to the suspended TiO_2 because it does not need additional post-treatment for the recovery of catalyst after oxidation. To preclude the separation procedure, the immobilization of the TiO_2 catalysts on certain supporting materials such as glass, fiber, or stainless steel has been frequently adopted as reviewed by Byrne et al. (1998) and these are listed in Table 2-3.

When the catalyst is immobilized, however, a considerable loss in the contact area between the immobilized photocatalyst and a light source limits its efficiency in the photocatalytic degradation of the organic substrates (Rachel et al., 2002; Shephard et al., 2002). In certain cases, the efficiency of photoactivities using the immobilized photocatalysts could be drastically declined to only 1/200th of that using TiO_2 slurry

Table 2-3. Methods of immobilization of TiO_2 and support substrates coated (Byrne et al., 1998).

Method of immobilization	Substrate coated	Ref.
Dip coating from suspension	Glass beads	Bideau et al., 1995
	Glass tubing	Matthews, 1987 and 1988
	Glass plate	Chester et al., 1993
	Glass fibers	Brezova et al., 1995
	Silica gel	Zhang et al., 1994
	Sand	Matthews, 1991
Sol gel related methods	Quartz	Fernandez et al., 1995
	Optical fibers	Tada and Honda, 1995
	Glass beads	Bideau et al., 1995
	Glass plate	Fernandez et al., 1995
	Tin oxide coated glass	Kim and Anderson, 1994
Oxidation of parent metal electrochemical	Titanium	Arsov and Efremova, 1992
Thermal	Titanium	Cámara et al., 1995
	Titanium alloy	Kudo et al., 1990
Anodization of $TiCl_3$	Tin oxide coated glass, Ti, Pt and Au	Kavan et al., 1993
Electrophoretic coating	Stainless steel	Fernandez et al., 1995
Aerosol powder coating	Hollow glass beads	Nair et al., 1993
Sputtering	Glass	Brudnik et al., 1991
Liquid phase disposition	Glass plate	Deki et al., 1996

due to not only the reduction of active area but also the high concentration of ionic species in the support that probably contributed to the recombination of charges in the photocatalyst leading to its deactivation (Rachel et al., 2002).

Recently, some researchers attempted to enlarge the surface areas of the TiO_2 film by forming a porous TiO_2 film (Guo et al., 2005; Zhao et al., 2008) or designing a new photoreactor (Hitchman and Tian, 2002; Xu et al., 2008). For example, Zhao et al. (2008) first prepared the micro-/nano-composite hierarchical TiO_2 films on glass substrates by electro-hydrodynamic (EHD) method. The experimental results show that the catalytic activities of hierarchical porous films were increased ca. 60–70% for mineralizing liquid-phase phenol comparing to that of nano-structured film. They suggested that the pores structure plays important roles in the photocatalytic characters of films photocatalyst. Hierarchical TiO_2 porous film produces continuously composite pore channels, providing the fast transport pathway for reactants, products and O_2 moving into and out of the catalytic framework.

On the other hand, Xu et al. (2008) developed a rotating disk photoelectrocatalytic (PEC) reactor with TiO_2/Ti thin film. This reactor combines highly effective thin film and conventional PEC process on a single TiO_2/Ti electrode. The upper part of the round TiO_2/Ti disk photoanode was coated with a thin film of wastewater and exposed to UV radiation in air. The lower part of the disk electrode was immersed in a wastewater solution to perform conventional PEC treatment. In conventional PEC reactor design, where the photoanode is completely immersed in solution, the radiation has to pass through the wall of the reactor and sample solution before it reaches the photoanode surface (Li et al., 2000; Yang et al., 2005). The average thickness of the thin wastewater film coated on the electrode is 75 μm. In a model system of 20–150 mg L^{-1} RB solutions, thin-film PEC removed total color and total organic carbon (TOC) by 27–84% and 7–48%, respectively, within 1 h, much higher than 3–55% and 0–30% removals by conventional PEC under the same treatment conditions. However, this film electrode without porous structure contains the aggregates of interconnected nanoparticles, which cannot sustain the development of a space charge layer (Hagfeld and Grätzel, 1995). Consequently, the photoelectron and photohole separation will be reduced and thus weaken the essential photoefficiency of TiO_2/Ti thin film, although a bias voltage is applied to the electrode (Jiang et al., 2003).

Based on the above results, there is a need to increase the total surface area of immobilized catalysts in the photoreactor by a better design with a high area-to-volume ratio between the catalysts and reactor and also better structured catalysts with higher photocatalytic activities.

2.2.2 Opportunity of TiO_2 Nanotubes

According to the mechanism illustrated in Figure 2-1, the overall quantum efficiency for interfacial charge transfer is determined by two critical processes: the competition between charge carrier recombination and trapping, followed by the competition between trapped carrier recombination and interfacial charge transfer. An increase in either the lifetime of charge carriers or the interfacial electron-transfer rate constant is expected to result in higher quantum efficiency for steady-state photolyses. This relationship has been verified by time-resolved microwave conductivity studies of TiO_2 (Martin et al., 1994), and also emphasizes the importance of the interfacial charge transfer rate constant and the charge-carrier recombination lifetime as contributing factors to TiO_2 photoreactivity. Accordingly, electron transport is a limiting factor in the performance of TiO_2 nanocrystallines, hampering progress in achieving higher efficiency. However, the structural disorder at the contact between two crystalline nanoparticles leads to enhanced scattering of free electrons, thus reducing electron mobility (Peng et al., 2003). In contrast, an ordered and strongly interconnected nanoscale architecture offers the potential for improved electron transport leading to higher photoefficiency. This has resulted in one-dimensional TiO_2 materials, such as nanowires, nanorods and hollow nanotubes, receiving a great deal of attention in recent years because they demonstrate a superior performance when compared to the bulk TiO_2 particles (Chen et al., 2005; Khan et al., 2006; Macak et al., 2007). Among these materials, hollow TiO_2 nanotubes that have surface area-related properties can further improve photocatalytic properties. Several nanotubular architectures have been investigated for potential enhancement of electron percolation pathways and light conversion as well as improved ion diffusion at the semiconductor-electrolyte interface (Chen et al., 2005; Mor et al., 2006c). Based on these results, the hollow TiO_2 nanotubes with high surface area seem to provide an opportunity for developing the TiO_2/UV process in water treatment. To date considerable efforts have been devoted to the preparation of various nanotubular TiO_2 catalysts by mainly the hydrothermal synthesis, template techniques and anodic oxidation methods.

2.3 Synthesis of TiO_2 Nanotubes

2.3.1 Hydrothermal Method

The hydrothermal synthesis, a simple method, was first developed by Kasuga et al. (1998), and extensively employed to synthesize TiO_2 nanotubes, nanoribbons and nanowires. Briefly, the TiO_2 precursor used for nanotube production is a commercially available TiO_2 powder (such as Degussa P25). The preparation is initiated by treating 2 g of the P25 powder with 70 mL of 10 M NaOH in a Teflon-lined autoclave at 130 ^{o}C for 24 h. After treatment and subsequent cooling, it is subjected to the precipitate from filtration to pH-value regulation by mixing it with 1 L HCl solutions of different concentrations. The final products are obtained by filtration with subsequent drying at 100 ^{o}C for 3 h. However, Du et al. (2001) claimed that the nanotubes prepared by the treatment of TiO_2 in aqueous NaOH solution were not the TiO_2 form but rather $H_2Ti_3O_7$. Meanwhile, Zhu et al. (2001) also developed a hydrothermal synthesis for the formation of titania whiskers and nanotubes with the assistance of sonication. In a typical synthesis, a mixture containing 150 mg of TiO_2 powder and 30 mL of 10 M aqueous NaOH solution is sonicated for 60 min, heat-treated at 110 °C for 4 h, and then washed by 0.1 M aqueous HNO_3 solution and deionized water. The products contain intermediates between $H_2Ti_3O_7{\cdot}0.5H_2O$ and TiO_2.

Tsai and Teng (2006) suggested that the structural features of nanotubes synthesized from NaOH treatment on TiO_2 were significantly dependent upon the different post-treatments. Apart from the crystalline structure of anatase TiO_2, some titanate structures, such as $A_2Ti_2O_5{\bullet}H_2O$, $A_2Ti_3O_7$, $H_2Ti_4O_9{\bullet}H_2O$ and lepidocrocite titanates, have been assigned as nanotube constituents (A = Na and/or H). Furthermore, they

Table 2-4. Nanotubes of different structures prepared from different processes (Tsai and Teng, 2006).

Precursor	NaOH treatment [a]	Post-treatment	Refs.
Nanotube Structure: Anatase TiO_2			
anatase	hydro/110/20	HCl + water	Kasuga et al. (1998)
rutile	chem/110/20	HCl + water	Kasuga et al. (1999)
anatase	chem/150/12	water	Seo et al. (2001)
anatase	hydro/110/20	HNO_3 + water	Zhang et al. (2002)
anatase/rutile	hydro/130/24	HCl	Tsai and Teng (2006)
Nanotube Structure: Anatase $TiO_2/H_2Ti_3O_7{\bullet}0.5H_2O$			
rutile	chemi/110/4[b]	HNO_3 + water	Zhu et al. (2001)
Nanotube Structure: $A_2Ti_2O_5{\bullet}H_2O$			
TiO_2 powder	chem/110/20	HCl + water	Yang et al. (2003)
anatase	chem/110/20	HCl + water	Zhang et al. (2004a)
Nanotube Structure: $A_2Ti_3O_7$			
anatase	hydro/130/72	HCl + water	Du et al. (2001)
anatase	hydro/130/72	HCl + water	Chen et al. (2002)
any crystals	hydro/130/72	water	Zhang et al. (2003b)
anatase	hydro/180/24	HCl + water	Yuan and Su (2004)
rutile	hydro/150/72	HCl + water	Thorne et al. (2005)
Nanotube Structure: $H_2Ti_4O_9{\bullet}H_2O$			
anatase/rutile	hydro/110/96	HCl + water	Nakahira et al. (2004)
Nanotube Structure: Lepidocrocite Titanates			
anatase	hydro/150/48	water + HCl	Ma et al. (2003)

[a] Treatment conditions refer to chemical or hydrothermal processes, temperature (°C) and duration (h), respectively.

[b] Sonication at 280 W before chemical treatment.

summarized the different nanotube structures proposed by different preparation conditions and the corresponding post-treatment processes as listed in Table 2-4.

2.3.2 Template-Assisted Synthesis

Replication processes have been applied to nanoelectrochemistry since the 1970s and one-step replication is among the first processes to produce nanoscopic pieces of material in a particular shape (Kawai and Ueda, 1975). This process usually results in structures that were “negatives” (negatypes) of the mold but in some cases polypyrrole or gold nanotubes were obtained as described by Martin (1991).

Template synthesis has the advantage that in principle any material which forms a unique nanostructure can be used as a mold to obtain negatype structures of a great variety of shapes. Although there are no fundamental limitations to the choice of a starting membrane, anodically formed porous alumina oxide (AAO) has the advantage that the dimensions of the porous nanostructure can be tuned over a wide range and it can be easily dissolved after the replication process (Martin, 1996; Piao et al., 2005). The size and density of the pores in the AAO matrix can be controlled by the anodizing voltage and subsequent etching procedures. Depending on the experimental parameters, samples with a regular honeycomb structure with holes of a size between 10 and 200 nm can be produced. In addition, the material shows a remarkable hardness, uniform pore size, high pore density together with its potentially low cost and relative ease with preparation. Hence, template synthesis using a highly ordered porous alumina membrane, has attracted a good deal of research interest. For example, Hoyer (1996a) first prepared titanium dioxide nanotubes by electrochemical deposition in AAO and a polymer mold, in which a two-step replication procedure was involved. During the first replication step, a negatype structure was formed, which served as a mold for the product. The second step yielded a copy of the mother template, finally producing a nanotubular structure. As mentioned above, the important part of the tubes is the free space in their interior. In the route presented here, the holes of the prepared tubes cross the whole thickness of the sample and both tube openings are accessible for chemical synthesis. The tubes can be filled by a variety of methods, including surfactant-assisted synthesis (Rao et al., 2001), chemical bath deposition (Zhang et al., 2004b), electrodeposition (Zhou et al., 2003; Kemell et al., 2007) and chemical vapor deposition (Schulz and Marks, 1994; He and Mohammad, 2006). Here, electrochemical deposition in a mold easily yields a compact porous film instead of nanotubes (Hoyer, 1996b), and the structural aspects of the deposition strongly depend on the pH, buffer capacity, current density, free space in the mold and diffusion of the ions in the solution.

The template method has been demonstrated to be effective in producing TiO_2 with a hollow structure, in which the TiO_2 nanoparticles were either deposited within the preformed tubular templates such as porous polymer latex and anodic aluminium oxide (Lakshmi et al., 1997; Caruso et al., 2001) by the sol–gel, electrochemical deposition or electrospinning methods to form one-dimensional TiO_2 hollow structures. However, these methods generally involve multiple (at least three) steps, including the fabrication of templates, the filling or coating of the surfaces of templates with TiO_2 (or a precursor to this material) and finally the selective removal of the templates. The quantity of nanostructures that can be obtained in each processing run is often limited. It will be an advantage if one can develop a simpler method that is capable of generating TiO_2 nanotubes in fewer steps.

2.3.3 Anodic Oxidation Technique

Zwilling and co-workers in 1999 first reported the anodization of titanium for an important surface treatment in chromic acid solution with and without hydrofluoric acid addition. Anodization was conducted under potentiostatic conditions at room temperature in a two-electrode cell. The standard procedure was to increase the potential between the specimen and a titanium cathode from 0 up to 5 or 10 V by five equal steps of 1 min each. The specimen was then maintained at the final voltage for variable times between 1 and 55 min. In their experiments, the thickness and morphology of the films were described as a function of the anodizing conditions and of the composition of the underlying substrate.

Grimes and co-workers in 2001 synthesized the uniform and highly-ordered TiO_2 nanotube arrays by anodic oxidation of a pure titanium sheet in an aqueous electrolyte containing 0.5-3.5 wt% HF (Gong et al., 2001) under 20 and 40 V. Instead of the electrolyte of HF/H_2O, other aqueous electrolytes, such as KF/NaF/H_2O (Cai et al., 2005), CH_3COOH/NH_4F (Tsuchiya et al., 2005), and organic electrolytes (Ruan et al., 2005) have been developed to create TiO_2 nanotube films. Based on these results, it was expected that in the anodization of titanium electrolyte composition is a critical determinant with regard to the resulting surface morphology, and hence properties of the anodic films. For example, Cai et al. (2005) reported the fabrication of self-organized titanium oxide nanotube arrays of enhanced surface area prepared by anodic oxidation of a pure titanium sheet in electrolyte solutions containing potassium fluoride or sodium fluoride. Although nanotube arrays of length greater than 500 nm were not possible with hydrofluoric acid containing electrolytes, they increased the nanotube length to approximately 4.4 μm by adjusting the pH of a KF-containing electrolyte to 4.5 with additives such as sulfuric acid, sodium hydroxide, sodium hydrogen sulfate and/or citric acid. The resulting nanotubes were composed of amorphous titanium oxide. On the other hand, varying the electrolyte bath temperature can also change the morphology of TiO_2 nanotubes. For example, nanotube arrays were grown by potentiostatic anodization of titanium foil at 20 V in an electrolyte of acetic acid + 0.5% HF mixed in 1:7 ratio, kept at four different electrolyte bath temperatures, 5, 25, 35 and 50 ^{o}C (Mor et al., 2005a). TiO_2 nanotubes fabricated at 5 and 25 ^{o}C, with resulting inner pore diameters of 76 nm showed that the nanotube wall thickness increases from 17 nm at 25 ^{o}C to 27 nm at 5 ^{o}C. This result confirmed the trend of increasing nanotube wall thickness as a consequence of a lower anodization temperature. In addition, the thickness and morphology of TiO_2 nanotube films are easily controlled by regulating the electrolyzing conditions such as the etching time, applied potential and the electrolyte composition.

To have a better understanding in straight titania nanotubes, Mor et al. (2006) further proposed a mechanistic model for the nanotube array formation. They suggested that the key processes responsible for anodic formation of nanoporous alumina (Patermarakis and Karayannis, 1995; Mei et al., 2003) and titania (Delplancke and Winand, 1988; Hwang, 1993) appeared to be the same. The key processes are: (1)

oxide growth at the surface of the metal occurs due to interaction of the metal with O^{2-} or OH^{-} ions (Parkhutik and Shershulsky, 1992). After the formation of an initial oxide layer, these anions migrate through the oxide layer reaching the metal/oxide interface where they react with the metal; (2) metal ion (Ti^{4+}) migration from the metal at the metal/oxide interface. Ti^{4+} cations will be ejected from the metal/oxide interface under application of an electric field that moves towards the oxide/electrolyte interface; (3) field assisted dissolution of the oxide at the oxide/electrolyte interface (Macdonald, 1993). Due to the applied electric field the Ti–O bond undergoes polarization and is weakened promoting dissolution of the metal cations. Ti^{4+} cations dissolve into the electrolyte and the free O^{2-} anions migrate towards the metal/oxide interface to interact with the metal; (4) chemical dissolution of the metal, or oxide, by the acidic electrolyte also takes place during anodization. Chemical dissolution of titania in the HF electrolyte plays a key role in the formation of nanotubes rather than a nanoporous structure.

To help understand the process of nanotube formation, a schematic diagram of the evolution of nanotube arrays at constant anodization voltage is shown in Figure 2-4. With the onset of anodization, a thin layer of oxide forms on the titanium surface (Figure 2-4a). Small pits originate in this oxide layer due to the localized dissolution

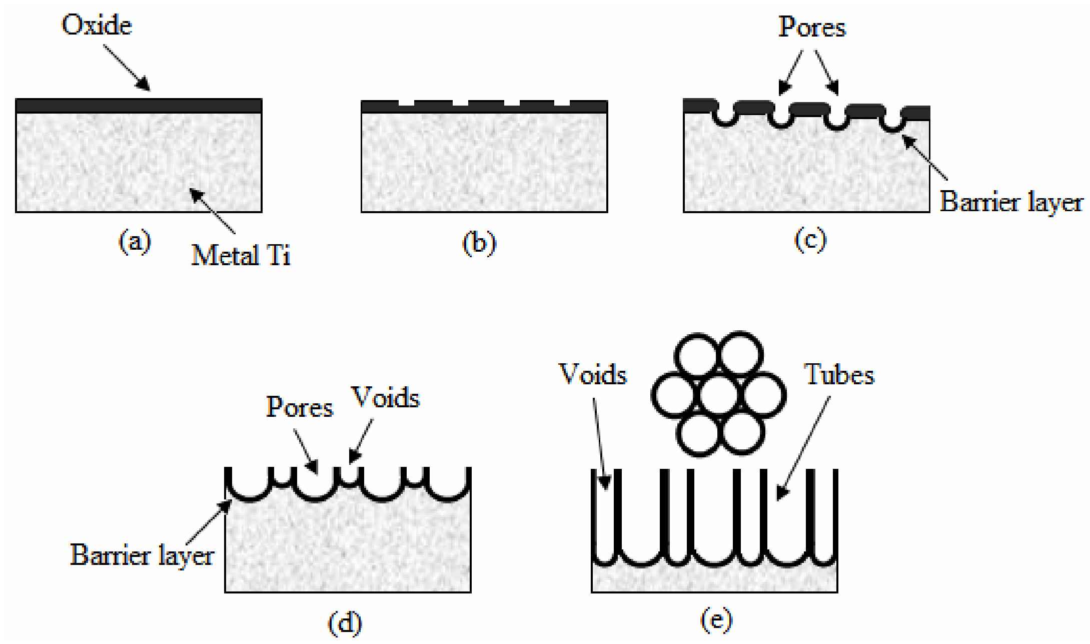

Figure 2-4. Schematic diagram of the evolution of nanotube arrays: (a) oxide layer formation; (b) pit formation on the oxide layer; (c) growth of the pit into scallop shaped pores; (d) metallic part between the pores undergoes oxidation and field assisted dissolution; and (e) fully developed nanotube arrays with a corresponding top view (Mor et al., 2006a).

of the oxide (Figure 2-4b) making the barrier layer at the bottom of the pits relatively thin which, in turn, increases the electric field intensity across the remaining barrier layer resulting in further pore growth (Figure 2-4c). The pore entrance is not affected by electric field-assisted dissolution and hence remains relatively narrow, while the electric field distribution in the curved bottom surface of the pore causes pore widening, as well as deepening of the pore. As the pores become deeper the electric field in these protruded metallic regions increases enhancing the field-assisted oxide growth and oxide dissolution; hence simultaneously with the pores well-defined inter-pore voids start forming (see Figure 2-4d). Thereafter, both voids and tubes grow in equilibrium. The nanotube length increases until the electrochemical etch rate equals the chemical dissolution rate of the top surface of the nanotubes.

2.4 Surface Modification of Anodic TiO_2 Nanotube Arrays

The anodized TiO_2 nanotube arrays allow for more efficient absorption of incident photons as well as decreased bulk recombination. This fact has been identified by Mor et al. (2005a) while also finding that the resulting quantum yield under 337 nm illumination was over 90% at high anodic polarization. Hence, the anodic TiO_2 nanotube film seems to be considered an ideal photocatalyst for UV applications. However, in its unmodified form it is rendered highly inefficient for visible light applications due to its wide band gap of 3.34 eV (Mor et al., 2005b). From the viewpoint of solar energy utilization, the development of a photocatalyst that can utilize visible light ($\lambda > 400$ nm) efficiently is indispensable. To utilize the visible light for photocatalysis, in recent years several different modifications to anodic TiO_2 nanotubes have been proposed and employed.

2.4.1 Dye-Sensitized TiO_2 Nanotubes

To extend the spectral response of TiO_2 from the UV range into the visible region, many different dyes were prepared and explored for sensitization (Polo et al., 2004). In last few years, this led to a substantial increase of light-to-electric energy conversion efficiency. Among the wide variety of dyes, polypyridyl complexes of Ru and Os with four pendant carboxyl groups, such as (*cis*-di(thiocyanato)–bis(2,2'-bipyridyl-4,4'- dicarboxylate)) ruthenium(II) dye (commercially known as N_3) and N719 dye (N719 = [tetrabutylammonium]$_2$[Ru(4-carboxylicacid-4'-carboxylate-2,2'- bipyridyl)$_2$(NCS)$_2$]) have become the most efficient and widely used dyes (Grätzel, 2003; Macák et al., 2005; Neale et al., 2005).

Since O’Regan and Grätzel (1991) reported on highly efficient TiO_2 based dye-sensitized solar cells (DSSCs), many attempts have been made to sensitize different substrates of TiO_2 such as single crystals (Nazeeruddin et al., 1993) and nanoparticulate (Grätzel, 2001) or nanoporous films (Nakade et al., 2003). The highly ordered TiO_2 nanotube arrays show the potential enhancement of electron percolation pathways and light conversion as well as improved ion diffusion at the semiconductor-electrolyte interface (Varghese et al., 2005). This has resulted in dye-sensitization of self-organized TiO_2 nanotubes recently receiving considerable attention. For example, Macák et al. (2005) reported on dye-sensitization of self-organized TiO_2 nanotubes and the photoelectrochemical response of this system. The tubes were grown by Ti anodization in fluoride containing electrolytes and after annealing the tubes to anatase they were sensitized with Ru-dye (N_3). They found an $IPCE_{max}$ of 3.3% for the ‘‘long’’ tubes (at 540 nm) and further claimed that the dye-sensitized TiO_2 nanotubes had a considerable light conversion efficiency. Zhu et al. (2007) investigated the charge transport and recombination properties of the TiO_2 nanotube (TNT) and nanoparticle (TNP) films used in DSSCs where all the films were sensitized by N719 dye. They also found that the light-harvesting efficiency of TNT-based DSSCs were higher than that of TNP-based DSSCs, resulting from the stronger light scattering effects of the former. At the same time, the former photocurrent densities were also higher than that of the latter, despite their photovoltages being comparable. Finally, they suggested that an investigation of the consequences of these morphological changes on the photoconversion processes would likely improve significantly the photoconversion efficiency of TNT-based DSSCs.

Among these organic dye sensitizers, $Ru(bpy)_3^{2+}$ and its derivatives seem to be one of the most successful and widely used in solar cells (Kalyanasundaram, 1982;

Rensmo et al., 1999). However, the dye-sensitized TiO_2 films are prepared generally by immersing into dye ethanol or acetonitrile solution and only in the acidic pH region. The dip-coating method makes it difficult to control the thickness of the dye layers, while the prepared dye-layers easily exhibit desorbed or dissolved behaviour. As a result, it is not sufficiently stable in aquatic environment.

2.4.2 Nitrogen-Doped TiO_2 Nanotubes

Recently the band-gap engineering of TiO_2 by non-metal doping has been receiving attention. Asahi and co-workers (2001) performed densities of states calculations on the effect of substitutional doping and identified nitrogen as the most effective dopant due to its comparable ionic radius and because its p-states contributed to band gap narrowing by mixing with the p-states of oxygen (Morikawa et al., 2001). However, Lee et al. (2005) contradicted this assessment in their report where their density functional calculations indicate that while nitrogen doping produces isolated N 2p states above the valence band maximum of TiO_2, the mixing of N with O 2p states is too weak to achieve appreciable band-narrowing. Based on this idea, there has recently been a great deal of interests in this area documenting different experimental approaches towards nitrogen doping of anodic TiO_2 nanotubes (Ghicov et al., 2006; Vitiello et al., 2006).

Schmuki and co-workers first reported the N-doping of anodic TiO_2 nanotubes based on two methods: ion implantation (Ghicov et al., 2006) and heat treatment in ammonia (Vitiello et al., 2006). In the former, TiO_2 nanotubes were produced by self-organized electrochemical oxidation of titanium at 20 V for 0.5 h, and then the tubes were N-ion implanted at 60 keV accelerating energy and at two nominal fluencies, 1×10^{15} and 1×10^{16} ions cm^{-2}. Two peaks could be distinguished clearly: one at 400 eV, a well-screened γ-N state (essentially adsorbed N); and another at 396 eV, an atomic β-N state (essentially atomic N in form of $TiO_{2-x}N_x$). These results demonstrated that nitrogen was not only successfully implanted in the structure but it was also present in a chemically bonded state (indicating that this type of nitrogen is the active doping species). They also investigated the effect of chromium (Cr)-ion implantation at relevant fluencies on the visible photoresponce of TiO_2 nanotubes layers (Ghicov et al., 2007). Photoelectrochemical measurements showed a visible photoresponse for the Cr^+-doped TiO_2 nanotubes. Although their results showed the successful preparation of N-doped or Cr-doped TiO_2 nanotubes, they did not further investigate the efficiency of these photocatalysts or the application in environment purification under visible light irradiation. Moreover, the ion implantation process is often accompanied by undesired radiation defects introduced in the TiO_2. The created defects act as a recombination centre for the photogenerated charge carriers, a drawback for visible light based applications.

2.4.3 Carbon/Sulfur-Doped TiO_2 Nanotubes

Park et al. (2006) reported that carbon doping of the TiO_2 nanotubular layers was successfully achieved by the reduction of carbon monoxide, CO. These catalysts are found to show much higher photocurrent densities and more efficient water splitting under visible-light illumination (> 420 nm) than pure TiO_2 nanotube arrays. The total photocurrent was more than 20 times higher than that with a P25 nanoparticulate film under white-light illumination. Hahn et al. (2007) also reported a similar observation on $TiO_{2-x}C_x$ nanotubular arrays prepared by a non-destructive thermal treatment at 500 ^oC under a mixed flux of N_2 and acetylene. They claimed that this heating approach was promising for achieving a significant photocurrent response in the whole range of visible light but that the photocatalytic efficiency of C-doped TiO_2 nanotubes was not further studied. Mohapatra et al. (2007) have also prepared the carbon-doped titania nanotube arrays by the sonoelectrochemical anodization method using ethylene glycol and ammonium fluoride solution. In their work, the application of $TiO_{2-x}C_x$ nanotube arrays as a photoanode and Pt/TiO_2 as a cathode in a PEC cell was shown, and this PEC cell was found to be highly efficient for hydrogen generation by water photoelectrolysis.

Tang and Li (2008) first fabricated the sulfur-doped TiO_2 nanotubular arrays by annealing at 380 °C for 14 h with a heating/cooling rate of 0.75 °C min^{-1} and a H_2S flux of 10 mL min^{-1}. Their experiments indicated that the sulfur atom content might gradually decrease along the nanotubes from the top to the bottom, depending on the doping temperature and duration; the sulfur-doped TiO_2 nanotubular arrays were sensitive to visible light and could form a sustainable steady photocurrent under visible light illumination. Ho et al. (2006) developed a one-step low-temperature hydrothermal route for the synthesis of S-doped TiO_2 photocatalysts from TiS_2 and HCl. In their study, sulfur could be efficiently doped into the anatase lattice under hydrothermal conditions. The photocatalytic activities of the S-doped TiO_2 were evaluated through the degradation of 4-chlorophenol under visible light irradiation and finally showed that the S-doped TiO_2 prepared by this hydrothermal approach had a higher photocatalytic activity than that obtained by the traditional high-temperature thermal annealing method. Unfortunately, since sulfur has a larger ionic radius than that of oxygen atom, it can be expected that sulfur could considerably modify the electronic structure of TiO_2 and lead to a greater instability in photocatalytic processes. This is an important point for the practical application of a photocatalyst in the environment, however it is not mentioned in their study.

2.4.4 Multi-Nonmetal-Doped TiO_2 Nanotubes

Lei et al. (2007) claimed that multi-non-metal-doped TiO_2 nanotubes could be fabricated by electrochemical anodization of Ti in the mixed acid electrolyte. The key step was to adjust the electrolyte composition. In order to dope TiO_2 nanotubes with N, F and I, they carried out all anodization experiments at room temperature by using the mixed acid electrolyte of 1/12 M $C_2H_2O_4 \cdot 2H_2O$ and 1.0 wt% HIO_3 containing 0.5 wt% NH_4F and the anodization voltage of 20 V. Although XPS measurements indicated the traces of N, F and I in TiO_2 nanotubes, most of them were essentially attributed to the adsorbed forms but not the presence of Ti–N bonds formed when the N atoms replace the oxygen in the TiO_2 crystal lattice. Further, Lei and co-workers developed a N-F-codoped TiO_2 nanotube electrode by using the $C_2H_2O_4.2H_2O$ and NH_4F electrolyte and further evaluated the effectiveness of the electrode by the degradation of methyl orange solution under UV irradiation (Su et al., 2008). It was found that there was an obvious synergetic effect between the electrochemical and photocatalytic processes, which was attributed to the utilization of photoelectrocatalytic technique using high-aspect-ratio TiO_2 nanotubes and the promoting effect of N-F-codoping on the catalytic activities. Hence, their results indicate that the possibility exists for electrochemical incorporation of anionic dopants during the anodization process. However, the mechanism of a one-step doping process is still unclear and needs further investigation.

2.4.5 CdS-Coated TiO_2 Nanotubes

CdS-coated TiO_2 nanotube arrays were fabricated by cathodic reduction with a conventional three-electrode system comprising an Ag/AgCl reference electrode and Cd counter electrode (Chen et al., 2006). A mixed solution of saturated elemental sulfur in benzene with 0.6 M $CdCl_2$ in dimethyl sulfoxide (DMSO) was used as the electrolyte. The resulting CdS–TiO_2 photoelectrode had an as-fabricated bandgap of 2.53 and 2.41 eV bandgap after sintering at 350 ^{o}C in N_2 ambient, and showed a higher visible light photocurrent as compared to a plain TiO_2 nanotube array electrode. This coupling of the semiconductors should have a beneficial role in improving charge separation, however, CdS photoeatalysis increased the toxicity due to CdS photocorrosion. Reuterglrdh and Iangphasuk (1997) investigated the decolourization of RB5 treated by CdS photocatalysis and found that the toxicity dramatically increased due to the dissolution of CdS, as confirmed by the determination of [Cd^{2+}]. Although the CdS photocatalytic degradation of RB5 wastewater was more rapid than for TiO_2, it still cannot be applied in real water treatment because of CdS dissolution and post oxidation toxicity.

2.5 Application of TiO_2 Nanotubes in Environmental Purification

2.5.1 Application of Powdery TiO_2 Nanotubes

The properties of functional materials are strongly dependent on their microstructure. Nanotubular materials possess many special properties for potential application in the area of electronics, optics, catalysis and energy storage/conversion. Recently, many researchers have focused on the synthesis of hollow TiO_2 nanotubes using the hydrothermal methods (generally producing powdery TiO_2 nanotubes) and the application to environment purification. For example, Hou et al. (2007) successfully synthesized the SnO_2/TiO_2 nanotubes composite photocatalysts by means of a simple solvothermal process. Methylene blue (MB) being the target pollutant, they investigated the photocatalytic performance and the results demonstrated that the composite photocatalysts with proper amount of SnO_2 loading have better photocatalytic activities than the pure TiO_2 nanotubes. The best photocatalytic activity was obtained in the case of 5 wt% SnO_2 loading. Also, Yu et al. (2007) prepared one-dimensional TiO_2 hollow structures consisting of primary particles (10–55 nm) were prepared by a one-step templated process. The one-step formation of the TiO_2 hollow structures was based on the template-directed deposition and the *in situ* template-sacrificial (dissolution) reaction of vanadium oxide nanobelts. The prepared TiO_2 hollow structures exhibited obvious photocatalytic activities for the photocatalytic degradation of methyl orange aqueous solution, but lower than that of the conventional powdered photocatalysts such as Degussa P25.

Zhang et al. (2004a) reported that nanotubed titanic acid ($H_2Ti_2O_4(OH)_2$) was prepared from nanotubed sodium titanate ($Na_2Ti_2O_4(OH)_2$) by an ion exchange reaction in a pH = 1 HCl solution, and evaluated the photocatalytic behaviour of nanotubed $H_2Ti_2O_4(OH)_2$ by propylene oxidation removal. The result showed that the photocatalytic activities of both $H_2Ti_2O_4(OH)_2$ and $H_2Ti_2O_5$ are very low, only about 60% that of raw anatase TiO_2. Once the formation of anatase phase begins, the photocatalytic activities increase dramatically, but the nanotubed ($H_2Ti_2O_4(OH)_2$) was found to be thermally unstable.

It is well known that when TiO_2 is exposed to UV light, electrons in the uppermost valence band will jump to the conduction band and create conduction band electrons and valence band holes. In most instances, the valence-band holes and conduction-band electrons easily undergo a fast recombination, which is responsible for the low photocatalytic efficiency. To suppress the rate of hole-electron recombination, Chen et al. (2005) designed a TiO_2-based p-n junction nanotube photocatalyst where the outside layer of the tube was TiO_2 a p-type and the inside was platinum as a n-type, respectively. In their research, the specific surface area of the p-n TiO_2/Pt nanotubes was estimated to be 40–60 $m^2 g^{-1}$, almost the same as the Degussa P25 (50 $m^2 g^{-1}$), while the modified nanotubes showed a great enhancement of photocatalytic activity, about 4 times higher than that of Degussa P25. Regarding these results, they explained that when the outside of the tube (TiO_2) was exposed to UV light, electrons in the uppermost valence band would jump to the conduction band and flow to the platinum layer. As a result, the p-n junction nanotubes might separate the electron-hole pairs and then improve photocatalytic activities.

2.5.2 Limitation of Powdery TiO_2 Nanotubes

As mentioned above, such TiO_2 nanotubes obtained by the hydrothermal and template-assisted methods are usually in a powdery form. In a photocatalytic process, powdery TiO_2 nanotubes are suspended in a rigorously mixed solution. The reaction commences upon the irradiation of slurry by a UV with the appropriate wavelength. A potential problem arises when the concentration of TiO_2 powder is so high that the solution becomes turbid and the penetration of UV is impeded. As a result, only TiO_2 in the vicinity of a UV source can be activated. The rest of TiO_2 at a distance from the UV cannot be activated due to the lack of UV irradiation. This so-called "shadowing effect" has been observed in previous studies (Wei and Wan, 1991). The second limitation involves the separation of powdery TiO_2 nanotubes from the treated water. The TiO_2 powders are very difficult to remove because of their small size. Recently, some attempts have been made to effectively separate TiO_2 photocatalysts, as mentioned previously, by coagulation, membrane separation and magnetic separation. Coagulation technique may contribute to the industrial application in a titanium dioxide-suspended reactor for the treatment of wastewater. However, the TiO_2 particles recovered from the precipitates need several further treatment steps prior to reuse; moreover, this method has another problem related to the production of chemical sludge. Employment of membrane processes provides an opportunity to separate the catalyst from a treated solution and provide high quality water. However, when a catalyst in suspension is applied, the membrane fouling is often observed, especially in case of MF and UF membranes. Moreover, the quality of permeate is not very high, as small molecules can pass easily through the membranes used, even in case of NF. In addition, low membrane life time and high operating cost would limit the practical application of membranes in wastewater treatment. Titania-coated magnetic particles have been proposed as a means to enhance the separation of the catalyst from treated water by the application of an external magnetic field. However, there are two major difficulties in employing titania-coated magnetic materials as a photocatalyst: (1) low photoactivities arising from the low crystallinity of titania and (2) photodissolution of the iron oxide. In summary, these techniques developed recently can not well solve the separation issue of TiO_2 powder. Hence, this gives rise to the opportunity for developing the immobilized TiO_2 nanotube films in water purification.

2.5.3 Application of Anodic TiO_2 Nanotubes Films

As mentioned above, the TiO_2 nanotubes directly grown from titanium metal substrate have good mechanical adhesion strength and electronic conductivity. Anodization of titanium not only develops a novel approach to engineering titanium dioxide nanostructures but it also explores wider applications in solar energy conversion, water splitting, gas sensors and in particular environmental purification.

However, thus far there have been limited reports warranting attention based on the photocatalysis of anodic TNT film under UV or visible light irradiation.

Quan et al. (2005) first reported the environmental application of TNT film as a photoelectrode. Titanium oxide nanotubes successfully grew from a titanium plate by direct anodic oxidation with 0.2 wt% hydrofluoric acid in water being the supporting electrolyte. To investigate their potential for environmental application, degradation of pentachlorophenol in aqueous solution was carried out using photoelectrocatalytic (PEC) processes, comparing with electrochemical process (EP) and photocatalytic (PC). A significant photoelectrochemical synergetic effect was observed. The kinetic constant of PEC degradation of pentachlorophenol using TiO_2 nanotubes electrode was 86.5% higher than that using a traditional TiO_2 film electrode. Also, Xie (2006) studied the PEC process of an H_2O_2-assisted nanotubular TiO_2 electrode system by the degradation bisphenol A (BPA) in aqueous solutions. He claimed that H_2O_2 could act as a more powerful electron-trapper than an oxygen molecule. Both electrons captured by chemical H_2O_2 and electron transfer via external circuit can work together to promote electron–hole pair separation on TNT film, which ultimately contributes the hydroxyl radical generation as well as the photodegradation reaction of BPA, thus achieving a much better performance of

BPA degradation. In the two literature reports, the direct photolysis, photocatalysis and photoelectrocatalysis of TNT films were compared but the effect of nanotube structures, for example, crystallinity, pore size, tube length and wall thickness, on the photocatalytic activities, was ignored.

Further, Lai et al. (2006) investigated the effects of structure and morphology of the TNT arrays on their photocatalytic activities. The photocatalytic activities of the TNT arrays were evaluated by the removal of methylene blue in aqueous solution. It was observed that the crystal structure, morphologies and nanotube sizes were greatly influenced by anodization voltage and calcination temperature. The TNT arrays prepared at 20 V and calcined at 450 °C showed the highest photocatalytic activity due to an increase in the anatase crystal phase and an increase in surface area. Although in their research the crystallinity, tube length and inner diameter as affecting factors were investigated, the wall thickness of nanotubes, which is responsible for charge transfer and electron-hole separation, was ignored.

To utilize the visible light for TNT photocatalysis Lu et al. (2007) developed boron-doped TiO_2 nanotube arrays with visible activities by chemical vapor deposition treatment using trimethyl borate as the boron source with N_2 as the carrier gas. The photoelectrocatalytic activities of the prepared electrode were evaluated using pentachlorophenol as a test substance under UV and visible light irradiation. Under both UV and visible light irradiation (400–620 nm), the B-doped TiO_2 nanotube array electrode exhibited the higher photoconversion efficiency than the non-doped one. A notable photoconversion efficiency of 32% and 15% was achieved under high-pressure mercury lamp irradiation and under $\lambda > 290$ nm light irradiation, respectively. These ordered B-doped TiO_2 nanotube arrays are expected to be a good prospect in solar energy related and environmental purification related practical applications. However, they ignored the effect of exterior factors, such as solution pH, dissolved oxygen and anion on the photocatalytic capacity of TiO_2 nanotubes. It is known that the destruction rate of pollutants can be increased by adding dissolved oxygen to act as a sink for the electrons. Additionally, pH, the presence of anions and chemical species in the solution (acting as a scavenger) are factors affecting the decomposition of organic molecules and even their degradation pathways. Unfortunately, these factors have only been recognized recently and their effects on the photocatalytic activities of TiO_2 nanotube structures are not well understood.

In 2006, Zhang and co-workers reported experimental results on the removal of sodium dodecylbenzene sulfonate (SDBS), using silica/titania nanorods/nanotubes composite membrane with photocatalytic capability. This multifunctional composite membrane has been successfully prepared from colloidal *X*-silica/titania sols (*X* denotes molar percent of silica) by the sol–gel technique. They found that the small size titania particles with anatase phase played an important role in the formation of silica/titania nanorods/nanotubes composite membranes with photocatalytic capability. The percentage of anatase phase titania reached 93% when 20%-silica/titania nanorods/nanotubes composite membrane calcined at 400 ^{o}C for 2 h. Most (95%) of the pore volume was located in mesopores of diameters ranging from 1.4 to 10 nm. The removal of SDBS was achieved by 89% after 100 min by combining the photocatalysis with membrane filtration techniques. Although the SDBS was not completely decomposed by photocatalysis, the degradation of the SDBS helped to enhance composite membrane flux and prevent membrane fouling. It was possible to treat successfully surfactant wastewater using multifunctional silica/titania nanorods/nanotubes composite membrane by means of a continuous process. This could be interesting for industrial applications.

2.5.4 Application of TiO_2 Nanotubes Combined with Other Advanced Oxidation Technologies

Li and Liu (2005) reported an innovative E-H_2O_2/TiO_2 (E-H_2O_2 = electrogenerated hydrogen peroxide) photoelectrocatalytic (PEC) oxidation system for water and wastewater treatment. In their study, a TiO_2/Ti mesh electrode was applied in this photoreactor as the anode to conduct PEC oxidation, and a reticulated vitreous carbon (RVC) electrode was used as the cathode to electrogenerate hydrogen peroxide simultaneously. The TiO_2/Ti mesh electrode was prepared with a modified anodic oxidation process in a quadrielectrolyte (H_2SO_4-H_3PO_4-H_2O_2-HF) solution. However, the obtained TiO_2/Ti film looked like a porous honeycomb rather than a nanotube array. Photocatalytic oxidation (PC) and PEC oxidation of 2,4,6-trichlorophenol (TCP) in an aqueous solution were performed under various experimental conditions. Experimental results showed that the TiO_2/Ti electrode, anodized in the H_2SO_4-H_3PO_4-H_2O_2-HF solution, had higher photocatalytic activities than the TiO_2/Ti electrode anodized in the H_2SO_4 solution. Furthermore, the E-H_2O_2 on the RVC electrode can significantly enhance the PEC oxidation of TCP in aqueous solution. The rate of TCP degradation in such an E-H_2O_2-assisted TiO_2 PEC reaction was 5.0 times that of the TiO_2 PC reaction and 2.3 times that of the TiO_2 PEC reaction.

Pan et al. (2007) reported the COD removal of landfill leachate solution by using the system of O_3/UV/TiO_2 nanotubes where TiO_2 nanotubes were prepared by a hydrothemeral method. They found that the removal rate of COD by using O_3/UV/TiO_2 nanotubes in 60 min was 21% better than using O_3/UV/P25 (Degussa, Germany), and 33% better than using O_3/UV (Yingze Corp., China). In landfill leachate solution, the maximal adsorption of COD on 0.5 g TiO_2 nanotubes, contributing 10% of the total COD removal rate, was 1.34 times that of 0.5 g P25 at 293 K. The overall apparent rate constant of O_3/UV/TiO_2 nanotubes was 1.19 times higher that that of O_3/UV/P25 and 1.80 times higher than that of O_3/UV.

Recently, Zhang et al. (2008) investigated the degradation of azo dye, methyl orange in aqueous solution with sonophotoelectrocatalytic process, where the TiO_2 nanotubes were used as an electrode in photoelectrocatalytic (PEC), sonophotoelectrocatalytic (SPEC) processes or as a photocatalyst in photocatalytic (PC), sonophotocatalytic (SPC) processes. Experimental results showed that at the optimized experimental conditions, the rate constants of decolourization of dye were 0.0732 min^{-1} for SPEC process, 0.0523 min^{-1} for PEC process, 0.0073 min^{-1} for SPC process and 0.0035 min^{-1} for PC process, respectively. The rate constants indicated that there was a synergistic effect in the ultrasonic, electro-assisted and photocatalytic processes. Meanwhile, they evaluated the durability of TiO_2 nanotube electrode, which plays a key role in the practical application of such a SPEC degradation process.

In summary, the immobilized TiO_2 nanotube films used as photocatalysts for the removal of organic and inorganic contaminants in water is coming of age. The large surface area of the nanoporous film enables efficient light harvesting, which maximizes the amount of photogenerated charge. The ordered and interconnected nanoscale film architecture offers the potential for improved electron transport leading to higher photoefficiency (Mor et al., 2006b). A variety of TiO_2 nanotubes are in various stages of research and development, each possessing unique functionality, and the system of TiO_2 nanotubes combined with other advanced oxidation technologies is potentially applicable to the remediation of industrial effluents, groundwater, surface water and drinking water.

2.6 Summary

This chapter presents the pertinent literature in relation to the scope of this thesis. The review on the current preparation and modification of TiO_2 nanotubes inspires the author to develop an immobilized TiO_2 nanotube film as a photocatalyst in environmental purification. The fundamentals of the anodization process identify the stage at which highly-ordered TiO_2 nanotube arrays are formed, and the anodic TiO_2 nanotubes have recently become the focus of intensive research due to its large surface area, strong light absorption, good mechanical adhesion strength and high reactivity. However, the review on the current application of TiO_2 nanotubes shows that the environmental application of anodic TiO_2 nanotube films is still in its infancy and disregarded. Hence, further understanding of the effects of nanotube structure and other exterior factors (such as solution pH, dissolved oxygen and anion) on photocatalytic activities and even developing a visible-induced photocatalyst is necessary to increase the applications of anodic TiO_2 nanotube films in the environment. Some research works will be described in subsequent chapters to address these important issues.

Chapter 3 – Materials and Methodology

3.1 Introduction

One of the objectives in this study is to evaluate the effects of intrinsic and exterior factors on the photoefficiency of anodic TiO_2 nanotube films. Based on the literature review in Chapter 2, it is clear that length, thickness and morphology of anodic TiO_2 nanotubes are easily controlled by regulating the electrolyzing conditions, while the intrinsic photoefficiency of TiO_2 nanotubes affected by morphology and structures is not well understood. In view of this, it is interesting to optimize the TiO_2 nanotubes, thus maximizing the photocatalytic activities. This chapter introduces the preparation of catalysts (e.g. TiO_2 nanotubes and polymer-sensitized TiO_2 nanotubes) by electrochemical process and the characterization by field-emission scanning electron microscopy (FESEM), X-ray diffraction (XRD), X-ray photoelectron spectroscopy (XPS) and UV–visible spectrophotometer. The photocatalytic activities of prepared catalysts were evaluated by the degradation of a target compound (such as 2,3-dicholophenol or diphenamid) in aqueous solutions. Also in this chapter various analytical methods, for example, HPLC, LC-MS and ^{1}H-NMR, were employed to identify the degradation degree of target compounds and the corresponding intermediates produced in the photocatalytic processes.

3.2 Materials

All solvents and chemicals were used as received without further purification. Titanium foils (140 μm thickness, 99.6% purity) were purchased from Goodfellow Cambridge Ltd. Titanium butoxide ($Ti(BuO)_4$), acetic acid (AC), ethanol, ammonia, ammonium fluoride (NH_4F) and acetonitrile (ACN) were purchased from Aldrich Chemical Company. Monomer of thiophene (99.5%) was purchased from ACROS, and 3-methylthiophene (99%), 3-hexylthiophene (99%) and thiophenecarboxylic were purchased from Aldrich Chemical Company. Electrolyte of boron fluoride-ethyl ether (BFEE) was purchased from Aldrich Chemical Company. Other chemicals were obtained as analytical grade reagents. Deionized distilled water (DDW) was used throughout the experiments.

Target compounds of 2,3-dichlorophenol (99%), diphenamid (99.9%) and 2-chlororesorcinol (98%) were purchased from Aldrich Chemical Company. The molecular weights and structures of the target compounds are listed in Table 3-1.

Table 3-1. Molecular weights (MW) and structures of the target compounds.

Abbreviations	Compounds	MW (g mol^{-1})	Structures
2,3-DCP	2,3-dichlorophenol	163	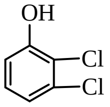
2-CR	2-chlororesorcinol	144.5	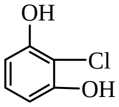
DPA	diphenamid	239	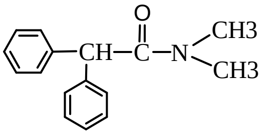

3.3 Preparation of Photocatalysts

3.3.1 Preparation of Anodic TiO_2 Nanotube Films

A large piece of raw titanium foil was cut into small rectangular pieces of 30 mm × 10 mm, which were ultrasonically cleaned in an acetone-ethanol solution and then washed with DDW prior to anodization. An anodic oxidation process was conducted in a dual-electrode reaction chamber, in which the cleaned Ti foil was used as the anode and a platinum foil (40 mm × 10 mm) was applied as the cathode. Two electrodes with a distance of 2 cm were submerged into an electrolyte solution containing 0.1 M NH_4F at pH 1.5 adjusted by H_2SO_4 and a DC electrophoresis power supply (EPS 600) was used to provide different electrical potentials between two electrodes during the anodic oxidation reaction. Here, the employment of NH_4F/H_2SO_4 was aimed to suppress the formation of HF for eliminating the etching rate of HF and thus leading to form a good tubular structure. All anodization experiments were conducted at room temperature (~20 °C) and the anodizing voltage of 25 V was kept constant for 1 h (unless otherwise mentioned). During anodization the color of the titanium oxide layer normally changed from purple to blue, and then finally gray. The resulting TiO_2 nanotubular array-films on Ti substrate were then rinsed by DDW and subsequently calcined in air at different temperatures of 300, 500 and 800 ^oC for 1 h, respectively.

3.3.2 Preparation of TiO_2 Thin Films

To compare the photocatalytic activities of TNT films, a TiO_2 thin film on Ti substrate was also prepared by a sol-gel method similar to that in the literature (Yu et al., 2001). Briefly, titanium butoxide (5 mL) and acetic acid (0.84 mL) were dissolved in ethanol (20 mL). After stirring vigorously for 1 h at room temperature, a mixed solution of water (0.26 mL) and ethanol (5 mL) was added dropwise to the above solution with a burette under stirring. The resultant alkoxide solution was kept standing at room temperature for hydrolysis reaction for 2 h, resulting in the TiO_2 sol. The chemical composition of the starting alkoxide solution was $Ti(OC_4H_9)_4$:

C_2H_5OH: AC: H_2O = 1:20:1:3 in molar ratio. Titanium foils (30 mm × 10 mm) were used as the substrates for thin films. The films were formed on the substrates from a coating solution by dipping-withdrawing in ambient atmosphere. The substrates coated with gel films were heat-treated at the same temperature for the same time in air. The withdrawal speed was 1 mm s^{-1} and the TiO_2 films were repeated the 5-times cycle from withdrawing to heat treatment based on reports by Yu et al. (2001) that the TiO_2 film obtained based on a repeat cycle of 5 times had perfect photocatalytic activities.

3.3.3 Preparation of Polymer-Sensitized TiO_2 Nanotube Films

An electrochemical polymerization process was employed to prepare the polythiophene-sensitized TNT composites in a one-compartment cell (see Figure 3-1), in which the TNT film calcined at 500 ^oC as the anode and a Pt sheet (40 mm × 10 mm) as the cathode (a counter electrode) were immersed in the BFEE electrolyte solution, while a saturated calomel electrode (SCE) was also used as the reference electrode. Three electrodes were connected with a potentiostat-galavanostat (ZF-9 ZhengFang Company, Shanghai). The working and counter electrodes were placed 1.0 cm apart. The electrolyte solution consisted of fresh BFEE and various amounts of thiophene as requested, where BFEE furnished the conducting medium (Eley, 1963). The electrolyte solution was deoxygenated by bubbling nitrogen gas before the electrochemical polymerization. The polythiophene layers were coated on the TNT films by the electrochemical polymerization process at 1.3 V (vs. SCE) potentiostatically for 1 min. This low potential avoids any degradation of the polymer and any side reactions between the electrolytes and electrodes due to the occurrence of overoxidation at 1.45–1.55 V (Chen and Xue, 2005). The thickness of polythiophene layers was controlled by the concentrations of thiophene monomers (1, 3 and 5 mM) in the BFEE electrolyte solution, corresponding to three composites named “PTh1/TNT”, “PTh3/TNT” and “PTh5/TNT”, respectively. All the resulting composite films were washed repeatedly with diethyl ether and DDW, and then dried at 80 ^{o}C under vacuum for 6 h before characterization.

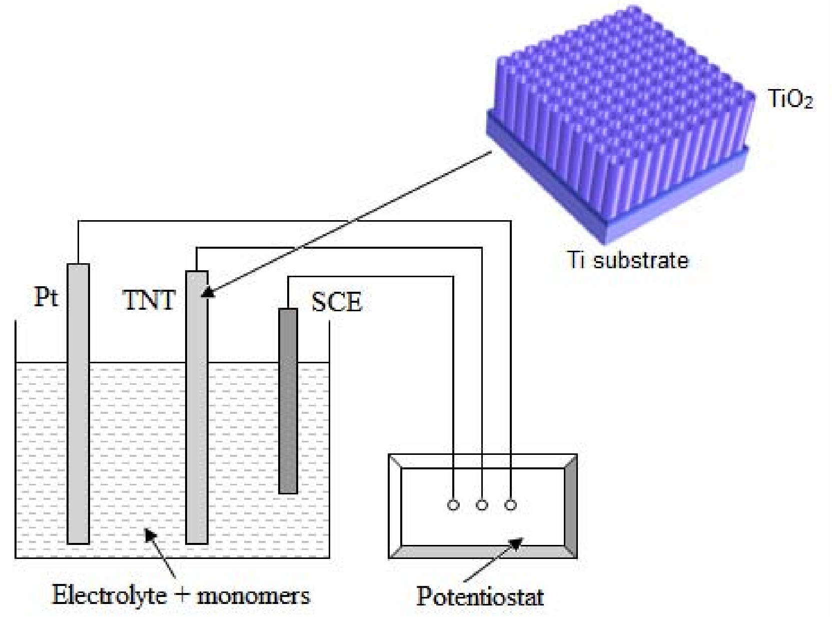

Figure 3-1. Schematic diagram of electrochemical reaction set-up.

For comparison, a pure polythiophene film was prepared by depositing polythiophene onto an optical ITO-glass electrode instead of on the TNT film by electrochemical polymerization in the BFEE electrolyte solution with a thiophene concentration of 5 mM at 1.3 V for 1 min and was named “PTh/ITO”.

To understand the influence of the side chains of polythiophene on the photocatalytic activities, substituted polythiophene derivatives, such as poly3-methylthiophene (P3Meth), poly3-hexylthiophene (P3Hexth) and poly3-thiophenecarboxylic acid (P3ThCA), were also synthesized by the potentiostatic electropolymerization method. It should be noted that unlike the former polymers, for P3ThCA the presence of carboxylic acid group in structure, an electron-withdrawing subunit, increases the potential of electrooxidative polymerization. Bargon et al. (1983) reported that for the electropolymerization of 3-thiophenecarboxylic acid (3ThCA), a high oxidation potential (2.28 V vs Ag/Ag^+) was necessary to obtain a conducting polymer. Hence, the potential of 2.3 V vs. SCE was applied in the case of 3ThCA electropolymerization, while other experimental conditions remained unchanged.

3.4 Characterization of Photocatalysts

3.4.1 Surface Morphology Analysis

Surface morphology of the resulting samples was observed by field-emission scanning electron microscopy (FESEM; JSM6300, Japan) with 3 kV and elemental analysis was performed by energy dispersive X-ray (EDX) spectroscopy. All of the samples were first dried in the vacuum oven at 80 ^{o}C and subsequently coated by a gold layer with 208HR high resolution sputter coater for FESEM and EDX applications.

3.4.2 X-Ray Diffraction Analysis

To determine the phase composition and crystal structure of the resulting samples, X-ray diffraction (XRD) measurement was carried out at room temperature using a Bruker D8 Discover XRD with diffracted beam graphite monochromator at 50 kV and 40 mA (Cu K_α with $\lambda = 1.54187$ Å). Data collection was carried out in a time step–scan mode with 0.03° per step in the angular range of 20–75° in 2θ at 1 s per step.

3.4.3 X-Ray Photoelectron Spectroscopy

Information on the chemical states of the samples was obtained from X-ray photoelectron spectroscopy (XPS, SKL-12), using a VG CLAM 4 multichannel hemispherical analyzer with ion-pumped sample analysis chamber. The residual pressure in the analysis chamber was maintained below 10^{-9} Torr during data acquisition. All the binding energies were referenced to the C 1s peak of the surface adventitious carbon. The X-ray photoelectron spectra were referenced to the C 1s peak at 284.6 eV resulting from the adventitious hydrocarbon (i.e. from the XPS instrument itself) present on the sample surface.

3.4.4 UV-Vis Spectrophotometer

UV–visible spectrophotometer (Perkin Elmer, Lambda 20) was used to directly record the diffuse reflectance spectra (DRS) of the resulting samples. Baseline correction was done using a calibrated sample of barium sulphate ($BaSO_4$). The spectra were recorded at room temperature in air, in the wavelength range of 250–800 nm.

3.4.5 Zeta Potential Measurement

To investigate the surface charges of photocatalysts in aqueous solution, zeta potential measurements were carried out using a Malvern Zetasizer 3000 (Malvern, UK). TiO_2 nanotubes were peeled off from TNT films to be TNT powder and then the obtained TNT powder was used to prepare its suspension of 0.1 g L^{-1} and dispersed ultrasonically for 2 h. Degussa P25 was also used to prepare its suspension with the same concentration for comparison. The 2 M HCl and 2 M NaOH solutions were used to adjust pH to the desired values. As a result, the isoelectric point of the catalysts was obtained by the measurement of the zeta-potential.

3.5 Equipment and Experimental Procedures

A schematic diagram of the batch-scale photoreaction set-up is shown in Figure 3-2. A UV-photochemical reaction system (Figure 3-2a) consisted of a quartz reactor with a magnetic stirrer, an 8-W medium pressure mercury lamp (Institute of Electrical Light Source, Beijing, China) as an external UV light source (unless mentioned otherwise), one piece of TNT film with 3 cm^2 of area as the photocatalyst and 25 mL of target compound aqueous solution (20 mg L^{-1}). The photoemission spectrum of the medium pressure mercury lamp is illustrated in Figure 3-3a, which mainly provides UV-Vis light in the range of 240–440 nm. A distance between the lamp and the top surface of solutions was 6 cm and the reactor received a light intensity of 5.96 W m^{-2}, which was determined using a UA-340 light meter (CE, Lutron, Taiwan).

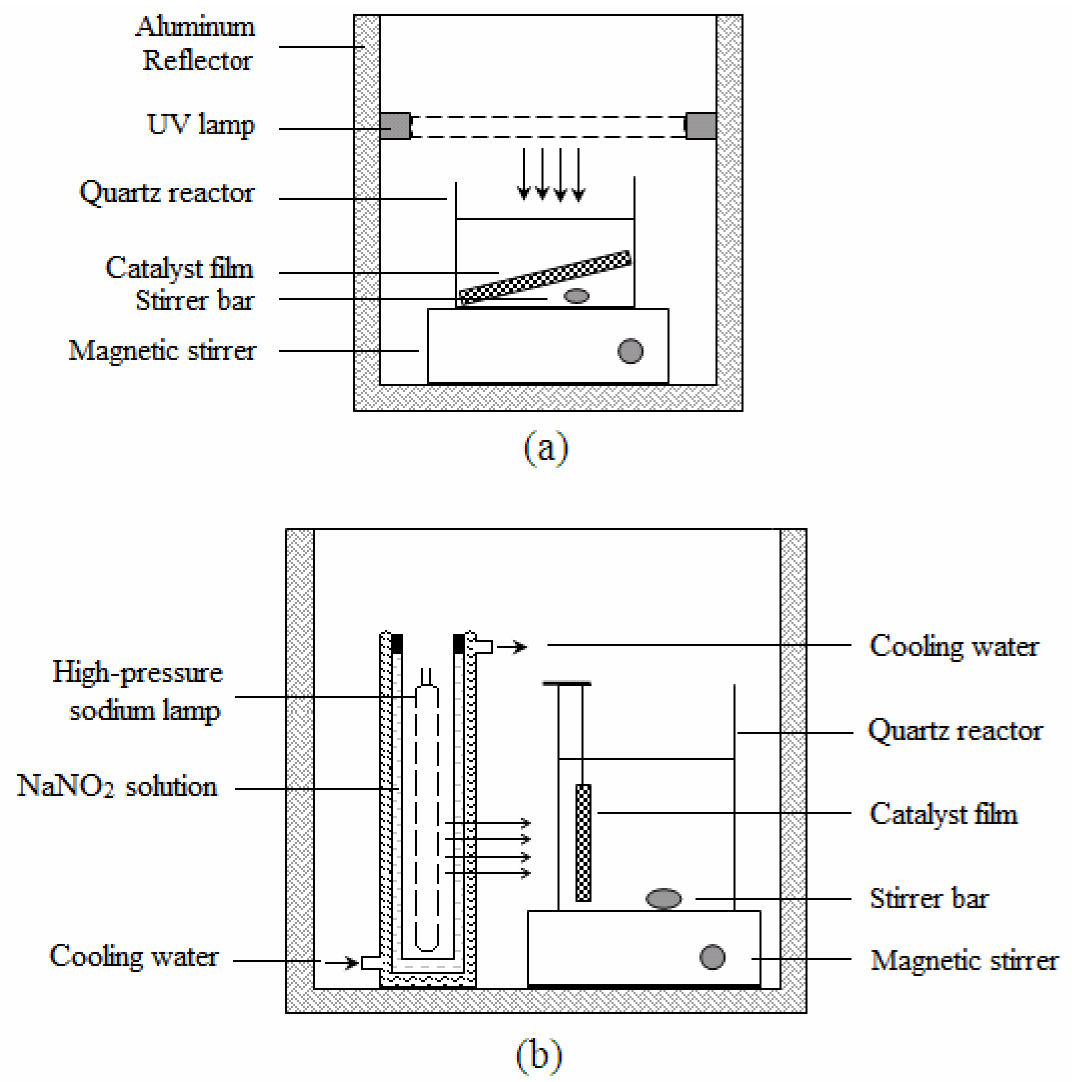

Figure 3-2. Schematic diagrams of the batch-scale photoreactors under UV light illumination (a) and visible light illumination (b).

A visible-photoreactor (Figure 3-2b) consisted of a quartz reactor with a magnetic stirrer, a 110-W high pressure sodium lamp (Institute of Electrical Light Source, Beijing, China), in which the lamp as an external visible light source was positioned inside the cylindrical Pyrex vessel surrounded by a circulating water jacket (Pyrex). The photoemission spectrum of the high pressure sodium lamp is illustrated in Figure 3-3b, which mainly provides visible light in the range of 400–800 nm, as we earlier reported (Li et al., 2001). To completely eliminate any UV radiation at a cutoff wavelength of 400 nm, a 1.0 M $NaNO_2$ aqueous solution as a UV cut-off filter was placed inside the Pyrex jacket. A distance between the lamp and the surface of solution was ~9 cm and the light intensity of the reaction system was 156.95 W m^{-2}. The resulting catalyst films with an area of 3 cm^2 were placed in 25 mL of aqueous 2,3-DCP solution with an initial concentration of 20 mg L^{-1}.

Prior to photoreaction, the aqueous mixture was magnetically stirred in the dark for 60 min to reach adsorption/desorption equilibrium. The reaction solution with stirring was then irradiated by the visible light. During the photoreaction, samples were collected at different time intervals for analysis.

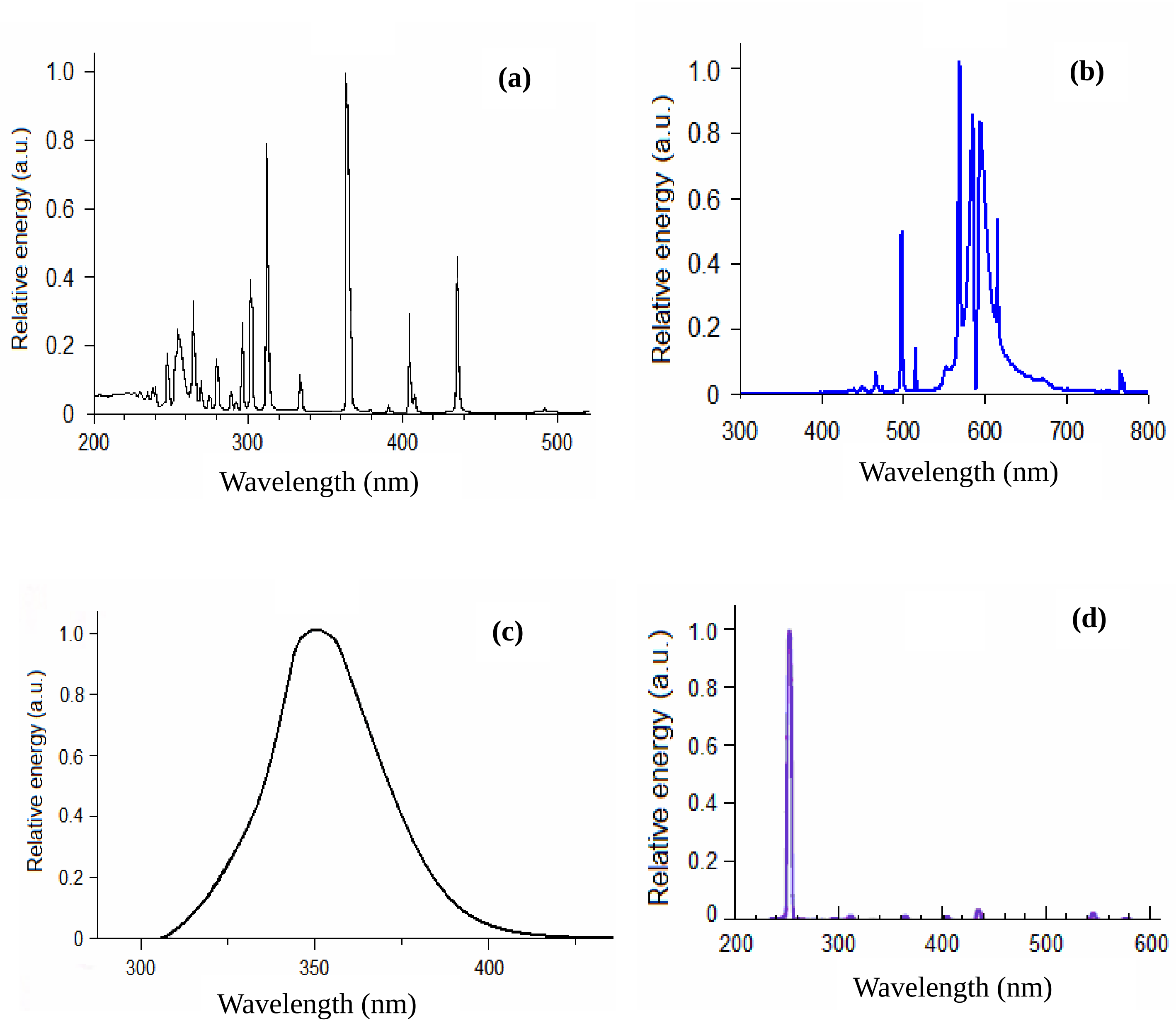

Figure 3-3. Photoemission spectra of the medium pressure mercury lamp (a), the high pressure sodium lamp (b), the black blue lamp (c) and the germicidal lamp (d).

3.6 Analytical Methods

3.6.1 HPLC

High performance liquid chromatography (HPLC) system is now widely used to analyze organic compounds because of some of its advantages such as high sensitivity, good reproducibility and ease of handling. Hence, in this study the concentrations of organic compounds (2,3-DCP or DPA) were measured by HPLC system (Finnigan SpectraSYSTEM P4000), as shown in Figure 3-4, consisting of a Pinnacle II C18 reverse-phase column (5 μm, 4.6 mm × 250 mm) and a UV detector (UV 6000LP). The mobile phase of acetonitrile/water (v:v = 3:2) was flowed at 1.0 mL min^{-1}. The wavelengths of the UV detector were set at 200 nm (for 2,3-DCP) and 218 nm (for DPA), respectively.

Figure 3-4. HPLC for the analysis of organic compounds.

3.6.2 LC/ESI-MS

During the mechanism study of DPA degradation, a Finnigan LCQ^{TM} DUO ion trap mass spectrometer (MS) coupled to the Finnigan SpectraSYSTEM$^{®}$ LC was used to verify the reaction intermediates through electrospray ionization (ESI) associated with a negative operational mode ($[M-H]^-$ ions). This LC system was composed of a solvent degasser, quaternary gradient pump, inert autosampler with a 20 μL injection loop and photodiode array UV detector. The eluent was partitioned by the Pinnacle II C18 column (5 μm, 4.6 mm × 250 mm). The mobile-phase gradient was programmed as follows: the elution was carried out with a gradient flow of 75% deionized distilled water including 5 mM ammonium acetate (DDW/AC) and 25% acetonitrile (ACN) for 3 min, followed by 55% DDW/AC and 45% ACN for 4 min, 10% DDW/AC and 90% ACN for 5 min, and finally 2% DDW/AC and 98% ACN for 3 min. The total running time was 15 min. The LC eluent was directed to the ESI detector for the detection of negative ions $[M-H]^-$ and positive ions $[M+H]^+$. The ESI probe was installed with sheath and auxiliary gasses at 60 and 20 units respectively. The MS conditions were as follows: the capillary temperature was set at 250 ^{o}C with a voltage of 46 V and a spray voltage of 4.5 kV. The mass spectrometer was operated in the negative ion mode in the m/z 50-500 range for LC-MS and LC-MS/MS.

3.6.3 ^{1}H-NMR Analysis

In order to unambiguously identify the intermediate products of 2,3-DCP and DPA degradation, ^{1}H-NMR analysis, a special feature of this study versus previous contributions (D'Oliveira et al., 1993), was employed. Since the sensitivity of the NMR detection is generally lower than that of HPLC, 2,3-DCP and DPA solutions with high initial concentrations of 300 and 130 mg L^{-1}, respectively, were used in the experiments and 1 mL of samples was taken in a NMR tube at different time intervals. For quantitative ^{1}H-NMR measurements, 50 μL of deuterated water (D_2O) containing a required internal standard of tetramethylsilane (TMS, δ 0.00 ppm) was added into the above NMR tubes before analysis. All one-dimensional (1D) and two-dimensional (2D) ^{1}H-NMR spectra were recorded at ambient temperature using a NMR spectrometer (Bruker Avance 600 MHz) equipped with a TCI cryoprobe, as shown in Figure 3-5. The strong water signals were suppressed using excitation sculpting with gradients. For 2D correlation spectroscopy (COSY), 64 scans with 2048 data points were acquired for each of the 512 increments and acquisition time was 12 h. To minimize missing out the intermediates of low concentrations during the NMR analysis, organic extraction was employed using chloroform (HPLC grade) for the water samples after completed reaction. The extraction solution was evaporated to dry completely using a vacuum pump at 20 °C and the resulting samples were dissolved in 0.5 mL $CDCl_3$ containing an internal referencing TMS standard for NMR analysis.

Figure 3-5. ^{1}H-NMR for the analysis of organic compounds.

3.6.4 DOC Analysis and Chloride Ion Measurement

The concentration of dissolved organic carbon (DOC) in solutions was determined by a total organic carbon analyzer (Shimadzu TOC-5000A) equipped with an auto-sampler (ASI-5000). O_2 as a carrier gas was used in the detecting system. Carbon can exist in two forms in the solution: inorganic and organic. Inorganic carbon is a pH-dependent parameter that exists in water as CO_3^{2-} or HCO_3^-, or in an acidic solution as dissolved CO_2. Organic carbon is theoretically defined to be carbon that exists as products of nature, altered or partially decomposed products of nature, or man-made products. In this study, dissolved organic carbon = total carbon (TC) – inorganic carbon (IC). TC was measured by injecting the obtained samples into a heated reaction chamber packed with an oxidative catalyst. The water would be vaporized and the organic carbon would be oxidized to CO_2 and H_2O. The CO_2 was transported in the carrier-gas streams and was measured by means of a nondispersive infrared analyzer. IC was measured by injecting the samples into a separated reaction chamber with phosphoric acid. Under the acidic condition, all inorganic carbon was converted to CO_2 and measured. On the other hand, a series of standard solutions in the range of 10-100 mg L^{-1} for TC and 1-10 mg L^{-1} for IC were prepared for calibration before the analysis of samples.

On the other hand, a UV-Vis spectrophotometer (Spectronic Genesys 2) was also used to further determine the chloride ions released from the 2,3-DCP degradation after the reaction with mercury thiocyanate (Janda et al., 2004). Briefly, 1.0 mL of the prepared sample as well as the deionized distilled water (sample blank) was filled in the sample cell. 1.0 mL of ammonium ferric sulfate solution (60 g L^{-1}) and

0.5 mL of mercuric thiocyanate ethanol solution (4 g L^{-1}) were also added into the above cell. Finally, the sample cells left for 2 min were inserted and measured at 460 nm by the UV-Vis spectrophotometer with WinSpec software.

3.7 Quality Assurance and Quality Control (QA/QC)

QA/QC of the analytical methods used to obtained data is important to ensure the accuracy and precision of experimental data.

HPLC analysis for determining the concentrations of 2,3-DCP and DPA

A 5-point calibration curve was established by injecting an appropriate amount (20 μL) of standard solutions with different concentrations at 5, 10, 15, 20 and 40 mg L^{-1} into the HPLC system. The calibration curve was prepared by plotting the peak areas against the corresponding concentrations of the standard solutions. Consequently, the slope, y-intercept, and the R^2 value from the calibration curve were obtained, where $R^2 > 0.999$ was used as a suitable criterion in our experiments. With the calibration curve, the concentrations (in mg L^{-1}) of 2,3-DCP and DPA in the test solution were calculated with a relative error of < 5%.

Chloride analysis

Duplicate analysis was performed on chloride measurement and the relative errors between the results of each analysis were found to be within 7% and the detection limit of the UV-Vis spectroscopy method was 0.03 mg L^{-1}.

TOC analysis

Before every TOC test, a blank and potassium hydrogen phthalate standard solution were used to establish working curves between 0 and 100 mg L^{-1}. Calibration curves were analyzed by Microsoft Excel software using R^2-correlation coefficients. The minimum acceptable correlation coefficient was 0.9991 and the detection limit of the method was 0.05 mg L^{-1}.

Chapter 4 – Characterization and Photocatalytic Activities of TiO_2 Nanotube Films

4.1 Introduction

TiO_2 nanotubes as photocatalysts have begun to be gain significant attention related to environmental applications (Quan et al., 2005; Dechakiatkrai et al., 2007). To date, however, there are only limited reports about the effect of their structures on photocatalytic behaviour. Although Lai et al. (2006) investigated the effect of crystallinity and length of TiO_2 nanotubes on the photodegradation of methylene blue in aqueous solution, they ignored the effect of tube wall thickness on the photocatalytic ability, which might play a key role on the charge transfer and the separation of electron-hole pairs. Calcination temperature is another key parameter to determine the overall photocatalytic activities of TiO_2 catalysts. Although many reports published within recent years involved the effects of calcination temperature on the photocatalytic activities of TiO_2 nanotubes, the results were not in agreement between each other. For example, Zhu et al. (2004) found that the as-prepared titanates nanotubes without calcination exhibited decent photocatalytic activities for the photocatalytic oxidation of sulforhodamine but Yu et al. (2006) claimed that no photoactivities of TiO_2 nanotubes obtained by hydrothermal technique was observed when the calcination temperature was below 300 °C. Therefore, it is necessary to further investigate the influence of calcination temperature on the photoactivities of the anodic TiO_2 nanotubes.

This chapter describes the detailed study on the photoactivities of TiO_2 nanotube films as a function of structure factors including pore size, tube length, tube wall thickness and crystallinity, in which 2,3-dicholophenol (2,3-DCP) was used as a model chemical and its degradation with different TiO_2 nanotube films under UV illumination was investigated in aqueous solution. From the results of this study, the photocatalytic activities of TNT films with structural specificity and functional novelty can be better understood.

4.2 Characterization of TNT Films

4.2.1 FESEM of TNT Films

The formation of TiO_2 nanotube arrays on the surface of titanium depends on both reactions of electrochemical etching and chemical dissolution. Since the interaction between two reactions could significantly affect the morphology and structure of TNT films, it would be a key factor to influence the photocatalytic activities of catalysts. In this study aqueous 0.1 M NH_4F solution was used as an electrolyte to prepare seven TNT film samples (S1-S7) under various anodization conditions as summarized in Table 4-1.

Table 4-1. Anodization conditions and the size of TiO_2 nanotubes.

Sample ID	V^a (v)	t^b (h)	T^c (^oC)	WT^d (nm)	L^e (μm)
S1	10	1	23	–	–
S2	15	1	23	40 ± 5	0.29 ± 0.05
S3	18	1	23	30 ± 5	0.32 ± 0.05
S4	25	0.3	23	35 ± 5	0.20 ± 0.03
S5	25	1	23	28 ± 5	0.31 ± 0.03
S6	25	10	23	33 ± 5	2.38 ± 0.05
S7	25	1	5	50 ± 5	0.32 ± 0.04

[a] Applied voltage
[b] Reaction time
[c] Reaction temperature
[d] Wall thickness of nanotubes
[e] Length of nanotubes

A TiO_2 thin film on Ti substrate was also prepared by the sol–gel method for comparison. These as-prepared samples were then calcined at 500 °C for 1 h. The calcined final samples were first examined by FESEM and their images are shown in Figure 4-1. It can be seen that the TiO_2 film had a nonporous structure and its thickness is about 1 μm. The SEM images of TNT films showed that the S1 anodized at a low voltage of 10 V for 1 h had only a few pits; the S2 at 15 V showed a partial porous structure; and the S3 at 18 V and S5 at 25 V had complete porous structures with well-aligned nanotube arrays. These results indicated that the formation of the well-aligned TNT arrays at a voltage below 18 V was difficult due to weak electrochemical etching reaction and that 25 V would be a sufficient electrical potential to adequately develop the TNT arrays on the Ti surface.

To study the effect of anodizing time on the structure of the nanotubes, three experiments were conducted at 25 V for different times of 0.3, 1 and 10 h. It was found that the length of TiO_2 nanotubes was significantly increased with the increased anodizing time: 0.20 μm for 0.3 h, 0.31 μm for 1 h and 2.38 μm for 10 h, respectively. These results indicated that the tube length was significantly affected by anodizing time.

Mor et al. (2005a) reported that the thickness of the anodic nanotube walls can be controlled via anodization bath temperature. To obtain the TiO_2 nanotubes with different wall thickness to compare their photocatalytic activities, the TNT film of S7 was anodized at a lower temperature of 5 ^{o}C while other TNT films were anodized at 23 ^{o}C.

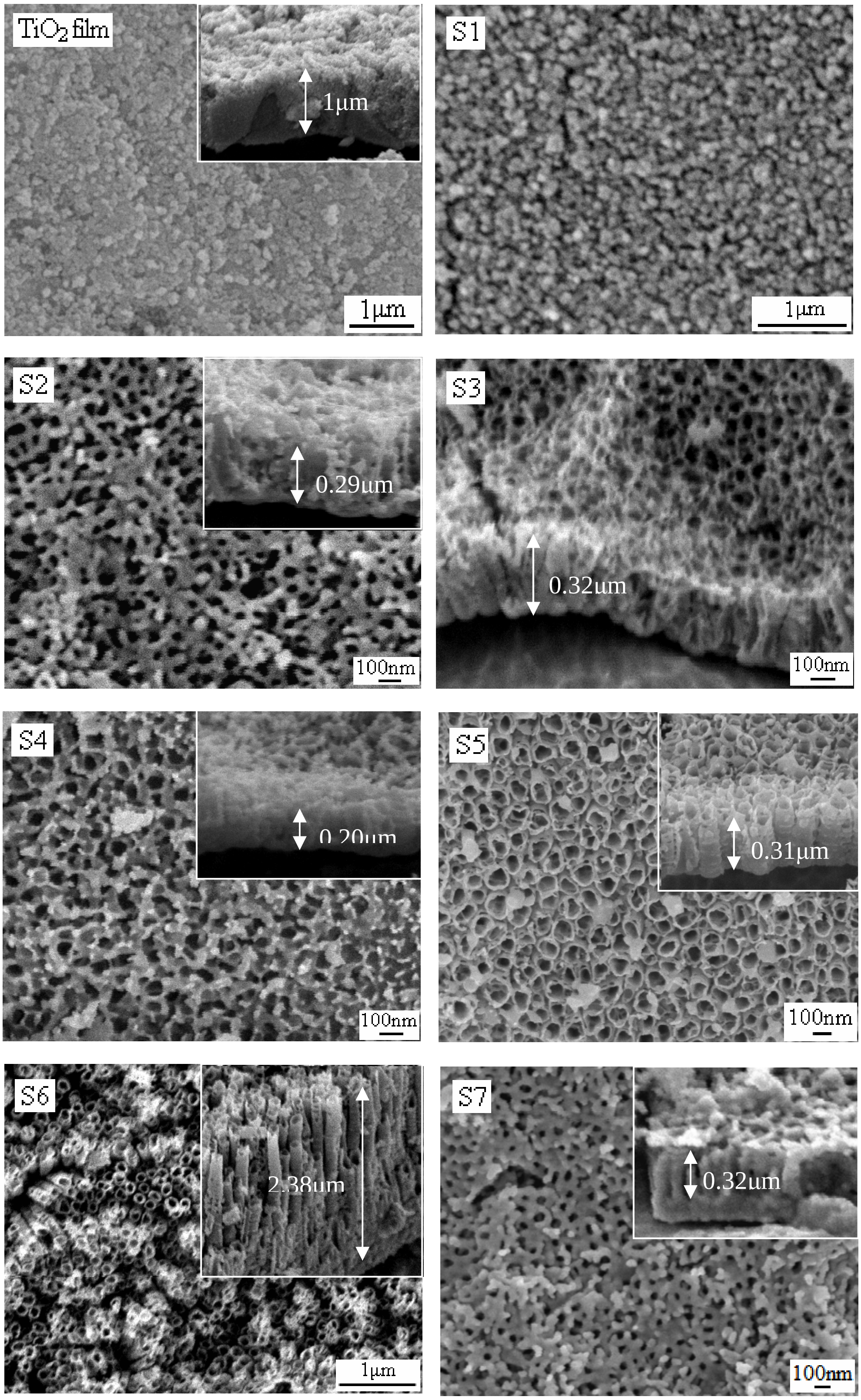

Figure 4-1. FESEM images of samples calcined at 500 ^{o}C for 1 h.

It was found that S7 had a highly disturbed porous structure with similar nanotube length but a thicker wall of ~50 nm compared to S5 (28 nm). The increased thickness of nanotube walls should be a consequence of using the lower anodization temperature. Although the formation of TiO_2 nanotubes is a result of the competition between the electrochemical etching of Ti and the chemical dissolution of TiO_2 occurring in the electrolyte solution during anodization process (Mor et al., 2006a), the chemical dissolution would be a limiting factor for the growth of nanotube length and wall, depending on the solution temperature. It is therefore believed that at low temperature the rate of the oxide dissolution reaction was slower than that of Ti etching, thus resulting in the formation of thicker nanotube walls.

4.2.2 XRD and XPS of TNT Films

One XRD pattern of Ti foil and four XRD patterns of S5 annealed at different temperatures from 300 to 800 °C are shown in Figure 4-2. It can be seen that the nanotubes without calcination (pattern 2) maintained an amorphous structure, which means that the low-voltage anodization only formed amorphous TiO_2 nanotubes but did not lead to TiO_2 crystallization. The patterns 3-5 show the crystallization calcined at 300, 500 and 800 °C, respectively, in which amorphous regions were gradually crystallized to form anatase/rutile phases.

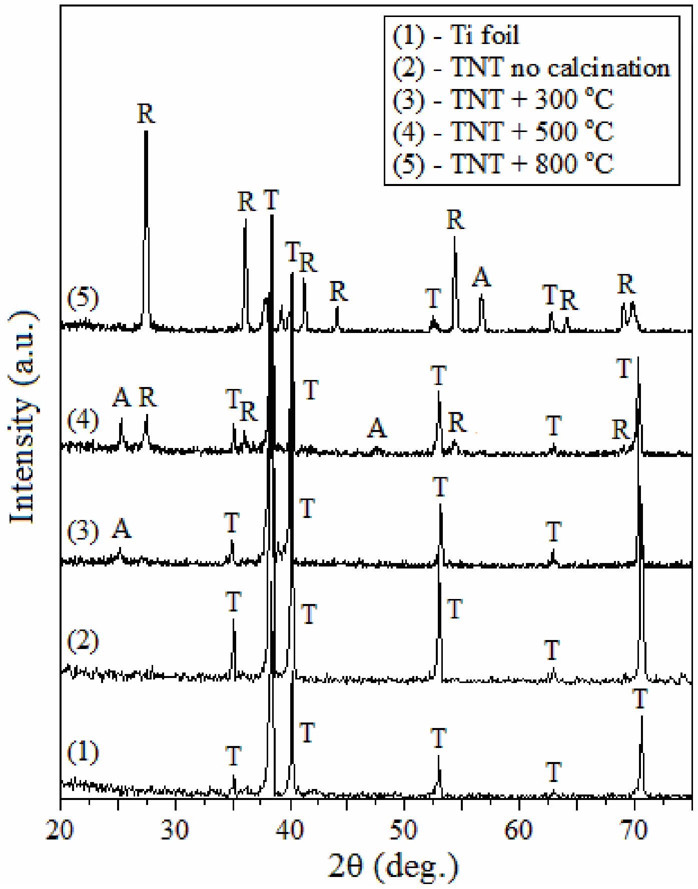

Figure 4-2. XRD patterns of fresh Ti foil and S5 calcined at different temperatures: A, anatase; R, rutile; T, titanium.

Further observation shows that the relative intensities of anatase and rutile diffraction peaks in each product are different for the new TiO_2 layer obtained at different calcination temperatures. It can be seen that at 300 °C (pattern 3), there was only a small diffraction peak of anatase at 25.35^o (101) but no rutile diffraction peaks occurred. This result reflects that the phase transformation to anatase or rutile was not fully achieved at 300 °C and still contained some inactive amorphous phase. While calcined at 500 °C, the sample (pattern 4) possessed characteristic peaks at

25.35^{o} (101), 27.5^{o} (110), 36.1^{o} (101), 48.1^{o} (200), 54.3^{o} (211) and 69.8^{o} (220), respectively. According to the XRD indexation, the crystal form of TNT is a mixture of rutile and anatase phases in good agreement with previous reports (Uchikoshi et al., 2004; Eder et al., 2006). According to the equation $f\mathrm{r} = 1.26I\mathrm{r}/(I\mathrm{a} + 1.26I\mathrm{r})$ (Wu et al., 2005), the mass fraction of rutile ($f\mathrm{r}$) in this sample was calculated by measuring the intensity of the strongest (110) and (101) diffraction peaks of rutile ($I\mathrm{r}$) and anatase ($I\mathrm{a}$), respectively to be ca. 52%. At 800 °C (pattern 5), the diffraction peak of anatase (101) disappeared completely and the rutile peak (110) became very strong. It is reasonable to infer from these results that the anatase phase was transformed into the rutile phase during heat-treatment at high temperature. Furthermore, the critical nanotube disintegration after calcination at 800 °C can be observed in the SEM image of Figure 4-3.

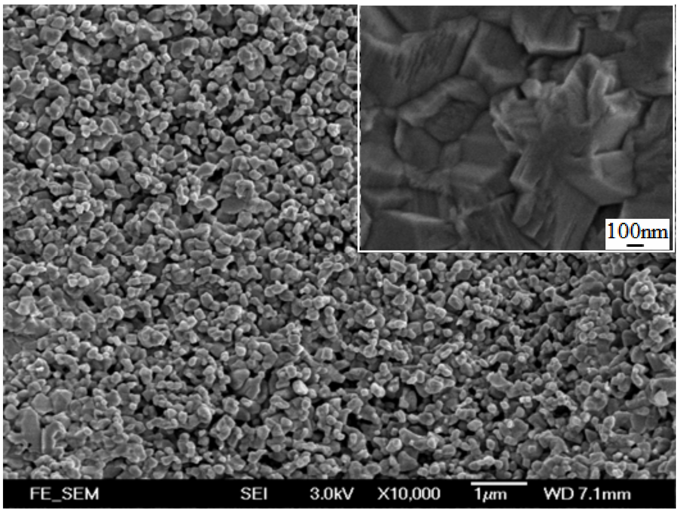

Figure 4-3. FESEM images of S5 calcined at 800 ^{o}C.

It is worth mentioning that Varghese et al. (2003) observed a similar morphology as that the nanotube structure completely collapsed at 880 °C leaving dense rutile crystallites.

To study the surface composition and chemical states of the obtained nanotubes, the S5 was also analyzed by XPS and its XPS spectra are shown in Figure 4-4. The individual peaks of O 1s at 529.5 eV, and Ti 2p at 458.2 and 463.9 eV can be clearly seen in the high-resolution spectra, which mean that the chemical state of the sample is Ti^{4+} bonded with oxygen (Ti^{4+}–O). Meanwhile, the spectra show a trace amount of carbon (C 1s), which should be ascribed to the adventitious hydrocarbon from the XPS sample preparation. In our experiment no evidence of other trace elements from electrolyte solution such as nitrogen (N), fluorine (F) or sulfur (S) was obtained. This confirmed that the elements of N, F and S were not incorporated into the TiO_2 crystal lattice during the anodization even though these elements were constrained in the electrolyte solution as NH_4F and H_2SO_4. Furthermore, the XRD spectra of TNT samples also give no indication of any TiO_xF_y, TiO_xN_y or TiO_xS_y existing in the samples, which confirms that the electrolyte elements did not enter either rutile or anatase lattice in such a low-voltage anodization process.

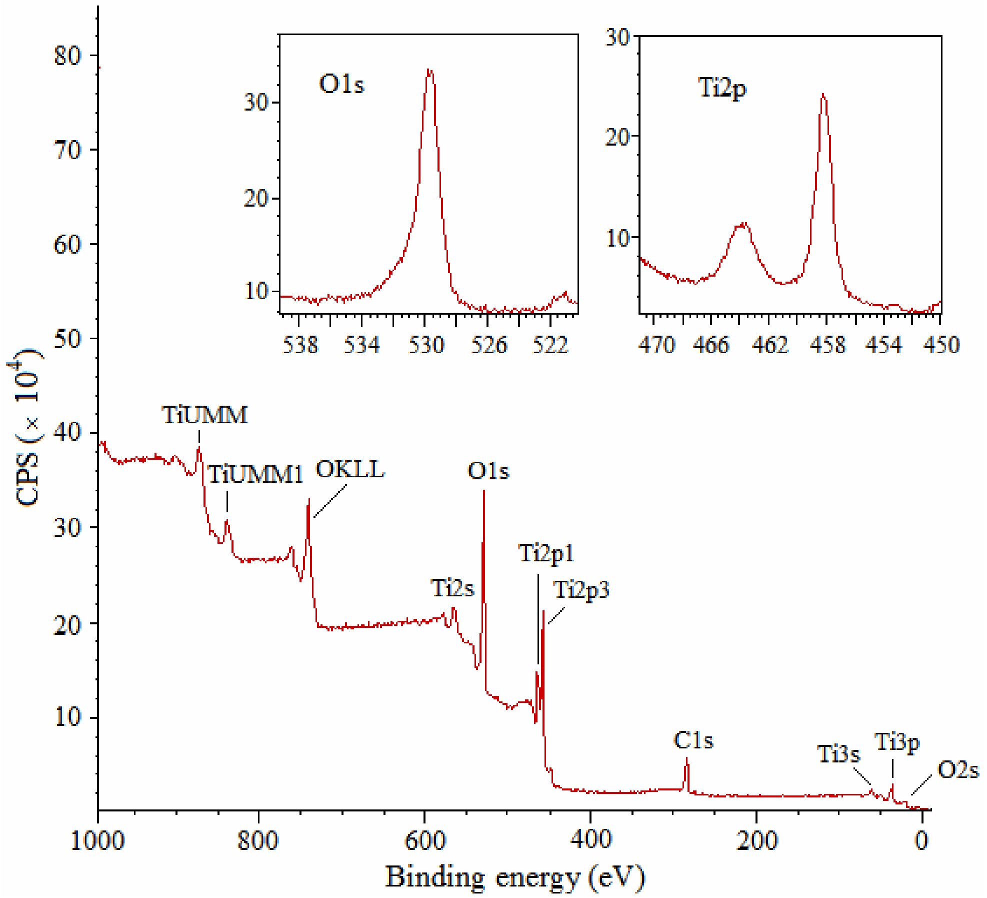

Figure 4-4. XPS spectra of S5 calcined at 500 °C in air for 1 h.

4.3 Effects of TNT Structure on the Photocatalytic Activities

4.3.1 Effect of Surface Structure

The photocatalytic activities of the anodized TNT films with different surface structures (S1, S2 and S5) were evaluated in the photodegradation of 2,3-DCP in aqueous solution under UV light irradiation; and the TiO$_2$ film with the same area of 3 cm^2 was also prepared and heated at the same temperature, 500 °C, for comparison, as shown in Figure 4-5. The semi-log graphs of the 2,3-DCP degradation with different TNT films versus irradiation time yield straight lines, indicating the pseudo-first-order reaction kinetics. The reaction rate constants (k) were evaluated from the experimental data using the linear regression. In all cases R^2 (correlation coefficient) values are higher than 0.96, which indicate that the exponential model can describe well the kinetics for degradation of 2,3-DCP in this process.

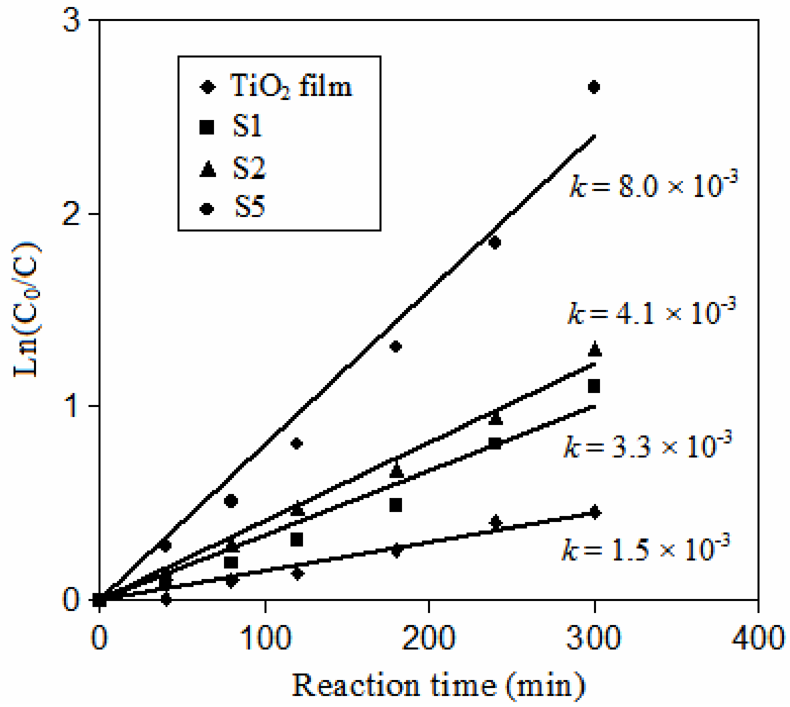

Figure 4-5. Effect of surface structures of anodized TNT films on the photocatalytic degradation of 2,3-DCP under UV light irradiation (C_0 = 20 mg L^{-1}).

It can be clearly observed from Figure 4-5 that the TiO_2 film showed the lowest photocatalytic activities with a corresponding k value of 1.5×10^{-3} min^{-1}. However, the TNT films (S1, S2 and S5) demonstrated the higher photocatalytic activities when compared to TiO_2 film. Among them, S5 showed the highest photoactivities with a corresponding k value of 8.0×10^{-3} min^{-1}, while S2 had $k = 4.1 \times 10^{-3}$ min^{-1} and S1 had $k = 3.3 \times 10^{-3}$ min^{-1}. This enhancement of photoactivities can be attributed to the difference of surface structures between the ordinary TiO_2 film and anodic TNT films. The TiO_2 thin film had a nonporous and tight solid structure with low specific surface area and poor charge mobility (see Figure 4-1), thus resulting in the low activities. In contrast, larger specific surface area of anodic TNT films allow more aqueous reactants to be adsorbed onto the outer and also inner surfaces of the photocatalysts, while the higher pore volume can favour a fast diffusion of various aqueous species during the photocatalytic reaction. All these factors contributed to the enhancement of photocatalytic activities. However, it should be noted that the factors resulting in the high photoactivities were strongly dependent upon the pore size and nanotubular structure of TNT films. As shown in Figure 4-1, S1 had only a few pits and was not a porous structure, S2 showed a partial porous structure and S5 had a complete porous structure with well-aligned nanotube arrays. These hollow and well-aligned nanotube arrays can produce a higher special surface area and favour the charge mobility, thus achieving the higher photoactivities. If it is believed that the degree of perfect tube-like structure benefits to form the large surface area and high pore volume, the well-aligned nanotubular structure of S5 is positively favourable to the highest photocatalytic activities when compared to other anodic samples.

4.3.2 Effect of Tube Length

To evaluate the effect of TiO_2 nanotube length on its photocatalytic activities, the degradation of aqueous 2,3-DCP solution in the presence of TNT samples (S3, S5 and S6) was carried out under UV light irradiation, respectively. These TNT films had similar nanotube wall thickness but different nanotube lengths (~0.31 μm for S3 and S5, and ~2.38 μm for S6). Also, the calcined TiO_2 film was used for comparison, as shown in Figure 4-6. As mentioned above, the TiO_2 film showed the lowest photocatalytic activities due to its nonporous solid structure and low specific surface area, while S3, S5 and S6 demonstrated the higher photocatalytic activities. This can be attributed to the combination of several factors including the large surface area, hollow interior wall and porous structures. Considering the similar nanotubular structure and approximate wall thickness of three samples (S3, S5 and S6), the surface area of these TNT films depends on the tube length and should play an important role in enhancing the photocatalytic activities of TNT films.

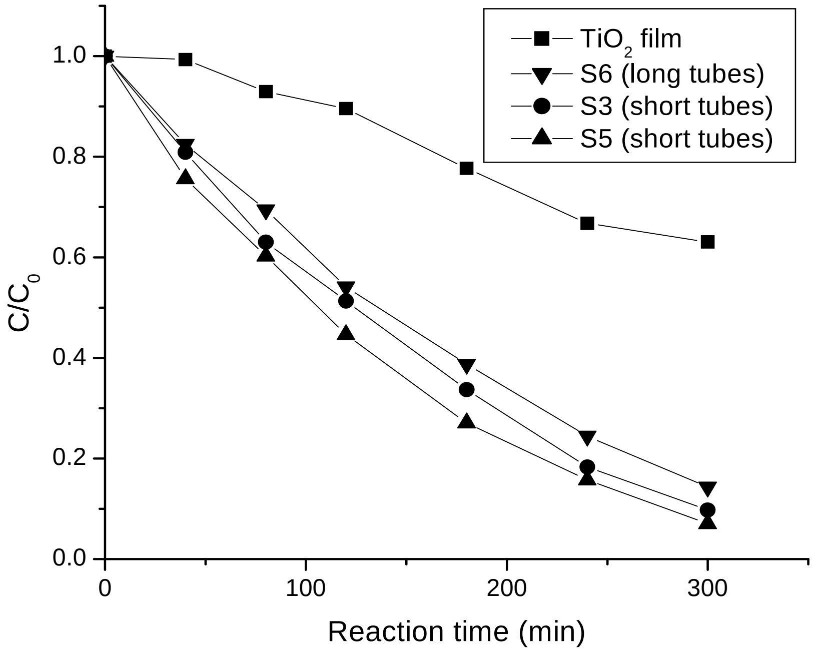

Figure 4-6. Effect of TiO_2 nanotube length on the photocatalytic degradation of 2,3-DCP under UV light irradiation (C_0 = 20 mg L^{-1}).

It can be noted that S3 and S5 with a similar nanotube length of ~0.31 μm exhibited a similar degree of 2,3-DCP degradation (90% and 93%, respectively), which were higher than that (81.2%) of S6 with the longer nanotubes of 2.38 μm. The fact that the photoactivities declined with the longer nanotubes may be attributed to the limited depth of incident photon penetration through the nanotubes and the diffusion of reactant inside nanotubes (Zhuang et al., 2007). It is generally believed that both the absorption of the incident photons and adsorption of 2,3-DCP by the TNT films should increase with the increasing of tube length, which are beneficial to achieving a greater photocatalytic degradation rate. However, the light intensity usually attenuates as it penetrates the solid photocatalyst film. If the length of nanotubes is longer than the effective depth of light penetration, the lower part of nanotubes has difficulty to absorb UV light well. This means that the amount of absorbed incident photons by the TNT films will not further increase when the tube length exceeds a certain range. In fact, the existence of the optimal thickness of TiO_2 films for degrading organic pollutants in water (Chang et al., 2000) also demonstrated the limitation of the UV light penetration. In this study, the length of nanotubes corresponds to the thickness of films mentioned in previous literature (Chen et al., 2006; Hui et al., 2007). On the other hand, the diffusion of species controlling reactions takes place not only on the outer surface of TiO_2 nanotubes but also on the inner walls due to the capillarity structure. Under a stirring condition, the external diffusion may be improved, but the internal diffusion within the nanotubes is hardly affected. Hence, the longer nanotubes have a slower internal diffusion for reactants, which is detrimental to the reaction rate.

4.3.3 Effect of Tube Wall Thickness

It is known that the large surface area of nanoporous film can enhance the adsorption of pollutants in aqueous solution and also enable light harvesting with a higher amount of photogenerated charge. Electron transport from the interband states or excitants to the surface is a limiting factor in the performance of these porous nanocrystallines, and the trapping of electrons to the surface is extremely dependent on the crystal size (Chen et al., 1997). It is therefore worthwhile to investigate the effect of wall thickness of TiO_2 nanotubes on the photocatalytic activities. However, the reported data related to the effect of nanotube wall thickness on the photocatalytic activities are quite limited.

Figure 4-7 compared the efficiency of 2,3-DCP degradation with three TNT films (S3, S5 and S7), which had the similar nanotube length of ~0.31 μm but different nanotube wall thickness. In this set of experiments, S3 and S5 have a close wall thickness of ~30 nm (see Table 4-1) while S7 has a larger thickness of ~50 nm. Due to their well-aligned tube-like structures, S3, S5 and S7 showed higher activities when compared with the TiO_2 thin film. Among them S5 achieved the highest 2,3-DCP removal of up to 93% after 300 min under UV illumination, which is about 2.6 times that by the TiO_2 thin film. However, S7 achieved the degradation of 2,3-DCP by 78.5% only during the same period. The results showed that the TNT films with the thinner nanotube wall achieved the higher removal of 2,3-DCP after 300 min of UV illumination in an order of S5 > S3 > S7. It may be understood that when a TiO_2 semiconductor is irradiated, electrons and holes are generated but always recombine immediately. If the electrons and holes created do not recombine rapidly, they need to either be trapped in metastable states or migrate to the semiconductor surface separately. As the thickness becomes smaller, the surface states increase rapidly, thus reducing the nonradiative surface recombination (Bhargava et al., 1994). In other words, the thinner wall makes it easier for the excited electrons to migrate from bulk to surface and provides more accessible carriers trapped on catalyst surface for the photocatalysis, thus enhancing the photocatalytic efficiency. When comparing the affecting factors of nanotube wall thickness and length, it appears that the wall thickness is a more important parameter influencing the overall photocatalytic efficiency of the 2,3-DCP decomposition reaction than the tube length.

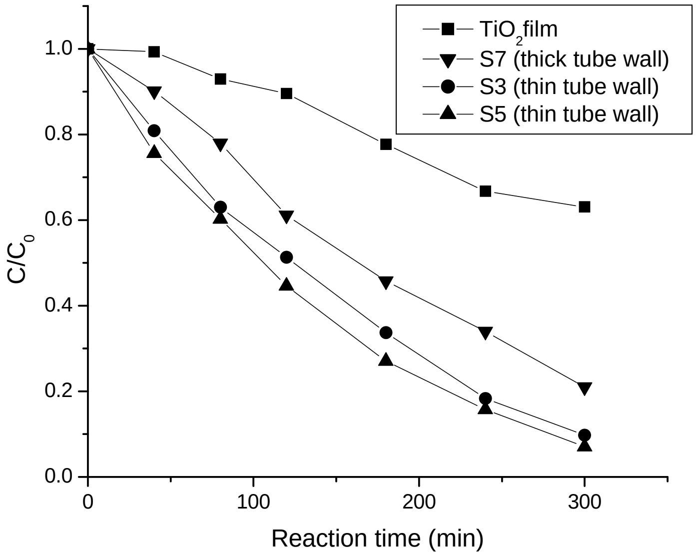

Figure 4-7. Effect of TiO_2 nanotube wall thickness on the photocatalytic degradation of 2,3-DCP under UV light irradiation (C_0 = 20 mg L^{-1}).

4.3.4 Effect of Calcination Temperature

The photocatalytic activities of the TiO_2 nanotubes after calcination at different temperatures were evaluated in terms of 2,3-DCP photodegradation in aqueous solutions. Figure 4-8 shows that the 2,3-DCP decay rate is strongly dependent on the calcination temperatures. It can be seen that the TNT film without calcination had very poor photocatalytic activities due to the amorphous structure. When calcined at 300 ^{o}C, however, the TNT film showed a certain degree of photocatalytic activities with a kinetic rate constant (k) of ca. 2.5×10^{-3} min^{-1}, which resulted from a low degree of crystallization of anatase phase (Chen et al., 2007). This result is different from the report by Yu et al. (2006), in which they found that the titanate nanotubes formed by a hydrothermal method, below the calcination temperature of 300 ^{o}C, showed no photocatalytic activities for the photooxidation of acetone in air. This difference in photocatalytic activities may be attributed to the different experimental conditions and the different crystal structure prepared by different methods. In the present study, the TNT film calcined at 500 ^{o}C achieved the highest degree of 2,3-DCP degradation with an apparent kinetic rate constant (k) of ca. 8.9×10^{-3} min^{-1}. These superior activities of the sample may be ascribed not only to their large specific surface area and high pore volume, but also the optimum crystallinity of anatase/rutile phase developed at this temperature. With further increasing of the calcination temperature to 800 °C, the photocatalytic activities of the TNT decreased significantly with a much lower *k* value of ca. 1.9 × 10^{-3} min^{-1} only. The decline of the photocatalytic activities for the TNT film calcined at the higher temperatures could be explained by the loss of anatase phase (see the XRD pattern in Figure 4-2) together with severe nanotube disintegration (see the SEM images in Figure 4-3). It is worth noting that when Qamar et al. (2008) investigated the influence of calcination temperature (from 300 to 900 °C) on the photocatalytic activities of titanate nanotubes, they also found that the as-prepared nanotubes calcined at 400-500 °C showed the best activities for the degradation of the dye followed by a decrease at higher temperatures, which is in good agreement with our result.

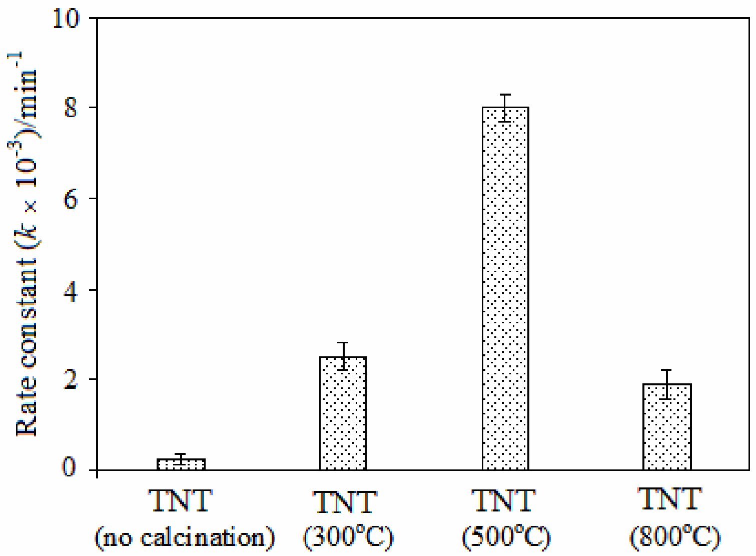

Figure 4-8. The dependence of rate constant of S5 on the calcination temperature. In all cases correlation coefficient (R^2) values are higher than 0.98.

4.4 Summary

In this chapter, different TiO_2 nanotube arrays were successfully prepared by the constant-potential anodization. XRD and XPS spectra of S5 confirmed that the anodic nanotubes contained TiO_2 only without incorporation of any electrolyte elements such as N, F and S. All of the anodic TNT films exhibited better photocatalytic activities for 2,3-DCP degradation in aqueous solution than that of the traditional TiO_2 film prepared by the sol–gel method and an optimal annealing temperature was found to be at 500 ^oC. Based on the experimental results, it can be concluded that morphology and structure of TiO_2 nanotubes, including tube wall thickness and tube length, are important factors in influencing the efficiency of the photocatalysis. Photocatalytic activities of TiO_2 nanotubes decreased with the increased nanotube wall thickness but were not proportional to their length. In comparing these factors, it was found that the nanotube wall thickness is a more important parameter in influencing the overall efficiency of the 2,3-DCP degradation reaction. On the other hand, the crystalline phase is also one of key factors affecting the photocatalytic activities of TiO_2 nanotubes. The S5 sample calcined at 500 ^oC for 1 h with a high degree of crystallinity exhibited the highest photocatalytic activities as compared with other samples calcined at 300 and 800 ^oC. Based on this study, it may be inferred that the surface structure, nanotube length, nanotube wall thickness and calcination temperature of an anodic TiO_2 nanotube film play very crucial roles in determining its photocatalytic activities.

Chapter 5 – Photocatalytic Degradation of 2,3-DCP with TiO_2 Nanotube Films and Effects of Dissolved Oxygen, pH and Anions

5.1 Introduction

The halogenated aromatics in aquatic bodies are mainly from industrial wastewater and the chlorination process of water purification and have been known to cause severe pollution problems (Bellar et al., 1974; Kinzell et al., 1979; Ku et al., 1996). Dichlorophenols (DCP), such as 2,3-DCP, 2,4-DCP, 2,5-DCP and 2,6-DCP, have limited degradation by most conventional biological processes due to their toxicity (Zheng et al., 2004; Ye and Shen, 2004). The photocatalysis with immobilized TiO_2 thin films may be developed to an effective process for reduction and removal of chlorophenols in water. Quan et al. (2005) reported that the degradation of pentachlorophenol (PCP) using an anodic TiO_2 nanotube film with a large surface area was much faster than that using a traditional TiO_2 thin film formed by a sol–gel method. Xie (2006) reported that an anodic TiO_2/Ti nanotubular film as a photoanode exhibited a good reactivity for the photoelectrocatalytic degradation of bisphenol A in aqueous solution. However, these work mainly focused on the aspect of material science, while the effects of key reaction conditions, such as dissolved oxygen (DO), pH and the anions commonly contained in wastewater, on the photocatalytic reaction of using the TiO_2 nanotube films have not been well investigated.

It is well known that dissolved oxygen (DO) can act as an electron acceptor to eliminate the recombination of photogenerated electron-hole pairs and the nanotubular TiO_2 surface with better separation of electrons and holes allows more efficient channelling of the charge carriers into useful reduction and oxidation reactions. The solution pH is one of the important environmental parameters significantly influences the physicochemical properties of semiconductors, including the charge on particle and the aggregation numbers of particles. With the effects on surface charge of the catalyst and speciation of the substrate, it follows that changing pH will result in changing reaction mechanisms and molecular interactions as intermediates are formed. Therefore, the effect of pH value should be considered when assessing the photocatalytic degradation reaction. On the other hand, the presence of various inorganic anions, such as SO_4^{2-}, Cl^-, $H_2PO_4^-$ and NO_3^- coexisting in various industrial effluents, may cause some negative effects on the photocatalytic decomposition of organic compounds (Chen et al., 1997; Hu et al., 2003). These anions are likely to retard the rates of organic compound oxidation by bidding for oxidizing radicals or by blocking the active sites of the TiO_2 catalyst.

Hence, this study aims at evaluating the influence of DO, pH and selected inorganic anions on the photocatalytic degradation of 2,3-dichlorophenol (2,3-DCP) in aqueous solution using the anodic TiO_2 nanotube films under UV light irradiation.

5.2 Photocatalytic Degradation of 2,3-DCP with TNT Films

Since the results in Chapter 4 showed that among the studied TNT samples ‘S5-TNT’ possessed the maximum photocatalytic activities, ‘S5-TNT’ films calcined in air at 500 ^{o}C temperature were used in current and future research work (unless mentioned otherwise). To have a better understanding of morphology and crystalline structure of this TNT film, the FESEM images and XRD patterns were extracted and integrated from the data in Chapter 4, as shown in Figure 5-1. It can be seen from Figure 5-1a that the TNT film has a tubular porous structure, on which TiO_2 nanotubes were well-aligned as uniform arrays with high density. While the inner diameter of the nanotubes was about 100 nm, the tube length was about 0.31 μm and the wall thickness was 28 nm on average. Figure 5-1b shows the XRD pattern of the TNT film calcined at 500 ^{o}C, in comparison with that of Ti foil. Clearly, the TNT film had characteristic peaks at 25.35^{o} (101), 27.5^{o} (110), 36.1^{o} (101), 48.1^{o} (200), 54.3^{o} (211) and 69.8^{o} (220), respectively. According to the XRD indexation, the crystal form of TNT is a mixture of rutile and anatase phases in good agreement with previous reports (Uchikoshi et al., 2004; Eder et al., 2006). From the FESEM and XRD results, it can be confirmed that the well-aligned TiO_2 nanotubular arrays grew on the Ti substrate successfully in aqueous NH_4F electrolyte solution during such a low-voltage (25 V) anodization process.

The photocatalytic activities of the TNT film were evaluated in terms of 2,3-DCP degradation in aqueous solution under UV illumination. A TiO_2 thin film with the same size was also prepared by the sol–gel method reported by Yu et al. (2001) and heated at the same temperature, 500 ^{o}C, for comparison. It had a nonporous structure and a film thickness of ~1.0 μm (shown in Chapter 4). Two experiments were conducted under the same experimental condition with an initial 2,3-DCP concentration of 20 mg L^{-1} and initial pH 5.3. The results are presented in Figure 5-2. It can clearly be observed that after 300 min reaction while the TiO_2 film degraded 2,3-DCP by less than 40%, the TNT film achieved the much higher removal by 93% with a factor of about 2.6 times. As mentioned in Chapter 4, such higher reaction activities of TNT film might result from several factors: larger surface area, hollow interior walls and a nanoscale-dimensional feature. The nanotube array architecture of the TNT film with a wall thickness of 28 nm ensures that the holes are never generated far from the semiconductor–electrolyte interface because the wall

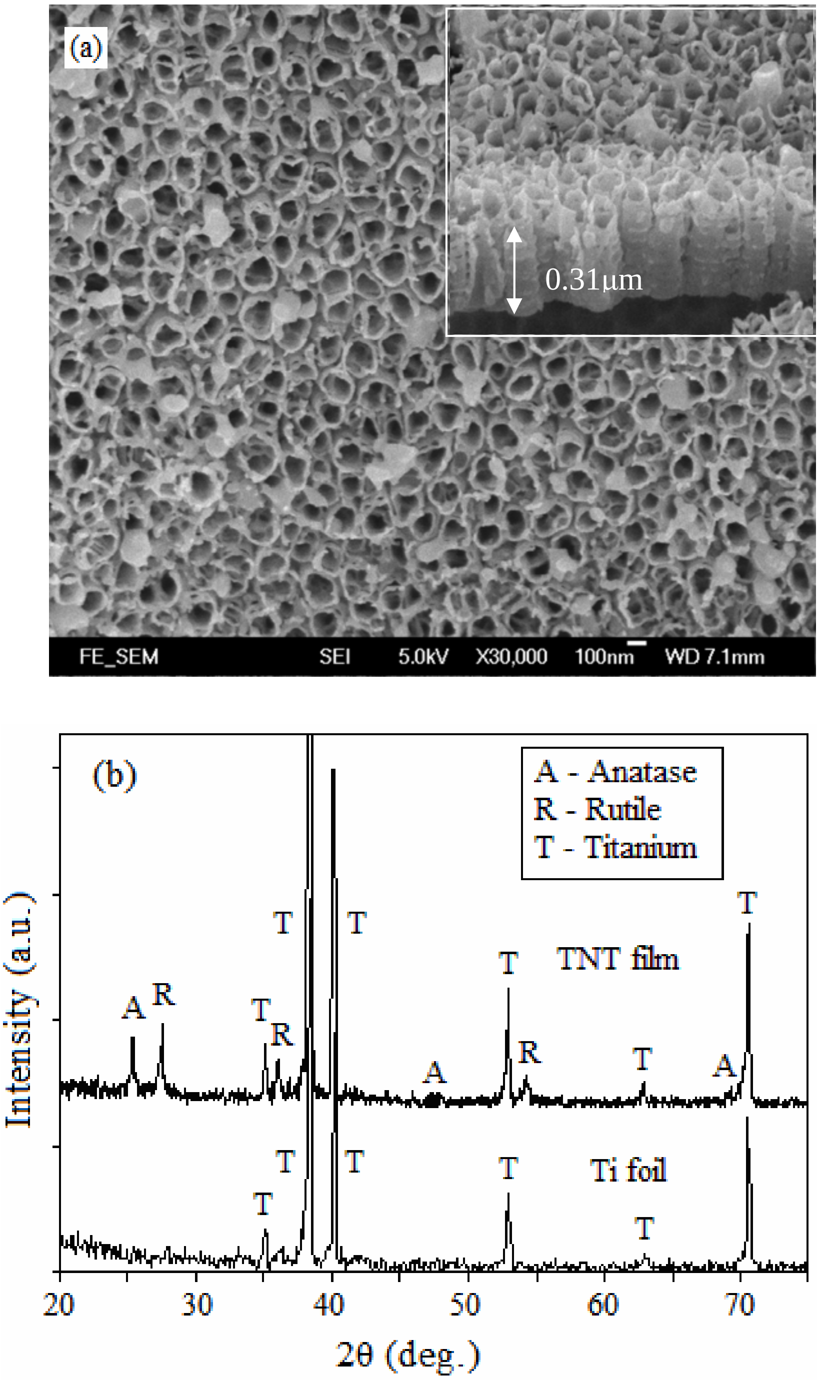

Figure 5-1. (a) FESEM images of TNT film; (b) XRD patterns of Ti foil and TNT film calcined at 500 ^{o}C for 1 h.

thickness is much less than the minority carrier diffusion length of $L_p \approx 100$ nm in TiO$_2$ (Hamnett, 1980), thus charge carrier separation takes place efficiently. In addition, the hollow feature of nanotubes enables the electrolyte species to permeate the entire internal and external surfaces. Paulose et al. (2006) suggested that this could cause the holes to reach the electrolyte surface through diffusion, which takes place on a scale of picoseconds, and finally also reduce the bulk recombination. Besides these, the tube-to-tube contact points (~5 nm) presented in Figure 5-1a may be another role responsible for the higher photoactivities of TNT film due to their quantum size effect and creation of a contact network between the nanotubes. This network allowed the charge carrier-transfer to become easier. Actually, this hypothesis has been confirmed by Varghese and co-workers (2003). They stated that the nanoscale geometry of the nanotubes, in particular the tube-to-tube contact points, is believed to be responsible for the outstanding hydrogen gas sensitivity (Varghese et al., 2004). On the other hand, Lubberhuizen et al. (2000) also claimed that strong scattering inside the nanoporous network leads to a long effective path-length of photons and finally to very effective light absorption. Hence, complete light absorption is achieved in nanoporous films with a thickness considerably smaller than the light absorption depth in bulk material.

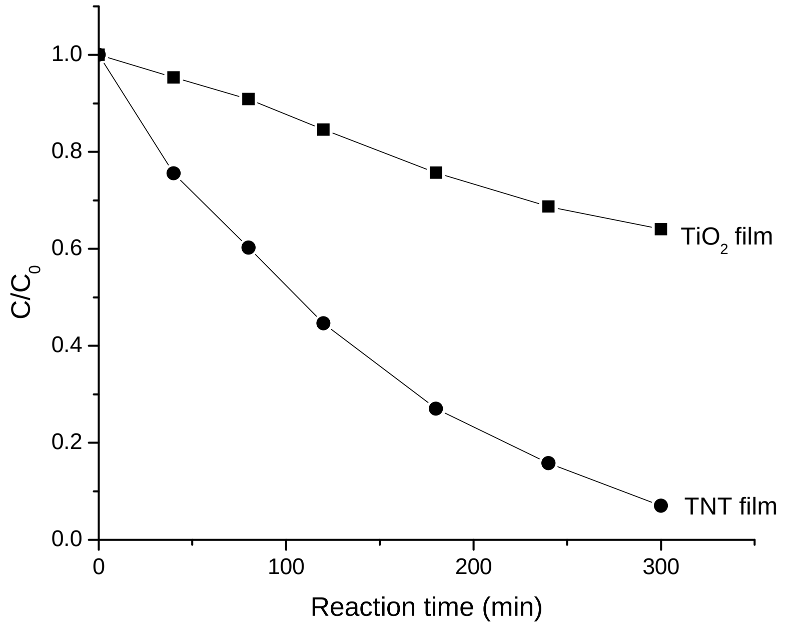

Figure 5-2. 2,3-DCP degradation with TiO_2 film and TNT film under UV illumination (Initial pH 5.3 and C_0 = 20 mg L^{-1}).

5.3 Effects of DO, pH and Anions on the TNT Photocatalysis

5.3.1 Effect of DO

The effect of DO concentration on 2,3-DCP degradation with the initial concentration of 20 mg L^{-1} at initial pH 5.3 was investigated in two sets of experiments using the TiO_2 film and TNT film by purging N_2, air or O_2 gas, respectively, and the results are shown in Figure 5-3. It is observed that after 300 min reaction under UV illumination, 2,3-DCP was degraded with the TiO_2 film by 49% at a high DO level of 33 mg L^{-1} (O_2), by 37% at a medium level of 8.1 mg L^{-1} (air), and by 29% at a low level of 0.3 mg L^{-1} (N_2), respectively. It is evident that for the TiO_2 film, increasing the DO concentration in the solution significantly increases the extent of 2,3-DCP degradation. Meanwhile, even at the very low DO concentration (N_2) the reaction rate was still significant. The similar result about the photocatalytic degradation of 4-chlorobenzoic acid using a TiO_2 thin film in a rotating disk photocatalytic reactor was also observed by Dionysiou et al. (2002). It has been reported that when molecular oxygen is used as an electron acceptor to trap and remove electrons from the surface of the titania particles for minimizing the build-up of free electrons, the reaction of adsorbed oxygen with photo-generated electrons at the surface of the titania catalyst is relatively slow and may be the rate-controlling step in photocatalytic oxidation reactions (Gerischer and Heller, 1991). Therefore, increasing the charge transfer rate from titania to molecular oxygen will increase the efficiency of photocatalysis for organic substrate photo-oxidation. If the adsorbed oxygen is in excess of the photo-generated electrons at the surface, the rate of electron transfer to molecular oxygen will be maximized. However, they are affected by the types and characteristics of titania through the efficiency of electron–hole generation, recombination, and also charge transfer reaction rates (Almquist and Biswas, 2001).

For the TNT film, it can be seen from Figure 5-3 that at the very low DO concentration (N_2), the removal of 2,3-DCP was achieved by as high as 81% after 300 min reaction. The large decay of 2,3-DCP in the absence of DO should be due to the unique nanotubular structure of TNT film, which owns a better separation of electron-hole and allows more efficient channelling of the charge carriers into the photochemical reactions. In fact, TiO_2 without DO can still perform the photocatalytic reactions due to the presence of photogenerated holes. Furthermore, the decomposition of 2,3-DCP increases to 93% in the presence of air and rises to 95% in the presence of oxygen, respectively. Only a slight enhancement of 2% from air to O_2 gas indicates that an air saturated water system can provide sufficient electron scavengers to accelerate the photocatalytic reaction using the TNT film under UV illumination.

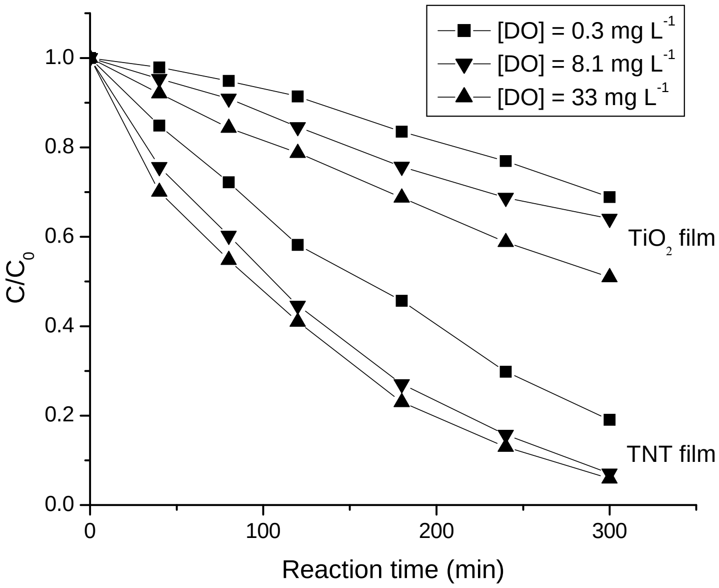

Figure 5-3. Effect of DO concentration on 2,3-DCP degradation with TiO_2 film and TNT film (Initial pH 5.3 and C_0 = 20 mg L^{-1}) by blowing different gases (N_2, air or O_2), respectively.

5.3.2 Effect of pH

Solution pH is one of the most important parameters that influence the photocatalytic reactions. To study the effect of pH on the photocatalytic degradation of 2,3-DCP, one set of experiments was carried out under the same experimental conditions but with different initial pH in the range of 3.4–10.9. The experimental results are shown in Table 5-1.

Table 5-1. Effect of solution pH on the 2,3-DCP degradation, dechlorination and DOC removal after 300 min reaction.

Test No.	pH		2,3-DCP degradation[a]		Dechlorination[b]	DOC reduction
	Initial	Final	k (min^{-1})	(%)	(%,Cl^-/Cl_{total})	(%)
1	3.4	3.0	0.007	90	52	47
2	5.3	3.4	0.008	93	57	40
3	7.8	3.8	0.011	96	74	37
4	10.9	7.1	0.024	100	99	20

[a] Photocatalytic degradation of 2,3-DCP is assumed to follow a pseudo-first-order reaction; k is the kinetic constant.

[b] Dechlorination was calculated on the basis of the total chlorine (Cl^-/Cl_{total}) in 2,3-DCP of 20 mg L^{-1}.

It is evident that at initial pH 3.4, the pseudo-first-order rate constant (k) of 2,3-DCP degradation was only 7×10^{-3} min^{-1} and the solution pH varied from 3.4 to 3.0 after 300 min UV irradiation. Instead, at initial pH 10.9 the k value reached 24×10^{-3}

min^{-1} (3.4 times higher than that at pH 3.4) and the corresponding pH of the solution dropped from 10.9 to 7.1. The results in Table 5-1 demonstrated that 2,3-DCP was degraded faster at the higher pH and some acidic products were formed from the 2,3-DCP degradation.

In general, medium pH has a complex effect on the photodegradation rates of chlorophenols depending on different molecular structures of chlorophenols as well as the semiconductors used in the oxidation process. Several studies showed that the removal efficiency of chlorophenols decreased with increasing pH values (Ku et al., 1996; Leyva et al., 1998; Quan et al., 2007). It is suggested that TiO_2 surface carries a net positive charge (pH_{zpc} 6.25) at low pH value, while the chlorophenols and intermediates are negatively charged naturally. Because of this, low pH value can facilitate the adsorption of the organic compounds and promote better photocatalytic degradation. In contrast, better removal efficiency of chlorophenols in alkaline condition has also been reported (Stafford et al., 1994; Serpone et al., 1995; Doong et al., 2001), which is consistent with our results. It is explained that the higher pH value can provide more hydroxide ions (OH^-) to react with holes to form hydroxyl radicals, subsequently enhancing the degradation rate of substituted phenols. The photocatalytic transformation of chlorophenols does not involve the •OH oxidation exclusively, and direct electron transfer and surface adsorption reactions also contribute to the disappearance of chlorophenols in TiO_2 (Stafford et al., 1994). Since the effect of pH can not be generalized, Gogate and Pandit (2004) recommended that laboratory scale studies are required for establishing the optimum pH conditions unless data are available in the literature with exactly similar operating conditions. In our case, the faster 2,3-DCP degradation occurring at the high pH may be attributed to two reasons: (1) more hydroxyl radicals are formed in alkaline solution with more OH^- ions and (2) it is easier for 2,3-DCP to absorb UV light energy at high pH, when the functional group of phenol is dissociated to the phenate ion due to its $pK_a = 7.7$ (Tehan et al., 2002) and the kinetic reaction constant has been found to be greater by several orders of magnitude (Langlais et al., 1991). The much higher reactivity of the dissociated compounds at the higher pH is believed to be via the attack of electrophilic species such as •OH radicals on the phenate ion, which should be faster with a greater electron density on the aromatic ring. In contrast, at low pH the undissociated species ($C_6H_3Cl_2OH$) is predominant. The hydrogen atom in polar O–H bond and the electronegative chlorine atom on o-chlorophenol may form intramolecular hydrogen bonding (O–H· · ·Cl) and develop a stable 5-membered ring. This hypothesis has been supported by a number of literature precedents (Brune et al., 1999; Kolla et al., 2004). By taking into account these, a possible coordination can be found in Scheme 5.1. In this way, there is an increase of the o-chlorophenol resonance structure in the ground electronic state and at the same time, an increase of the surroundings rigidity occurs due to formation of the chelate ring. Both effects may resist the attack of •OH radicals on the protonated phenol ring at low pH condition, evidently mirroring a corresponding decrease of the 2,3-DCP degradation.

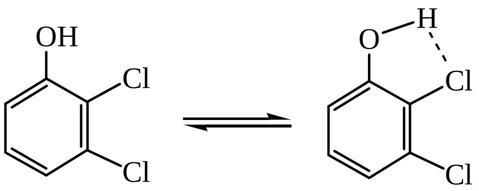

Scheme 5-1. Formation of intramolecular hydrogen bonding in 2,3-DCP molecular structure.

Table 5-1 also illustrates the pH dependency of the dechlorination of 2,3-DCP and DOC reduction using the TNT film. Similar to its degradation, the photocatalytic dechlorination of 2,3-DCP was observed to be faster at alkaline pH than that at acidic pH (pH 10.9 > 7.8 > 5.3 > 3.4). However, DOC reduction demonstrated an opposite result on the pH dependency, in which the photocatalytic reaction at initial pH 10.9 after 300 min UV irradiation lead to a significant release of chloride by 99% , whereas the loss of DOC was only 20%. In the case of acidic pH (pH 3.4 and

5.3), the dechlorination of 2,3-DCP was only 52% and 57% after 300 min, whereas the reduction of DOC reached 47% and 40%, respectively. These results indicate that the acidic condition is more favourable for the 2,3-DCP mineralization (further degradation) rather than its decomposition (initial degradation). This may be mainly attributed to the formation of organic intermediates in the photocatalytic reaction. Information on the intermediate concentrations at different pH and the pathway of 2,3-DCP degradation has been studied through the ^{1}H-NMR analysis as shown in Table 5-2.

Table 5-2 shows the ^{1}H-NMR spectral data of residual aromatic compounds and their corresponding concentrations at 12 h irradiation time for the photodegradation of 2,3-DCP with an initial concentration of 300 mg L^{-1} with different initial pH. It was clearly observed that the distribution of intermediates of 2,3-DCP was pH-dependent. Compound like 2-chlororesorcinol is the major intermediate from the decomposition of 2,3-DCP under three pH conditions (pH 3.4, 5.3 and 10.9). For example, the concentration of 2-chlororesorcinol at pH 10.9 reached 90 mg L^{-1}, which was critically higher than those at pH 3.4 (12.6 mg L^{-1}) and 5.3 (18.9 mg L^{-1}). Furthermore, at pH 10.9 the total concentration of residual compounds in the irradiated solution (including the residual 2,3-DCP and compounds **1**-**7**) is obviously

Table 5-2. Identification of intermediates from 2,3-DCP degradation by ^{1}H-NMR analysis.

Compound[a] No.	Proton	Chemical shifts (ppm)	Description[b]	Concentrations (mg L^{-1})		
				pH 3.4	pH 5.3	pH 10.9
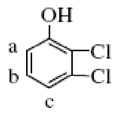 (2,3-dichlorophenol)	a b c	6.97 7.18 7.13	1H, d, J_{ab} = 9.85 1H, m, 1H, d, J_{cb} = 8.34	47.2	47.2	26.0
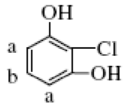 (2-chlororesorcinol)	a b	6.62 7.09	2H, d, J_{ab} = 9.1 1H, t, J_{ba} = 9.1	12.6	18.9	90.1
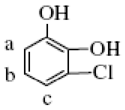 (3-chlorocatechol)	a b c	6.52 6.82 6.86	1H, d, J_{ab} = 8.9 1H, m, 1H, d, J_{bc} = 8.9	8.4	12.6	2.1
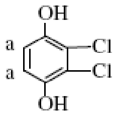 (2,3-dichloroquinol)	a	6.75	1H, s	2.3	2.3	2.3
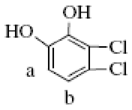 (5,6-dichlorocatechol)	a b	6.46 6.95	1H, d, J_{ab} = 8.7 1H, d, J_{ba} = 8.8	trace	trace	6.9
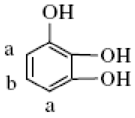 (Pyrogallol)	a b	6.40 6.61	2H, d, J_{ab} = 8.3 1H, t, J_{ba} = 8.1	2.7	1.8	2.7
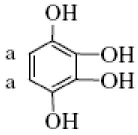 (1,2,3,4-benzenetetrol)	a	6.08	2H, s	4.2	2.1	10.5
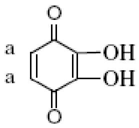 (2,3-dihydroxy-p-benzoquinone)	a	6.89	2H, s	1.7	1.7	1.6

[a] Different protons linked on benzene ring are marked as a, b and c, respectively.

[b] Singlet, doublet, triplet, and multilet are abbrivated as s, d, t and m, respectively; coupling constants (*J*) are given hertz.

higher than those at pH 3.4 and 5.3. This accumulated amount of 2-chlororesorcinol indicated its degradation more slowly under an alkaline condition rather than that under an acidic condition, resulting in lower DOC reduction under the alkaline condition. Furthermore, the different concentrations of intermediates detected at different pH values indicate that the solution media is susceptible to OH attack on the aromatic moiety.

Based on the organic intermediates identified by the ^{1}H-NMR analysis, a possible pathway of 2,3-DCP degradation in this reaction system can be proposed as shown in Figure 5-4. The reactions may mainly involve the addition of hydroxyl radicals to the organic substrate by three approaches of (a) hydroxylation of the aromatic ring, (b) substitution of chlorine by OH and (c) oxidation of hydroxylated hydroquinone to the corresponding quinine (Antonaraki et al., 2002). The routes (a) and (b) in Figure 5-4 was based on the dechlorination process, where the •OH substitution removes the chlorine in the ring, leading to formation of the hydroxyl derivatives (compounds **1**, **2** and **5**). Due to the stereochemical inhibition of *ortho*-chlorosubstituents, compound **1** is the major intermediate from the 2,3-DCP decomposition under three pH conditions.

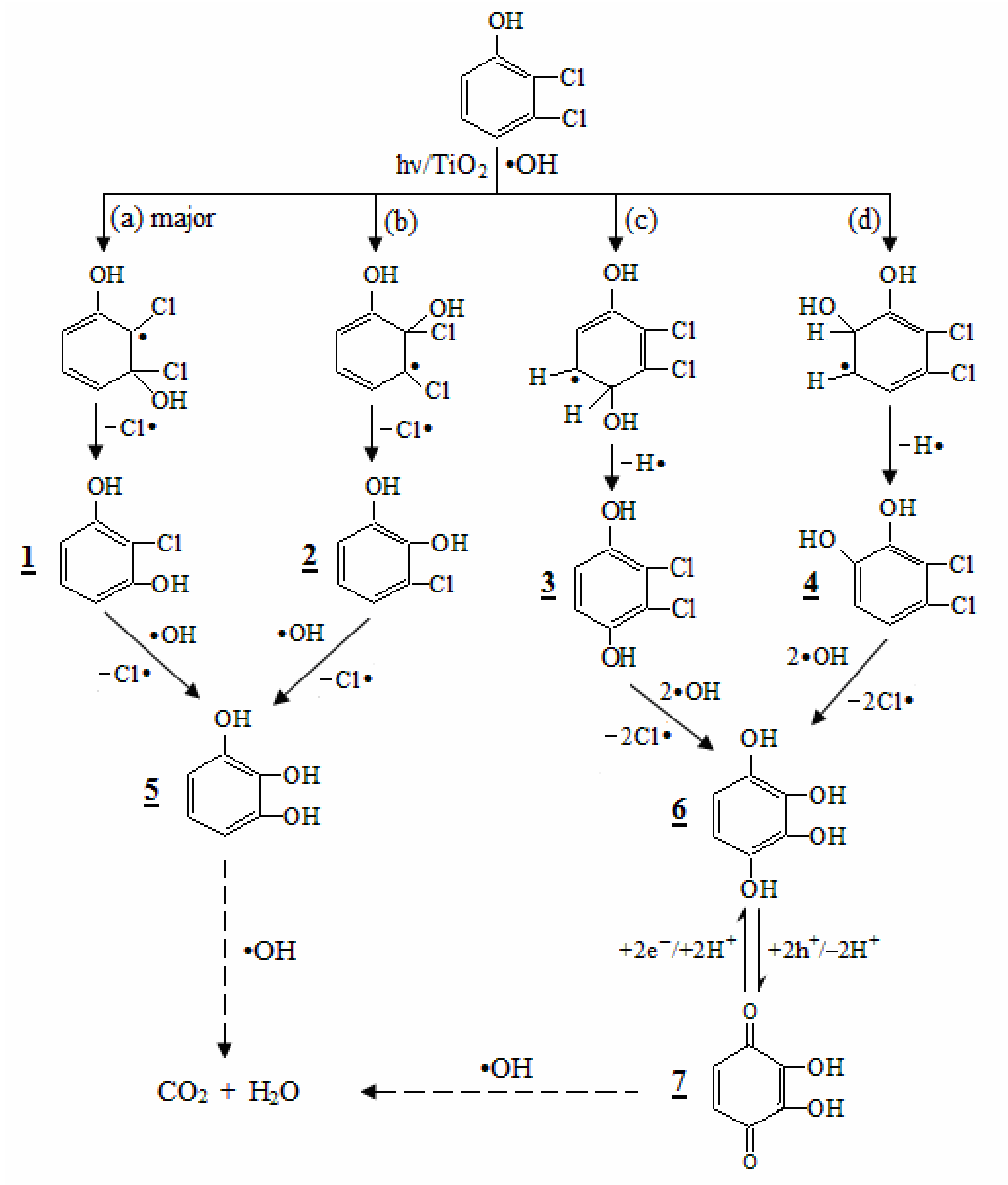

Figure 5-4.	Proposed pathways of the 2,3-DCP degradation in the TNT/UV system.

In general, the OH groups in the chlorophenol ring are *ortho* and *para* directing with activation, whereas Cl substituents are *ortho* and *para* directing with deactivation. When the OH radical, an electrophilic reagent, is attacking 2,3-DCP, it is expected to attack the electron rich positions and generate major *para*- or *ortho*-substituted intermediates (i.e. 3-chlorocatechol, 3,4-dichlorocatechol and 2,3-dichloroquinol). This seems to be the case in this study. Besides the *para*- or *ortho*-substituted intermediates in the present paper, a new intermediate, 2-chlororesorcinol, with the highest concentration was identified as a *meta*-substituted intermediate under three pH conditions, which is different from the previous report (D'Oliveira et al., 1993). This indicates that this ring position is attacked by •OH radicals preferentially, which can be attributed to the strong stereochemical inhibition of *ortho*-chlorosubstituents to •OH radical attack, due to the close proximity of OH and Cl groups on the aromatic ring (Tang and Huang, 1995) and/or to the formation of intramolecular hydrogen bonding between the OH and Cl groups in the aromatic ring (mentioned above). As a result, compound corresponding to a primary OH substitution at the *meta*-position was detected.

In the routes (c) and (d), the detected intermediates are all rationalized as being formed by hydrogen abstraction, followed by *para*- and *ortho*-hydroxylation of the ring, respectively. Hydroxyl radicals attack preferentially the aromatic moiety due to their electrophilic character to form the hydroxylated compounds **3** and **4**. The two products are then followed to dechlorinate through the •OH attack (compound **6**) and finally oxidized to corresponding quinine (compound **7**).

5.3.3 Effect of Anions

The existence of inorganic anions such as chloride, sulfate, carbonate, nitrate and phosphate is considerably common in wastewaters and also in natural water. The importance of the effect of anions on the photodegradation of pollutants has been remarkably recognized due to the occurrence of the competitive adsorption, resulting in the inhibitive effect on the photoreaction of organic pollutants. In this study, the initial pH 5.3 was employed and the effect of Cl^- on the photocatalytic degradation of 2,3-DCP in the TNT/UV system was first studied by adding NaCl into the reaction solution at different concentrations of 0.005, 0.05 and 0.1 M, The results are shown in Figure 5-5a. It can be seen that while the removal of 2,3-DCP without any anions was achieved by 93% after 300 min UV irradiation, it was achieved by 77% only at $[Cl^-]$ = 0.005 M and further down to 64% at $[Cl^-]$ = 0.1 M. This indicates that the rate of 2,3-DCP degradation decreased with an increased Cl^- concentration significantly. The observed inhibition effect is often explained by competitive adsorption (Chen et al., 1997). To understand the adsorption behavior of the TNT catalyst in aqueous solution, the TiO_2 nanotubes were peeled off from the TNT films and a powdery suspension was prepared to measure its point of zero charge (pzc) in the pH range of 3.3–10.7 as shown in Figure 5-6, where P25 powder with the same concentration was also used as

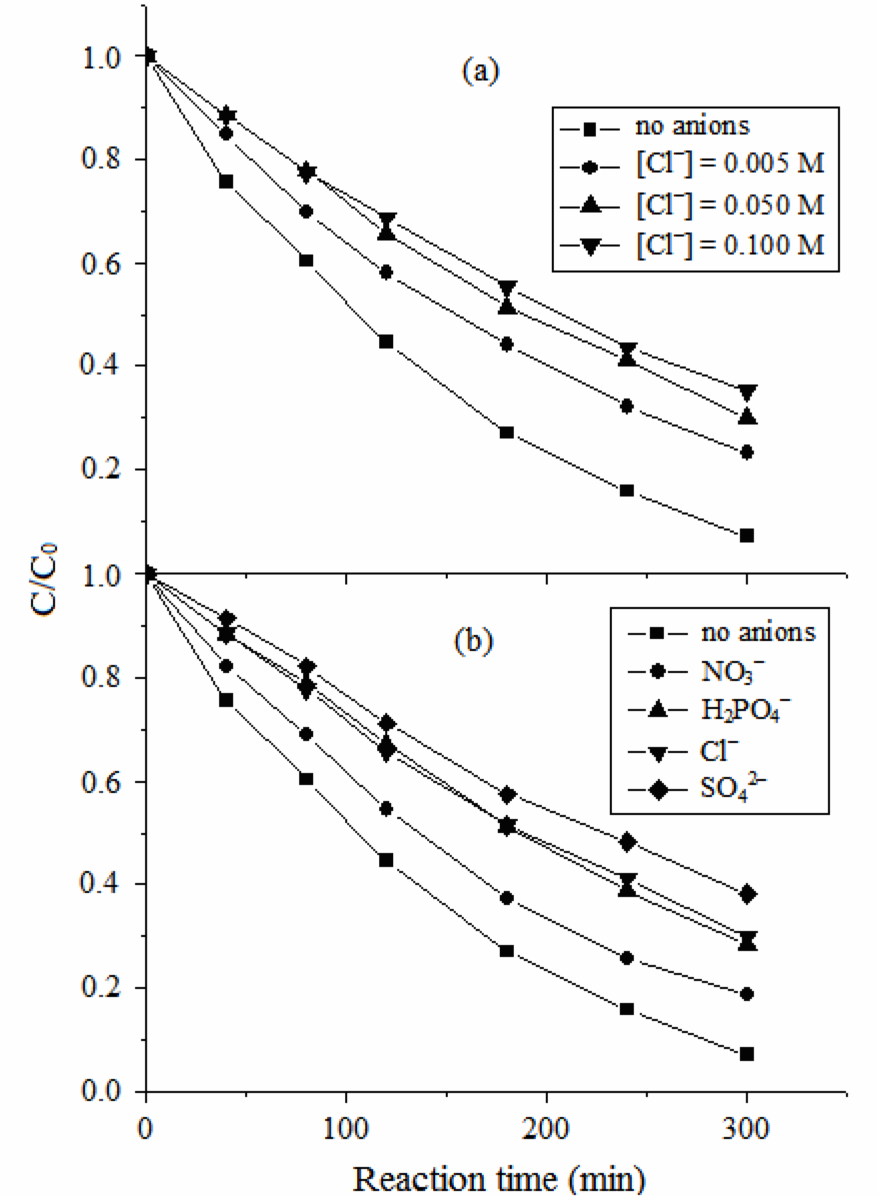

Figure 5-5. (a) Influence of Cl^- concentrations on the photocatalytic deactivation of TNT/UV system; (b) Photocatalytic deactivation in the presence of different anions (0.05 M) at initial pH 5.3: (●) no anion; (■) NO_3^-; (▲) $H_2PO_4^-$; (▼) Cl^-; (♦) SO_4^{2-}. Here, all experiments were carried out at initial pH 5.3 and C_0 = 20 mg L^{-1}.

a reference. It can be seen that the pzcs of P25 and TNT samples were at pH 6.21 and 5.23, respectively. The results demonstrated that the isoelectric point of TNT catalyst was very close to the reported value of pH 5.3 (Wang et al., 2006) and lower than that of P25 powder. This might be attributed to the formation of more functional groups (such as –OH and –COOH) on TNT surface. In fact, the photocatalytic process mainly occurs on the photocatalyst surface but not in the bulk solution. It is suggested that the isoelectric point would greatly influence the adsorption of organic substrates and its intermediates on the surface of photocatalysts during photoreaction (Hu et al., 2001). Hence, the TiO_2 nanotube surface is positively charged at pH < 5.2 and Cl^- can be easily adsorbed onto the positively charged surface of the catalyst by electrostatic attraction, leading to the competitive adsorption.

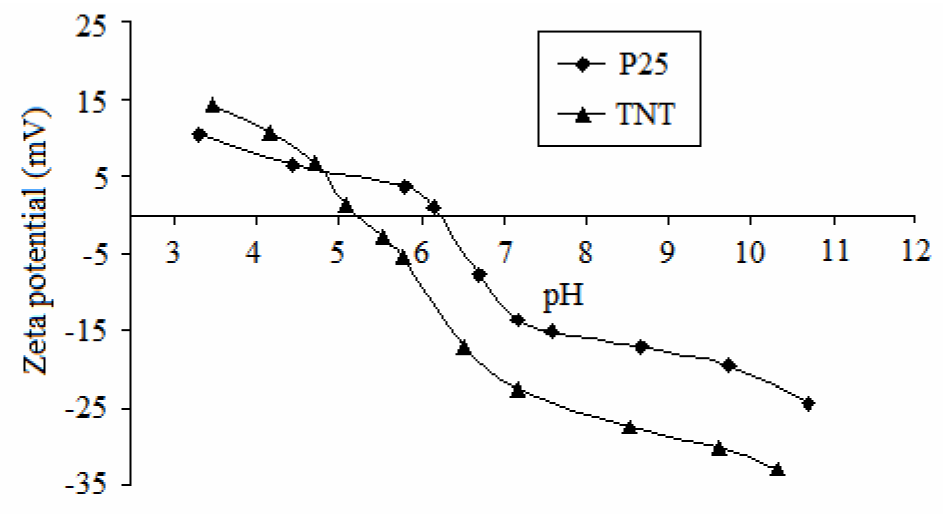

Figure 5-6. Zeta potential analysis of P25 and TNT samples as a function of pH.

The other probability is that chloride ions can act as scavengers of positive holes (h^+) and/or hydroxyl radical (•OH) through the following reactions:

$$Cl^- + h^+ \rightarrow Cl\bullet \qquad (1)$$

$$\bullet OH + Cl^- \rightarrow Cl\bullet + OH^- \qquad (2)$$

Meanwhile, the dichloride radical anion $Cl_2\bullet^-$ from the further reaction of Cl• with Cl^- (Eq. 3) is reactive with organic substances and the recombination of two chloride radicals $Cl\bullet/Cl_2\bullet^-$ (Eqs. 4 and 5) (Rincón and Pulgarin, 2004) are the source of molecular chlorine, thus ending the radicals transfer.

$$Cl\bullet + Cl^- \rightarrow Cl_2\bullet^- \qquad (3)$$

$$Cl_2\bullet^- + Cl_2\bullet^- \rightarrow Cl_2 + 2Cl^- \qquad (4)$$

$$Cl\bullet + Cl\bullet \rightarrow Cl_2 \qquad (5)$$

Since Cl• is less reactive than •OH, the excess Cl^- may have the inhibition effect on the photodegradation of 2,3-DCP in aqueous solution.

Figure 5-5b shows the effects of different anions (i.e. Cl^-, NO_3^-, $H_2PO_4^-$ and SO_4^{2-}) at the same concentration of 0.05 M. Compared to the control test in the aqueous 2,3-DCP solutions without anions, the existence of all anions reduced the 2,3-DCP degradation to a certain degree. Among them, the strongest inhibition of 2,3-DCP degradation resulted from SO_4^{2-} due to its ionic properties. At $pH < 5.3$, like Cl^-, SO_4^{2-} can inhibit the photodegradation of the chlorophenol through two ways of: (1)

competitive adsorption with the 2,3-DCP on the TNT film surface due to the higher ionic strength and (2) trapping positive holes and/or hydroxyl radical, where SO_4^{2-} can be led to the generation of less reactive radical $SO_4\bullet^-$. Actually, the divalence charge of SO_4^{2-} can lead to the stronger binding of the SO_4^{2-} with the catalyst, as compared with the single valence ions such as NO_3^-, Cl^- and $H_2PO_4^-$, thus resulting in the stronger competitive adsorption. For the addition of $H_2PO_4^-$, the behaviour of $H_2PO_4^-$ ions is similar to SO_4^{2-} ions, in that the $H_2PO_4^-$ reacted with h^+ and •OH to form $H_2PO4\bullet^-$, less reactive than that of h^+ and •OH. Formation of inorganic radical anions under these circumstances was also reported in some literature (Abdullah et al., 1990; Bekbölet et al., 1998; Hu et al., 2003). The addition of NO_3^- to the solution in this study showed a minor effect on the photocatalytic degradation of 2,3-DCP only. Abdullah et al. (1990) also reported that the presence of $NaNO_3$ had a negligible effect on the photodegradation of ethanol and 2-propanol under UV light irradiation. Based on the above discussion, the observed inhibition effect may therefore be explained by the combination of the competitive adsorption and the formation of less reactive radicals during the photocatalytic reaction.

5.4 Summary

The highly-ordered TiO_2 nanotube arrays were successfully formed on Ti foil by an anodic oxidation method. The experimental results showed that the anodic TNT film had higher photocatalytic activities than the conventional TiO_2 thin film prepared by a sol-gel method with a factor of about 2.6 times. DO acts as an effective electron acceptor to extend the hole's lifetime and to form the oxidizing species of •OH radicals, affecting the photoactivities of the TNT film. The effect of solution pH demonstrated that an alkaline condition is favourable to 2,3-DCP degradation and dechlorination but an acidic condition is more beneficial to further mineralization. The presence of NO_3^- had the weakest inhibition effect on the degradation of 2,3-DCP, while SO_4^{2-} had the strongest inhibition among NO_3^-, Cl^-, $H_2PO_4^-$ and SO_4^{2-}.

Chapter 6 – Mechanism and Pathways of Diphenamid Degradation by Photolysis and Photocatalysis with TiO_2 Nanotube Films

6.1 Introduction

Diphenamid (DPA) as a pre-emergent herbicide is widely employed for control of annual grasses and broadleaf weeds in tomato, potato, strawberry, peanut, and also in soybean plants (Krzeminski et al., 1966; Schultz and Tweedy, 1972). Early study on the loss of DPA in soil has shown that it is nonvolatile and its metabolites may persist in soil for several months (Weed Science Society of America, 1983). These factors could result in a long term contamination of surface and ground water, which becomes a potential risk for the environment.

Photochemical degradation of DPA in aqueous solution has been investigated by some researchers. Rosen (1967) studied the direct photodegradation of DPA, but the major products from DPA degradation upon UV and sunlight irradiation are not clear. Rahman et al. (2003) investigated the photodegradation of DPA affected by different reaction parameters such as pH, substrate concentration, catalyst concentration and the presence of electron acceptors in aqueous TiO_2 (P25) suspension. They identified five intermediates by using GC-MS technique and suggested a brief pathway of the

DPA degradation. However, due to the complexity of the DPA molecular structure, the five products identified in their study were definitely not sufficient to buildup a thorough pathway delineating the photocatalytic degradation of DPA. With the GC-MS analysis alone, a solvent extraction and/or sample derivation procedure is usually required, where the escaping of some polar intermediates and positional isomers from the MS detection was inevitable. Moreover, a 125-W medium pressure mercury lamp used in their experiment generally offers an emission in a broad band from 200 to 600 nm, which can result in the photolysis and photocatalysis processes simultaneously during the DPA degradation.

To our best knowledge from the previous literatures, so far it is not clear that how the DPA degradation and mineralization is preponderated by different reaction mechanisms of photolysis and photocatalysis. Therefore, the aim of present work is to further understand the reaction mechanisms and pathways of DPA degradation by photolysis with UVC alone and by photocatalysis with TiO_2/UVA through two sets of well-designed experiments.

6.2 Direct Photolysis and Photocatalysis of DPA

Two sets of experiments were conducted to degrade DPA by photolysis with UVC alone and by photocatalysis with TNT/UVA. In our experiments, the semi-logarithmic graphs of the DPA degradation versus irradiation time yielded straight lines and the reaction rate constants (*k*) were evaluated by fitting the experimental data with linear regression. As a result, in two cases correlation coefficient (R^2) values were higher than 0.97, as shown in Figure 6-1.

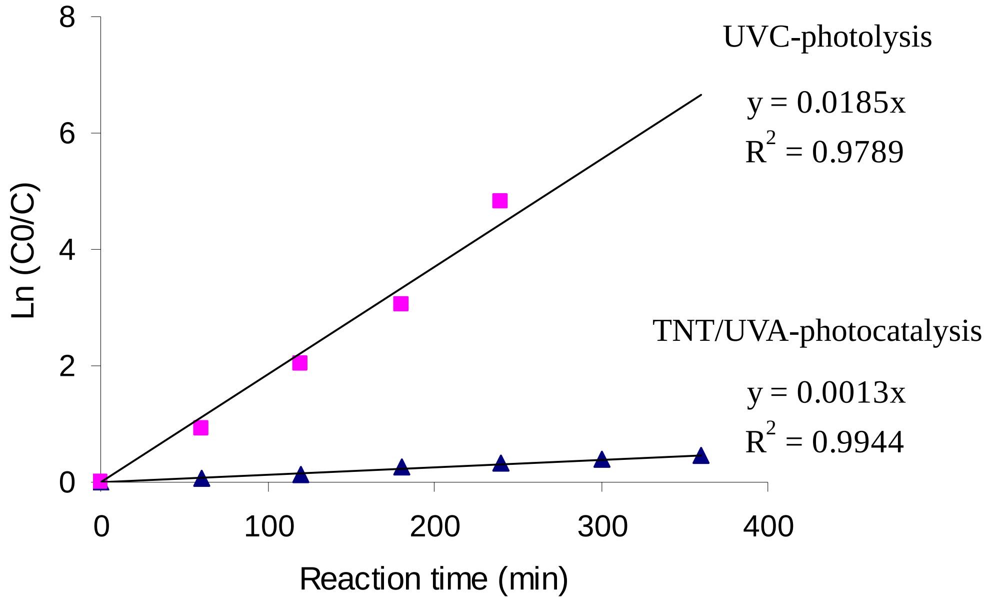

Figure 6-1. Direct photolysis and photocatalysis of DPA using different UV light irradiations of 254 and 350 nm (Initial pH 7.2 and C_0 = 20 mg L^{-1}).

This results means that the degradation of DPA follows the pseudo-first-order reaction with respect to the DPA concentration, which is in agreement with the previous report by Rahman et al. (2003).

The aqueous DPA solutions in the absence of TNT film at pH 3.5, 7.2 and 9.6 were first conducted under UVC and UVA illumination, respectively. To conduct a photocatalysis reaction without any effect of direct photolysis, aqueous DPA solution in the presence of TNT film was irradiated by the UVA light in the wavelength range of 318-400 nm under different pH conditions. The experimental results are presented in Table 6-1.

Table 6-1. Effects of solution pH on DPA degradation, kinetic constants and DOC removal in different systems after 360 min reaction. Here, C_0 = 20 mg L^{-1}.

System	DPA decay[a] (1–C/C_o, %)			k^b (min^{-1})			DOC removal[a] (%)		
	pH 3.5	pH 7.2	pH 9.6	pH 3.5	pH 7.2	pH 9.6	pH 3.5	pH 7.2	pH 9.6
UVC	100	100	100	0.0319	0.0185	0.0243	11	8	9
UVA	--[c]	--	--	--	--	--	--	--	--
TNT/UVA	63	51	42	0.0018	0.0013	0.0010	13	11	8

[a] All reactions were carried out for 360 min reaction.

[b] The DPA degradation is assumed to follow the pseudo-first order reaction.

[c] -- is nearly zero.

It can be seen while the direct photolysis by UVA showed almost no reduction of DPA after 360 min reaction time at three pH values, the direct photolysis by UVC showed that at pH 3.5, 7.2 and 9.6, DPA was degraded by 100% after 360 min, but the corresponding DOC was only reduced by 11%, 8% and 9%, respectively. These results indicate that DPA can not be degraded by direct photolysis under UVA illumination (350 nm) because of its main light absorption at ~260 nm, but it can be excited by UVC light (254 nm) and then quickly degraded through direct electron transfer reaction. Unfortunately, the direct UVC-photolysis had poor mineralization when the DOC removal is used to reflect the mineralization of DPA. The effect of pH on DPA degradation indicated that DPA was degraded from fast to slow as: pH 3.5 > 9.6 > 7.2. It can be attributed to the unique ionic states of DPA under acidic and alkaline conditions. Both the acidic and alkaline conditions favored UV absorption, as shown in Figure 6-2, resulting in faster homolytic or heterolytic breakages in the DPA molecules.

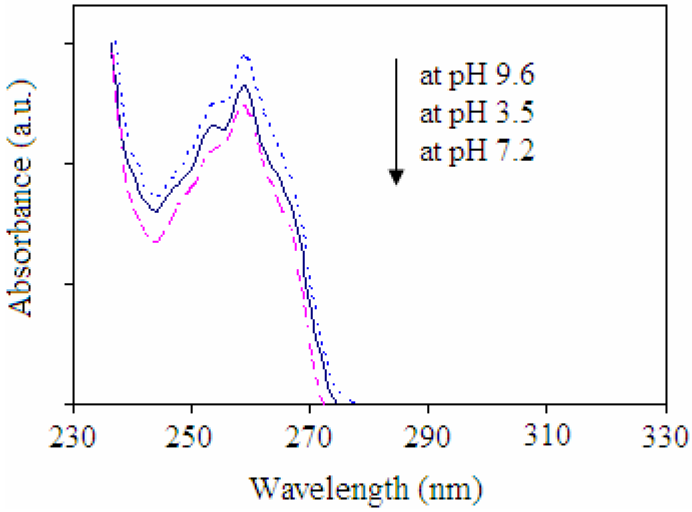

Figure 6-2. UV-visible spectra of aqueous DPA solutions at different pH media.

With the further photolysis reaction, some acidic products were formed from the DPA degradation, which leaded to the decrease of solution pH. For the case at pH 9.6, the reaction rate therefore was slowing down gradually.

For the photocatalysis of DPA, it can be seen from Table 6-1 that at pH 3.5, DPA was degraded by 63% and DOC was reduced by 13%, respectively after 360 min whereas at pH 9.6, DPA was degraded by 42% and DOC by 8%. These results indicate that DPA can be degraded by the photocatalysis with TNT/UVA, but much slower than that by the photolysis with UVC. Furthermore, it was found that under acidic and neutral conditions, the DOC removal by the TNT/UVA-photocatalysis (13% and 11%, respectively) was higher than that by photolysis (11% and 8%, respectively). These results might indicate that the photocatalysis process has a nature of poor selectivity for degrading different intermediates from the DPA degradation, which is beneficial to DPA mineralization, especially under the acidic condition, while the direct photolysis showed relatively lower DOC removals. Considering these results, a conclusion can be made that a mixed light source including UVC and UVA, such as a medium-pressure mercury lamp, seems more favorable for the photocatalytic degradation of DPA in aqueous solution.

In fact, photocatalysis by TiO_2 is known to produce •OH radicals in water, through the interface oxidation of hydroxide anions or water molecules adsorbed on the semiconductor surface by the holes photogenerated in the valence band of semiconductor. These produced •OH radicals initiate the degradation of aromatic compounds by direct attack to the aromatic rings, leading to the formation of hydroxylated intermediate species (to be discussed later). The holes may also induce the direct oxidation of molecules adsorbed on the semiconductor, leading to radical cations, and the subsequent interaction with oxygen-containing species. These two photocatalytic reaction paths frequently yield the same mineralized products (Hoffmann et al., 1995). Since the photocatalytic process mainly occurs on the photocatalyst surface, but not in the bulk solution, solution pH can affect the species adsorption on the catalyst surface and then further affect the reaction rate of DPA degradation as pH 3.5 > 7.2 > 9.6. This might be ascribed to the surface-charged properties of TiO_2 under different pH conditions, which has been claimed by many reports (Naskar et al., 1998; Bayarri et al., 2005).

In contrast, the mechanism of the direct UV-induced photolysis ($\lambda = 254$ nm) is based on the fact that the chemical species undergo the homogenerous reactions in solution, by which molecules are broken down into smaller molecules as a result of photodecomposition of the excited organic compounds. The sequence of events that could occur during a particular DPA photolytic decomposition is summarized below.

$DPA + h\nu \rightarrow DPA^* \rightarrow [DPA\bullet^+ + DPA\bullet^-]^*$ excitation of DPA (1)

$[DPA\bullet^+ + DPA\bullet^-]^* \rightarrow DPA + heat$ thermal deexcitation of DPA (2)

$[DPA\bullet^+ + DPA\bullet^-]^* \rightarrow I_{uv}$ formation of intermediates (3)

$[DPA\bullet^-]^* + O_2 \rightarrow DPA + O_2\bullet^-$ formaion of superoxide radical (4)

$O_2\bullet^- + I_{uv} \rightarrow products$ decomposition of intermediates (5)

$I_{uv} + h\nu \rightarrow I_{uv}^*$ excitation of intermediates (6)

$I_{uv}^* \rightarrow products$ decomposition of intermediates (7)

Here Eq. 1 involves the excitation of DPA, in which the photo-excited state of DPA^* takes one-electron from the ground state of DPA molecule to produce radical anion $DPA\bullet^-$. Subsequent reaction can either undergo thermal deexcitation (Eq. 2) via recombination of radical ions or photodecomposition to produce intermediate I_{uv} (Eq. 3). Radical anion ($DPA\bullet^-$) is the only species that can be responsible for the reaction with dissolved oxygen (Lee and Yoon, 2008), which suggests that $DPA\bullet^-$ transfers one-electron into dissolved oxygen to yield a superoxide radical ($O_2\bullet^-$), as described in Eq. 4. Although its oxidizing power is not very high, the superoxide radical is able to degrade some unstable intermediates with high absorption of UV light (Eq. 5).

Some intermediates I_{uv} can also absorb UV light to produce excited state intermediate I_{uv}^* as shown in Eq. 6, further undergoing the decomposition towards final products step by step (Eq. 7), but some can not. For example, Kochany and Maguire (1994) studied the sunlight photodegradation of metolachlor and found that metolachlor is relatively resistant to photolytic decomposition. When energy absorbed by intermediate molecules directly from UV light is not enough to cause the bond scission, this intermediate will show the resistant property. The formation of resistant intermediates merely explains the fact that generally direct photolysis has a lower degree of mineralization than that of photocatalysis with TiO_2. Therefore, it was found in this study that the direct 254 nm−UV photolysis was effective for degrading low concentration of DPA but only produced a limited degree of DPA mineralization.

6.3 Identification of Intermediates and Pathways

6.3.1 Identification of Intermediates

To better understand the reaction mechanisms of DPA photodegradation, the identification of principal intermediates and studying their evolution were carried out. Using the LC-MS and ^{1}H-NMR analyses, up to 20 intermediate compounds were identified according to the mass ion ($[M+H]^+$, $[M-H]^-$) peaks and the characteristic proton patterns. Table 6-2 summarized these results along with the proposed structures for the detected intermediates. In summary, there are three principal groups of intermediates were identified: (i) intermediates 1–4 from the reactions relevant to only the *N*-methyl oxidation or loss; (ii) intermediates 5–11 from the reactions of the hydroxylation of the aromatic ring; and (iii) intermediates 12–20 from the N-demethylation, oxidation and ring opening.

Figure 6-3 depicts the aliphatic regions (5.35–5.70 ppm) of the 1D-NMR and 2D-COSY spectra of DPA solutions after the irradiation by direct UVC process for 1 h and by TNT/UVA process for 24 h, respectively. This is the time at which the DPA degradation exceeded 50% and the concentrations of its products were sufficient to be observed clearly in the NMR analysis. In Figure 6-3a, spectra B and C (treated DPA) display four new methine singlets at 5.64, 5.52, 5.49 and 5.43 ppm as compared to that of spectrum A (untreated DPA), only a strong methane singlet at 5.88ppm, which reflects the formation of four intermediates after the treatment of DPA solutions in either UVC or TNT/UVA system. In addition, their chemical shifts distribute at, respectively, attributing to the proton signal of methine group. In addition, 2D-COSY analysis was conducted in this study to allowed identification of

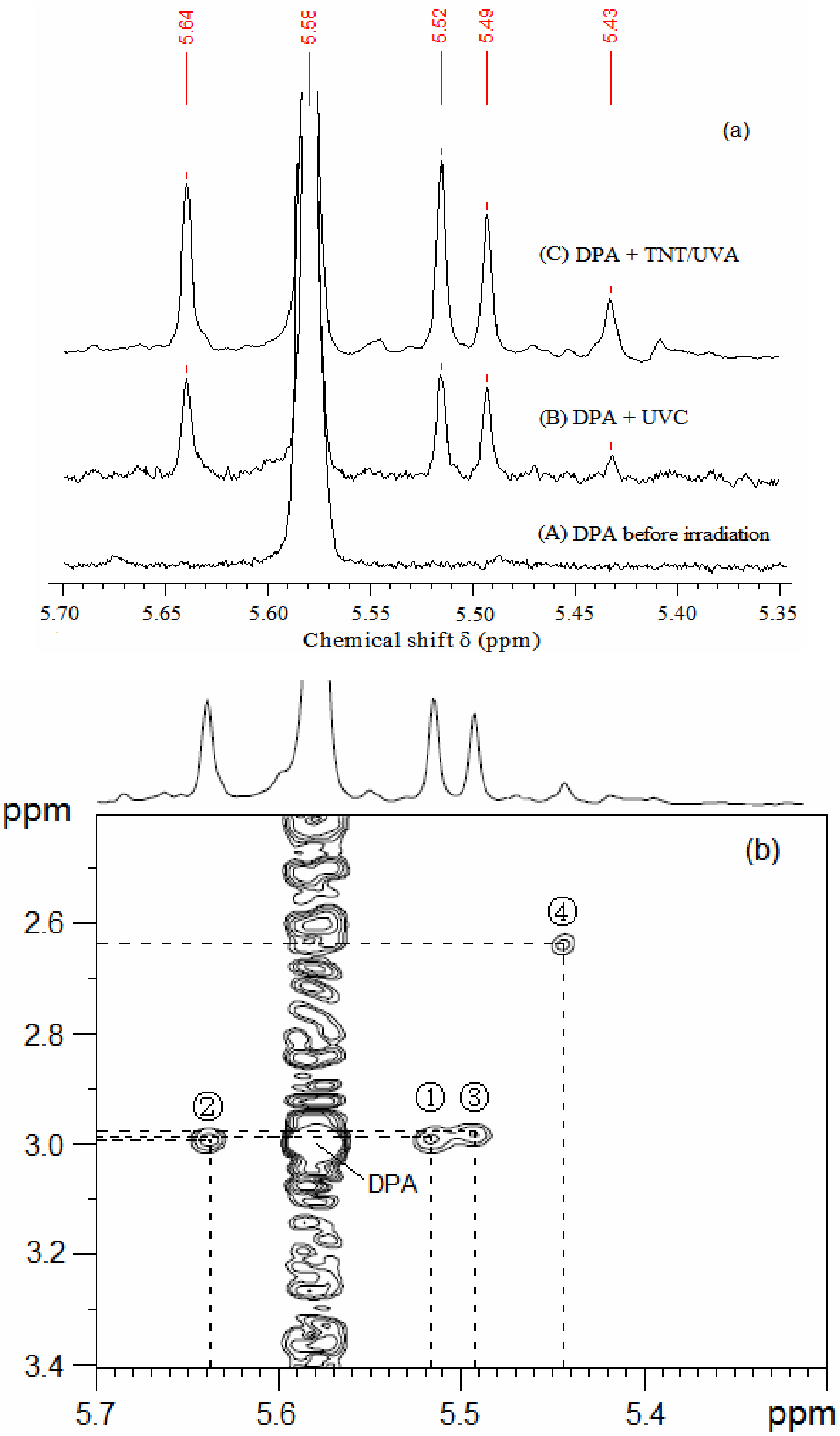

Figure 6-3. (a) 1D-^{1}H-NMR spectra of aqueous DPA solutions after treatment by UVC and TNT/UVA systems. (b) 2D-COSY spectra of proton signals of methine group in DPA and compounds 1–4 (treated by TNT/UVA system).

direct proton coupling information. Figure 6-3b shows the COSY spectrum of treated DPA solution in the region of 5.35–5.70 ppm (corresponding to the 1D spectrum shown in Figure 6-3a) against the methyl proton region of 2.5-3.4 ppm. Interestingly, correlation cross peaks were observed for all these methine resonances of the original DPA and new intermediates. The presence of these cross peaks, which correlates the methyl protons and methine protons, indicates that (1) the COSY method could detect the unusual long-range coupling interaction that extends to five bonds (^5J) shown in Scheme 1, which has been reported previously by Pavia et al. (2001) and (2) the methyl and methine groups must be present simultaneously in DPA and the intermediate molecules. The fact that they are chemically nonequivalent indicates that these four intermediates maintain the same methyl-N(R)-C(O)-CH- skeleton with some variations on the attaching groups.

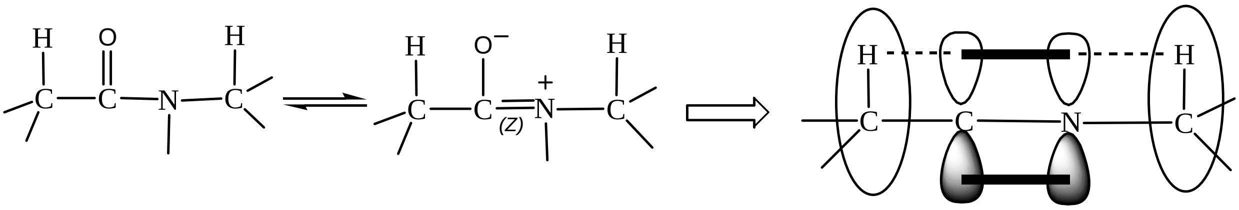

Scheme 6-1. Homoallylic coupling (^5J) in the DPA molecular structure.

Table 6-2. Products resulting from the direct UV and TNT-photocatalysed degradation of DPA by MS and ^{1}H-NMR analysis.

Compound No.	Structures[(a)]	MS data (m/z)	^{1}H-NMR data (δ, multiplicity[(b)], coupling constant)	Products of DPA degradation[(c)]	
				UVC	TNT/UVA

DPA	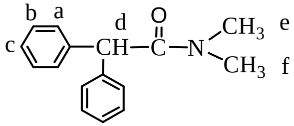	238 $(M-H)^{-}$
		240 $(M+H)^{+}$
		241 $(M+2H)^{++}$
			a: 7.22 (4H, d, J_{ab} = 8.56); b: 7.41 (4H, m);
			c: 7.35 (2H, t, J_{cb} = 7.18); d: 5.58 (1H, s);
			e: 3.04 (3H, s); f: 3.00 (3H, s)
				+	+

1	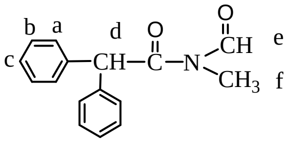	251 $(M-2H)^{--}$
		254 $(M+H)^{+}$
		255 $(M+2H)^{++}$
			a: 7.22 (4H, d, J_{ab} = 8.56); b: 7.41 (4H, m);
			c: 7.35 (2H, t, J_{cb} = 7.18); d: 5.52 (1H, s);
			e: 8.44 (1H, s); f: 3.11 (3H, s)
				+	+

2	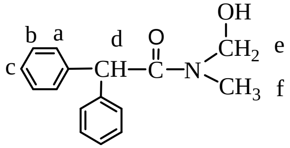	255 (M)
		256 $(M+H)^{+}$
		258 $(M+3H)^{+++}$
			a: 7.22 (4H, d, J_{ab} = 8.56); b: 7.41 (4H, m);
			c: 7.35 (2H, t, J_{cb} = 7.18); d: 5.64 (1H, s);
			e: 5.89 (2H, s); f: 3.04 (3H, s)
				+	+

3	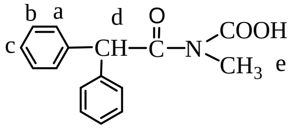	268 $(M-H)^{-}$
		270 $(M+H)^{+}$
		271 $(M+2H)^{+}$
			a: 7.22 (4H, d, J_{ab} = 8.56); b: 7.41 (4H, m);
			c: 7.35 (2H, t, J_{cb} = 7.18); d: 5.49 (1H, s);
			e: 3.08 (3H, s)
				+	+

4	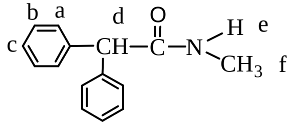	224 $(M-H)^{-}$
		226 $(M+H)^{+}$
		227 $(M+2H)^{++}$
			a: 7.22 (4H, d, J_{ab} = 8.56); b: 7.41 (4H, m);
			c: 7.35 (2H, t, J_{cb} = 7.18); d: 5.43 (1H, s);
			e: 7.51 (H, m); f: 2.99 (3H, d, J_{fe} = 4.05)
				+	+

5	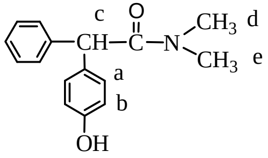	254 $(M-H)^{-}$
		256 $(M+H)^{+}$
		257 $(M+2H)^{++}$
			a: 7.10 (2H, d, J_{ab} = 9.11);
			b: 6.88 (2H, d, J_{ba} = 9.09);
			c: 5.58 (1H, s); d: 3.04 (3H, s); e: 3.00 (3H, s)
				trace	+

6	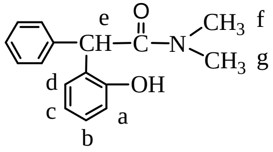	254 $(M-H)^{-}$
		256 $(M+H)^{+}$
		257 $(M+2H)^{++}$
			a: 6.91 (1H, d, J_{ab} = 8.79); b: 7.01 (1H, m);
			c: 7.01 (1H, m); d: 6.95 (1H, d, J_{dc} = 8.58);
			e: 5.58 (1H, s); f: 3.04 (3H, s); g: 3.00 (3H, s)
				trace	+

Table 6-2 (Continue)

Compound	Structures[(a)]	MS data	^{1}H-NMR data	Products of DPA degradation[(c)]	
No.		(m/z)	(δ, multiplicity[(b)], coupling constant)	UVC	TNT/UVA

7	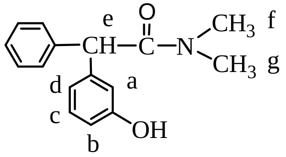	254 $(M-H)^-$
		256 $(M+H)^+$
		257 $(M+2H)^{++}$
			a: 6.71 (1H, s); b: 6.78 (1H, d, J_{bc} = 9.75);
			c: 7.09 (1H, m); d: 6.84 (1H, d, J_{dc} = 9.50);
			e: 5.58 (1H, s); f: 3.04 (3H, s); g: 3.00 (3H, s)
				trace	+

8[(d)]	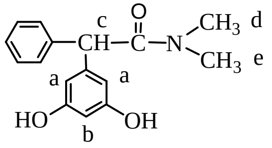	272 $(M+H)^+$ 273 $(M+2H)^{++}$ 274 $(M+3H)^{+++}$	a: 6.63 (2H, s); b: 6.57 (1H, s); c: 5.58 (1H, s); d: 3.04 (3H, s); e: 3.00 (3H, s)	–	trace
9[(d)]	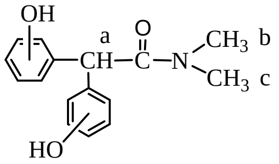	272 $(M+H)^+$ 273 $(M+2H)^{++}$ 274 $(M+3H)^{+++}$	a: 5.58 (1H, s); b: 3.04 (3H, s); c: 3.00 (3H, s)	–	trace
10[(d)]	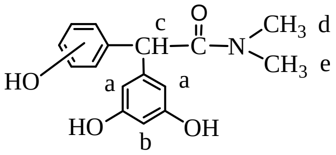	285 $(M-3H)^{---}$ 288 $(M+H)^+$ 290 $(M+3H)^{+++}$	a: 6.63 (2H, s); b: 6.57 (1H, s); c: 5.58 (1H, s); d: 3.04 (3H, s); e: 3.00 (3H, s)	–	trace
11[(d)]	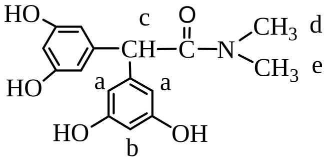	300 $(M-3H)^{---}$ 303 (M) 304 $(M+H)^+$ 306 $(M+3H)^{+++}$	a: 6.63 (2H, s); b: 6.57 (1H, s); c: 5.58 (1H, s); d: 3.04 (3H, s); e: 3.00 (3H, s)	–	trace
12[(d)]	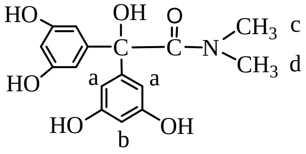	316 $(M-3H)^{---}$ 318 $(M-H)^-$ 322 $(M+3H)^{+++}$ 323 $(M+4H)^{++++}$	a: 6.63 (2H, s); b: 6.57 (1H, s); c: 5.58 (1H, s); d: 3.04 (3H, s);	–	trace
13[(d)]	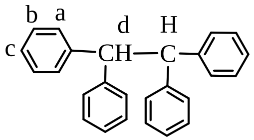	332 $(M-2H)^{--}$ 333 $(M-H)^-$ 336 $(M+2H)^{++}$	a: 7. 51(4H, d, J_{ab} = 8.22); b: 7.53 (4H, m); c: 7.45 (2H, t, J_{cb} = 8.14); d: 4.89 (1H, s);	+	–

Table 6-2 (Continue)

Compound No.	Structures(a)	MS data (m/z)	^{1}H-NMR data (δ, multiplicity(b), coupling constant)	Products of DPA degradation(c)	
				UVC	TNT/UVA
14(d)	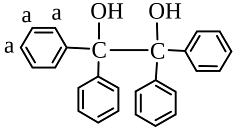	365 (M-H) 366 (M) $367\ (M+H)^+$	a: 7. 49 (5H,s)	+	–
15	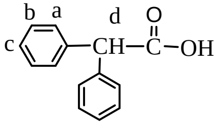	$211\ (M-H)^-$ 212 (M) $213\ (M+H)^+$	a: 7. 22 (4H, d, J_{ab} = 8.56); b: 7.41 (4H, m); c: 7.35 (2H, t, J_{cb} = 7.18); d: 5.12 (1H, s);	+	+
16	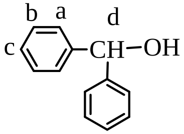	$183\ (M-H)^-$ 184 (M) $185\ (M+H)^+$	a: 7.39 (4H, d, J_{ab} = 8.02); b: 7.51 (4H, m); c: 7.47 (2H, t, J_{cb} = 8.81); d: 5.89 (1H, s);	+	+
17(d)	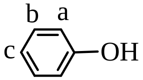	$93\ (M-H)^-$ 94 (M) $95\ (M+H)^+$	a: 6.85 (2H, d, J_{ab} = 6.54); b: 7.25 (2H, m); c: 6.99 (1H, t, J_{cb} = 7.55)	trace	trace
18	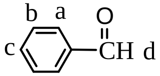	$105\ (M-H)^-$	a: 7.89 (2H, d, J_{ab} = 9.24); b: 7.51 (2H, m); c: 7.74 (1H, t, J_{cb} = 8.31); d: 9.34 (1H, s);	+	+
19	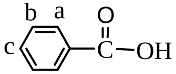	$121\ (M-H)^-$ 122 (M) $123\ (M+H)^+$	a: 8.16 (2H, d, J_{ab} = 9.20); b: 7.67 (2H, m); c: 7.49 (1H, t, J_{cb} = 8.12);	+	+
20(d)	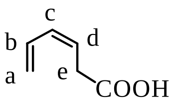	$111\ (M-H)^-$ 112 (M) $113\ (M+2H)^{++}$	a: 5.83 (2H, d, J_{ab} = 8.91); b: 6.15 (1H, m); c: 6.44 (1H, m); d: 5.97 (1H, m); e: 3.38 (2H, d, J_{ed} = 3.85);	+	–
21(d)	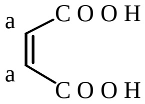	$115\ (M-H)^-$ $118\ (M+2H)^{++}$	a: 6.36 (2H, s)	–	+

(a) Different protons linked on molecular structures are marked as a, b, c, d, e and f, respectively.

(b) Singlet, doublet, triplet, and multilet are abbrivated as s, d, t and m, respectively; coupling constants (*J*) are given hertz.

(c) –, absence; +, presence.

(d) Identified in organic extracts only. The NMR spectra of organic extracts were not showed in the present paper.

Combining the information provided by chemical shift, integration, J coupling and multiplicity as well as MS data, the four intermediates can be identified as compounds 1–4 arising from oxidation or removal of terminal N-methyl group in DPA molecule.

Besides, other four types of cross peaks, similar to the nature of DPA molecule, were also observed in this COSY spectrum. They are nonequivalent, probably owing to the nuclear magnetization effect of the methyl neighbor group. Therefore, combining the specifical proton information with corresponding MS data, the four intermediates can be identified as compounds 1–4 arising from oxidation or removal of terminal N-methyl group in DPA molecule, simultaneously appearing in the UVC photolysis and TNT/UVA photocatalysis processes.

The second category of products (compounds 5–11) includes various phenolic compounds resulting from the hydroxylation of benzene ring during the UVC and TNT/UVA processes. Although MS data provided important information on the molecular weight, several positional isomers such as compounds 5, 6 and 7 could not be discriminated by MS analysis alone. Therefore, ^{1}H-NMR was used to get complementary information and, particularly, to localize the position of hydroxyl group on the benzene ring of these isomers. Since the chemical shift of ortho-proton of most phenolic compounds is 6.0–7.0 ppm in many literatures (Limiroli et al., 1996; Es-Safi et al., 2000), the evolution of main products belonging to this group is represented on the NMR spectra in the region of 6.0–7.2 ppm (see Figure 6-4).

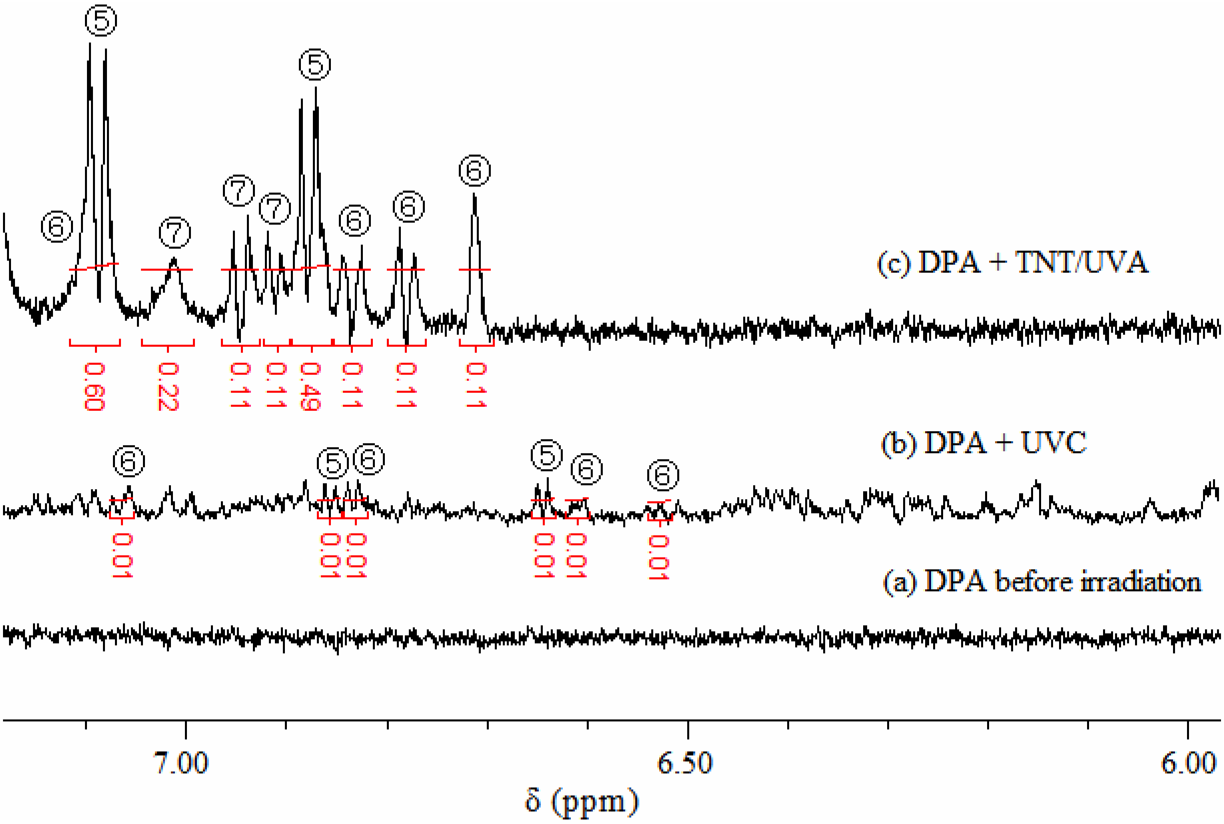

Figure 6-4. Relevant region of ^{1}H-NMR spectra of DPA (a) and its hydroxylation products 5, 6 and 7, obtained by UVC (b) and TNT/UVA (c) treatments.

It can be clearly observed that some strong proton signals occurred in the spectrum c. According to the mass of 256 m/z, compounds 5, 6 and 7 would be recognized with the mono-substitution by OH in the para-, ortho- and meta-position, respectively. While compounds 6 and 7 had the same concentration level, compound 5 showed the higher concentration level of about 4.5 times than that of 6 and 7. This result indicates that compound 5 is a major hydroxylated product from the DPA degradation by TNT/UVA due to the regioslective attack of •OH. This can be explained by the electron density of the benzene carbon sites and the steric hindering effects of the benzene ring substituents ($–CHCON(CH_3)_2$), where the para-position is more nucleophilic and accessible than the other two positions at ortho and meta orientation. In contrast, spectrum b in Figure 6-4 shows very low proton signals of compounds 5 and 6, indicating that the hydroxylation of benzene ring in DPA structure is not a dominating process by direct photolysis under UVC irradiation. It should be noted that the difference in chemical shifts of compounds 5 and 6 in both spectra b and c resulted from the effect of different final pH, such as pH 6.47 in the direct photolysis but pH 5.56 in the photocatalysis. Water samples were extracted by chloroform to concentrate the organics for further analysis. As a result, it was identified that some multi-hydroxylated products (compounds 8–12, n_{OH} = 2–5) appeared in the TNT/UVA process but not in the UVC process when corroborating with their mass ion peaks in MS spectra. (The NMR spectra of organic extracts are not presented in this paper.)

The third category of intermediates includes compounds 13–21. Among them, compounds 13 and 14 exhibited very high molecular mass (m/z = 334 and 366, respectively), indicating that they probably resulted from the reactions of dimerization under UVC irradiation. This hypothesis was supported by the absence of these compounds in the DPA degradation with TNT/UVA. In corroboration with the proton signals obtained from 1D- and 2D-NMR spectra, compounds 13 and 14 were identified as 1,1,2,2-tetraphenylethane and 1,1,2,2-tetraphenyl-1,2-ethanediol, respectively. Compound 15 showed a mass value of m/z = 212, corresponding to the removal of one N-dimethyl group and the addition of one OH group. With a $[M+H]^+$ quasimolecular mass of 185, compound 16 corresponds the CO removal of 15. Although the three proton signals from aromatic ring (δ = 7.39–7.51 ppm), are overlapped partially by the signals of other compounds, the characteristic proton signal from methine group (CH(OH), 5.89 (1H, s)) also support that compound 16 should be benzhydrol. Compounds 17 and 18, with a $[M-H]^-$ quasimolecular mass of 93 and 105 respectively, probably resulted from the scission fragments of compound 16, where the hydroxylation of phenyl fragment led to 17 and the carbonylation of benzyl fragment gave rise to 18. Compound 18 was further identified as benzaldehyde when corroborating with the proton signals in NMR spectra (a: 7.89 (2H, d, J_{ab} = 9.24); b: 7.51 (2H, m); c: 7.74 (1H, t, J_{cb} = 8.31); d: 9.34 (1H, s)). This compound, in general, will readily undergo the oxidation to benzoic acid when exposed to air. Thus, benzoic acid (compound 19) with a $[M+H]^+$ mass of m/z = 123 was also identified. Likewise, compounds 20 (m/z = 112) and 21 (m/z = 116), resulting from the oxidative opening of the aromatic ring, were identified as hexa-3,5-dienoic acid and maleic acid, respectively.

6.3.2 Degradation Pathways

Figure 6-5 illustrates the proposed pathways of DPA degradation by UVC irradiation alone, which may not include every possible reaction but covering the main processes according to the identified products. The major decay pathways include N-methyl oxidation and removal, scission of the N-CO or C-CO bond, dimerization and ring opening. The results have been compared to those from previous research with analogous degradation mechanisms such as tyrosine, phenylthioacetic acid and phenylurea derivatives photolysis (Jin et al., 1995; Filipiak et al., 2006), which supported our findings in this study. For specific intermediates, compound 1, arising from N-methyl oxidation, is considered to be a major primary intermediate in the

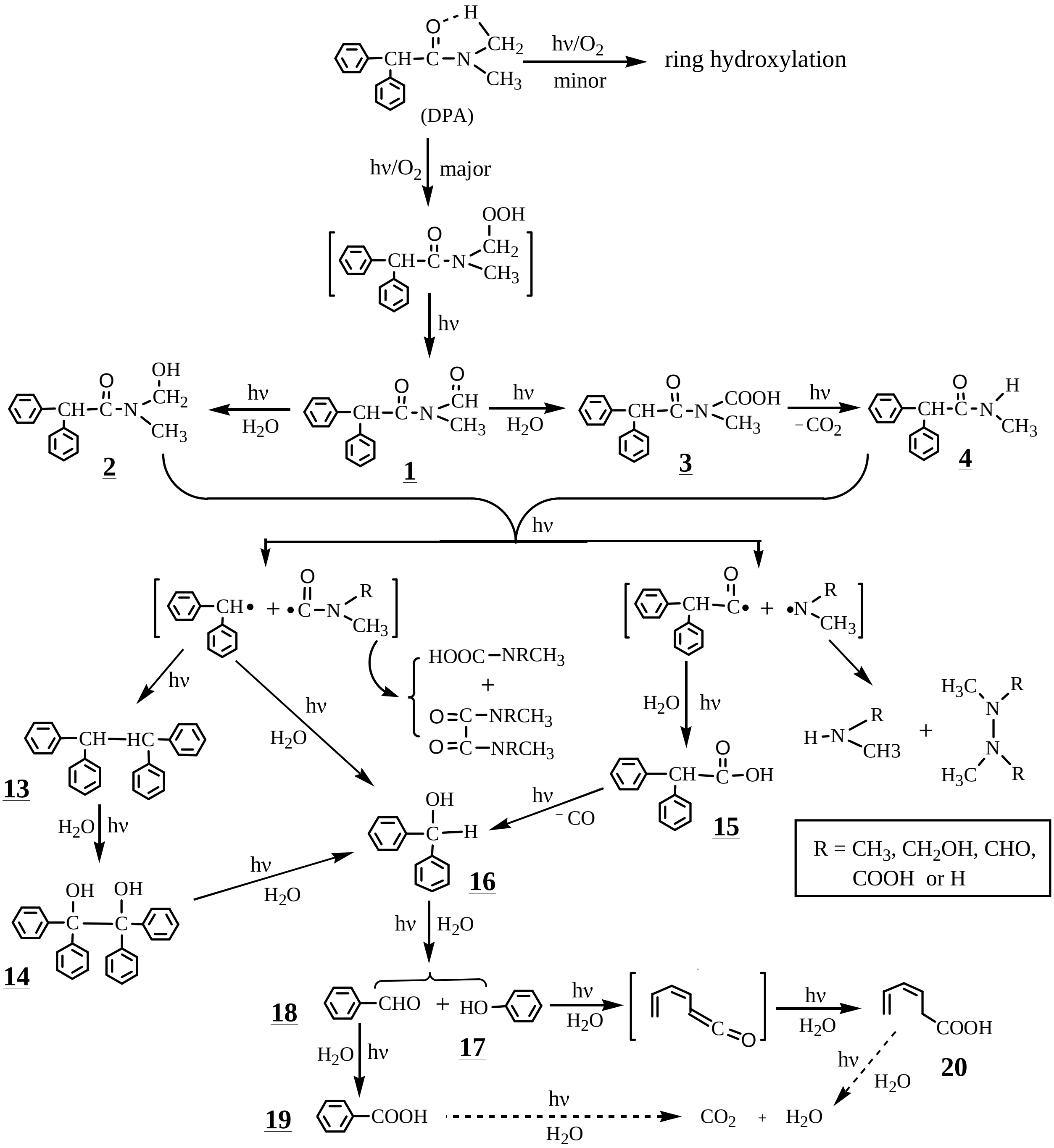

Figure 6-5. Proposed pathways of the DPA degradation by direct UVC-photolysis.

process (see Figure 6-3). The oxidation of terminal methyl group involves an intramolecular hydrogen bond between N-methyl and carbonyl groups in the excited state (Jirkovský et al., 1997), and then reacts with dissolved molecular oxygen to form formylated product [–N(CH_3)CHO]. This indicates the key role played by the photoexcited oxygen species in this case and the formation of the formylated product by oxidation of the *N*-methyl group was the major reaction observed. The subsequent reduction and further oxidation of compound 1 gave rise to products 2 and 3, in which compound 3 easily underwent the decarboxylation to yield 4 via photo-kolbe reactions (Krautler and Bard, 1978; Tahiri et al., 1998). The evolution profiles of compounds 1–4, as shown in Figure 6-3, offer useful information in supporting this pathway. On the other hand, no obvious products coming from further oxidation of the second N-methyl group were detected in our LC-MS and ^{1}H-NMR spectra. Despite hydroxylated products 5 and 6 were detected, the fact that they only existed at trace levels (see Figure 6-4) and implies that hydroxylation of aromatic ring was not a major pathway in the UVC photolysis process.

It is known that a 254 nm photon has an equivalent energy of 4.89 eV, which should be energetic enough to produce homolytic or heterolytic breakages in the molecules (Litter, 2005). Direct irradiation leads to the promotion of a molecule from the ground state to an excited state. Such excited states can undergo homolysis or heterolysis, among other processes. Therefore, it can be expected that further photolysis bond scission could take place, followed by radical recommendation or H-/(HO-) abstracting from water solvent. For instance, scission of the N-CO bond leads to yield the diphenylacetic acid (compound 15) while scission of the C-CO bond gives benzhydrol (compound 16) as a major intermediate and trace amount of compound 13.

Upon UVC irradiation, the cleavage of compound 16 can produce small molecules such as phenol (17) and benzaldehyde (18), where benzaldehyde can easily undergo further oxidation to form secondary intermediate benzoic acid (19) and phenol trends to undergoing the ring opening to form product 20. The observed product 20, belonging to an aliphatic polyene acid, could be transformed into CO_2 and H_2O. A similar pathway for phenol degradation by photolysis was proposed by Jin et al. (1995).

The mechanism of TiO_2 photocatalytic oxidation process has been discussed extensively and widely accepted that the •OH radicals act as primary oxidizing species causing the decomposition of organic pollutants. The reaction of these species with organic matter is fast and nonselective, due to the high oxidation potential. In the heterogeneous photocatalysis, hydroxylation of the aromatic ring and oxidation of the terminal N-methyl group seem to be the most frequently observed primary processes, as shown in Figure 6-6. Actually, Amine-Khodja et al. (2002) had identified substitution of chlorine or methoxy groups by hydroxyl on the ring and oxidation of N-methyl groups or N-demethylation on the urea moiety as the main reactions occurring in the heterogeneous photocatalytic degradation of metoxuron over illuminated TiO_2 semiconductor particles. In this study, the oxidation of N-methyl groups and N-demethylation on the urea moiety of DPA were also observed, as shown in Figure 6-7. These reactions were conducted through attack by hydroxyl radicals and reaction with oxygen. Like the DPA photolysis, the photocatalytic process also yielded four major products 1-4, which may be ascribed to the formation of intramolecular hydrogen bonding (C=O· · ·H) in DPA and then undergoes the attack of hydroxyl radicals. Actually, the 1-4 products of N-methyl oxidation and N-demethylation have also been reported as the main species formed in the photocatalytic transformation of diuron (Krýsová et al., 1998) and metoxuron (Khodja et al., 2002).

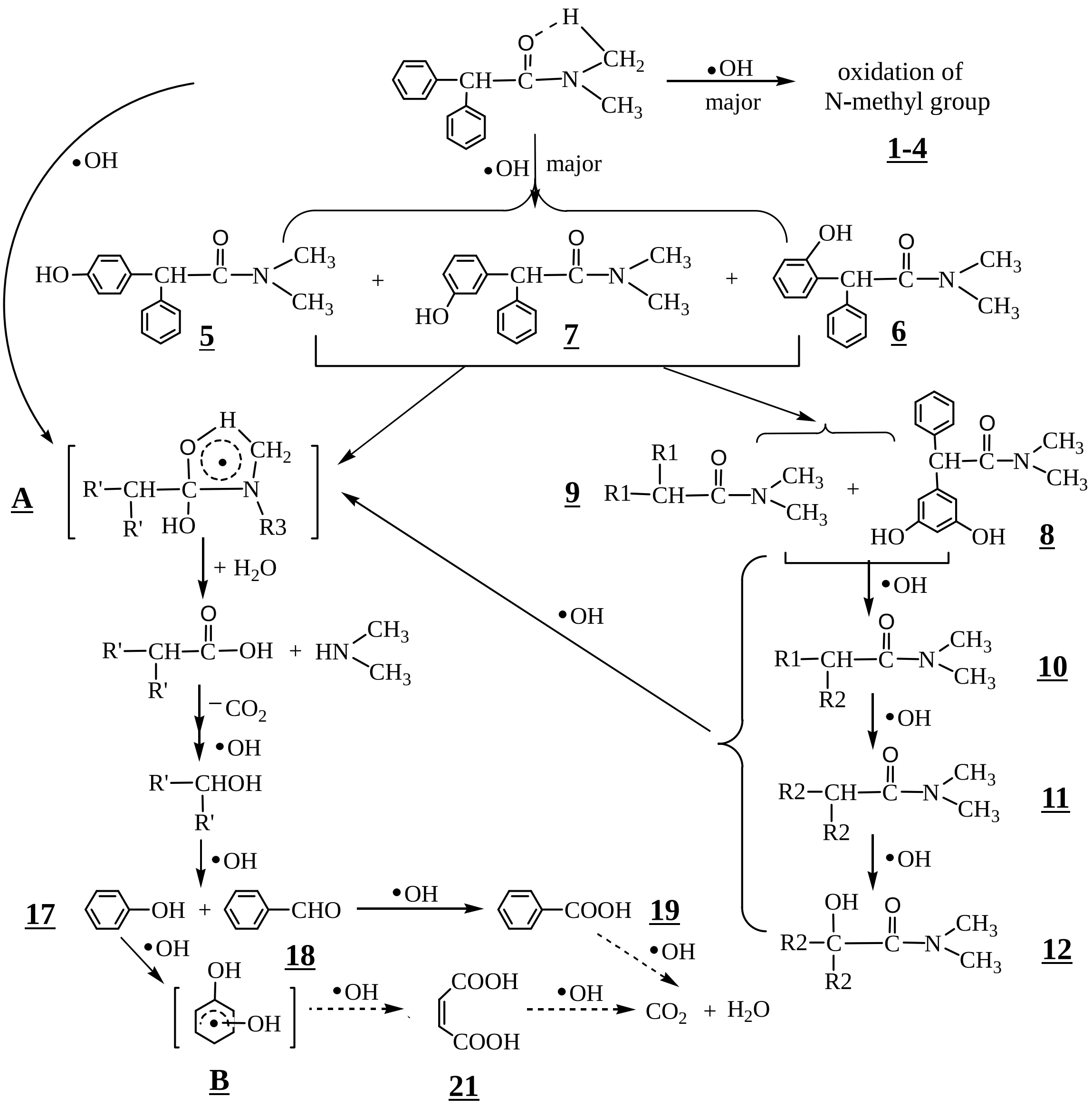

Figure 6-6. Proposed pathways of the DPA degradation by TNT/UVA-photocatalysis. Here, R1 is p- or m-phenolic ring; R2 is 3,5-diphenolic ring; and R' includes benzene ring of R1 and R2.

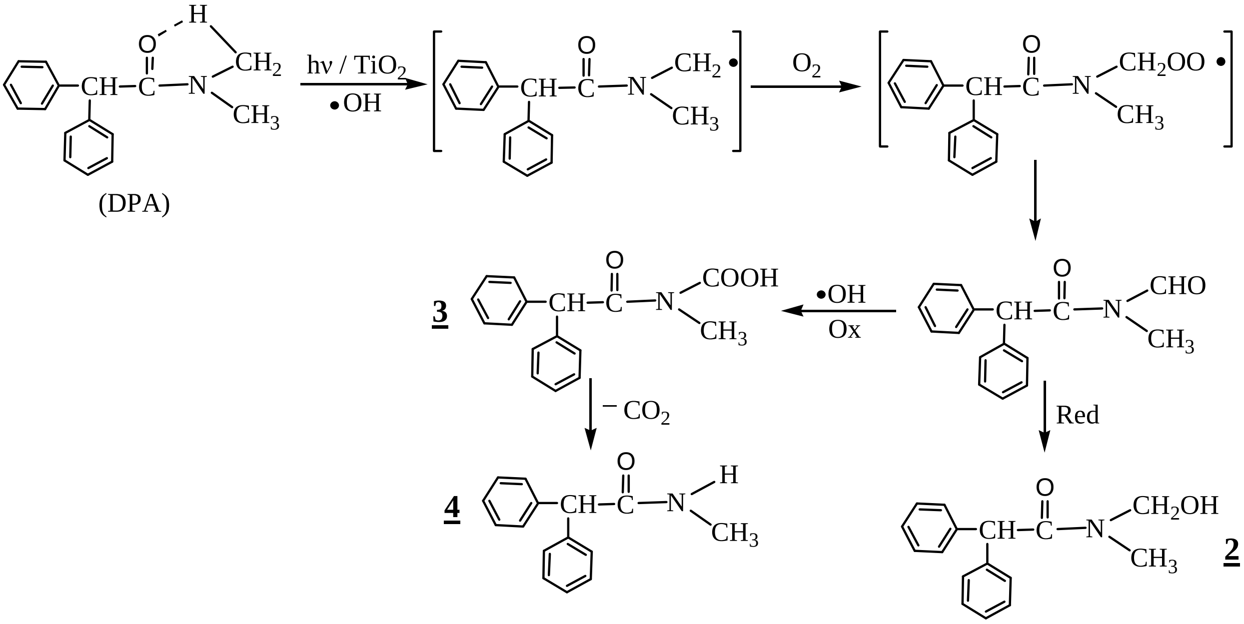

Figure 6-7. Mechanism of oxidation of N-methyl group in DPA molecules during the photocatalytic process.

A second target is the hydroxylation of aromatic ring. In this study, three isomeric ring-hydroxylation products (compounds 5, 6 and 7) were observed as major photoproducts, as shown in Figure 6-7. They were identified as the phenolic compounds mono-substituted by OH in para-, ortho- and meta-position, respectively, suggesting that the aromatic ring has an electron-donating effect, due to the electrophilicity of hydroxyl radicals. Among them, isomer 5 shows the highest concentration level, followed by isomers 6 and 7. These results indicate that monohydroxylation of aromatic ring with corresponding H abstraction by •OH attack not only is a major reaction step in the photocatalytic process but also takes place regioselectively on the aromatic ring. When further •OH attack, its subsequent reaction with oxidizing species yielded the multihydroxylated intermediates (compounds 8–12), such as di-, tri-, tetra- and quint-substitution phenolics. However, they had a low concentration, which reveals that the multihydroxylation reaction might occur as a minor route in the photocatalytic degradation of DPA. Further steps cause loss of dimethylamine to give the observed carboxylic acid derivative 15, followed by decarboxylation and to form compounds 17 and 18. These steps were also observed in the UV photolysis process.

The opening of the benzene ring after oxidation/hydroxylation yields maleic acid (compound 21). The ring opening possibly involves •OH attack to cleave the ring. It should be noted that the formation of maleic acid 21 in the photocatalytic process is different from the alkylcarboxylic acid 20 detected in photolytic reaction. This is possibly due to the formation of a hydroxycyclohexadienyl radical in photocatalysis process (e.g. radical B in Figure 6-6), confirmed by Aceituno et al. (2002). Based on the above analysis, the distribution of the main products reveals the essential natures of direct photolysis involving excited-state species and photocatalysis involving •OH radicals.

6.4 Summary

A detailed study on the DPA degradation by direct photolysis and photocatalysis indicates that DPA degradation under UVC illumination was achieved to a high degree with low level of mineralization, while the treatment with TNT/UVA revealed a lower degree of DPA degradation but with a relatively higher degree of mineralization. In this study, more than 20 intermediates were identified through LC-MS and ^{1}H-NMR analyses and the possible pathways of DPA degradation by direct photolysis and photocatalysis were proposed based on the indentified intermediate products and the main reactions involved. These results provide useful information to better understand the reaction mechanism of DPA degradation by direct photolysis and photocatalysis. These results provide useful information to better understand the reaction mechanism of DPA degradation by direct photolysis and photocatalysis.

Chapter 7 – Visible-induced Photocatalysis with Polymer-sensitized TiO_2 Nanotube Films

7.1 Introduction

Polythiophene and its derivatives, a kind of sulfur-containing conjugated polymer, are photochemically and thermally stable under photoirradiation, which have been often used as sensitizers in polymer-sensitized TiO_2 photovoltaic devices (Yanagida et al., 2004; Zafer et al., 2005). Furthermore, they have also been used as catalysts to degrade organic pollutants in the environment (Wen et al., 2000). Besides, it is interesting that the polythiophene and its derivatives do not undergo degradation under UV radiation in the presence of TiO_2, which has been widely confirmed in literature (Wen et al., 2000; Muktha et al., 2007; Song et al., 2007). In the present study, we therefore chose polythiophene as a photosensitizer to be attached on the anodic TiO_2 nanotube films through an electropolymerization technique and thereby investigated the photocatalytic reactivity of polythiophene-TiO_2 composites under visible light irradiation. The roles of polythiophene layers on TiO_2 nanotubes and the effects of various factors on the sensitized photoactivities were also studied with details. This study aims to utilize the ability of polymer sensitization by visible light and provide better understanding of the mediated electron-transfer process and interactive oxidation reaction of the functionalized polymer/TiO_2 composites.

7.2 Characterization of PTh/TNT Photocatalysts

7.2.1 Morphology and Elemental Composition

The morphology and elemental composition of as-formed TNT and PTh/TNT films were first examined by FESEM and EDX analyses and the results are shown in Figure 7-1. From the SEM image of TNT film in Figure 7-1a1, it can clearly be observed that the highly ordered and perforated porous TNT arrays with a wall-thickness of ~12 nm and a tube length of ~350 nm are well formed on the Ti substrate. When viewed from an angle perpendicular to the surface, the TNT arrays appear to be highly-uniform tubular, and their tube mouths are open and smooth. The EDX spectrum of the TNT film in Figure 7-1a2 showed two signals of Ti (K_α and K_β) at 4.51 and 4.93 keV, respectively, and also two additional signals of a L_α peak of Ti and a K_α peak of O at 0.53 KeV. In addition to the above peaks, no peaks representing other elements were detected in the EDX analysis and XPS spectra (not shown here). These results indicate that the anodic TNT films prepared in this study consisted only of Ti and O but no other elements, such as N, F or S existing in the

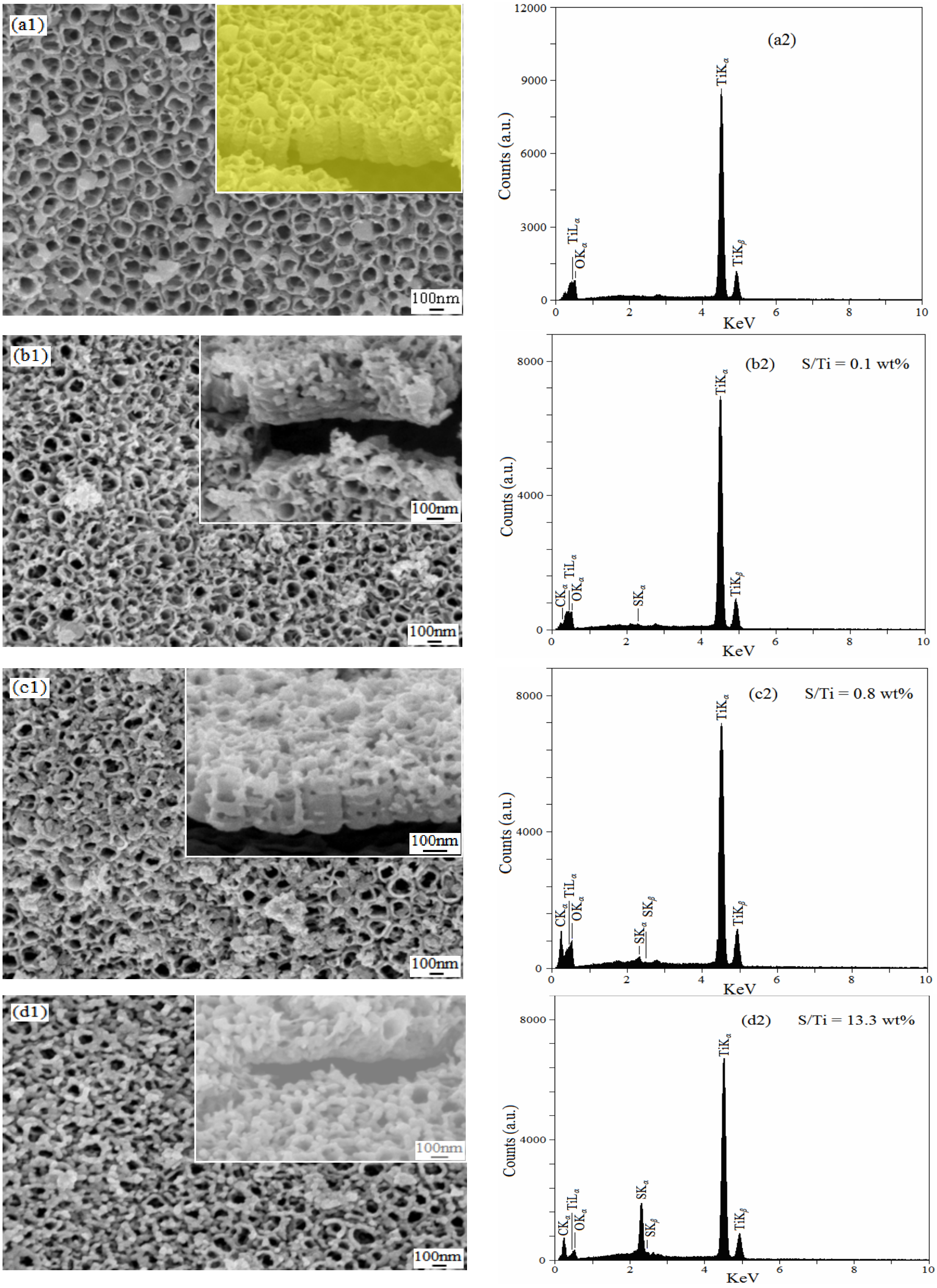

Figure 7-1. FESEM images of TNT and its composites: (a1) TNT; (b1) PTh1/TNT; (c1) PTh3/TNT; and (d1) PTh5/TNT; (a2), (b2), (c2) and (d2) are their corresponding EDX spectra, respectively.

electrolyte solution, were doped into the lattice of TiO_2 in the low-voltage anodization process. Figure 7-1b-d shows the SEM images and EDX spectra of PTh1/TNT, PTh3/TNT and PTh5/TNT composites, respectively. It was observed that unlike the pure TNT film, the polythiophene layer formed on TNT substrate yielded the rough pore mouth and also some disordered aggregates on the wall surface of the TNT arrays (b1). Comparing three composites (PTh1/TNT, PTh3/TNT and PTh5/TNT), it can be found that the higher strength of thiophene in the electrolyte BFEE solution formed the thicker polythiophene layer with its extension to the top and inner wall of TiO_2 nanotubes (see c1 and d1). This phenomenon might result from the higher current density through the electrolyte solution, since a fixed potential was applied at 1.3 V (vs. SCE). Current-time response curves for the polymerization of thiophene at different monomer concentrations are shown in Figure 7-2. These curves demonstrated a same pattern that current density varied violently initial time and gradually stabilized to approach a plateau, which is similar to other earlier reports (Hillman and Mallen, 1987; Miller et al., 1987). It can be seen that the stabilized current density was higher with the higher concentration of monomer (5 mM). The relevant behaviour for the current as a function of time has been described in metal deposition (Horwood, 1985).

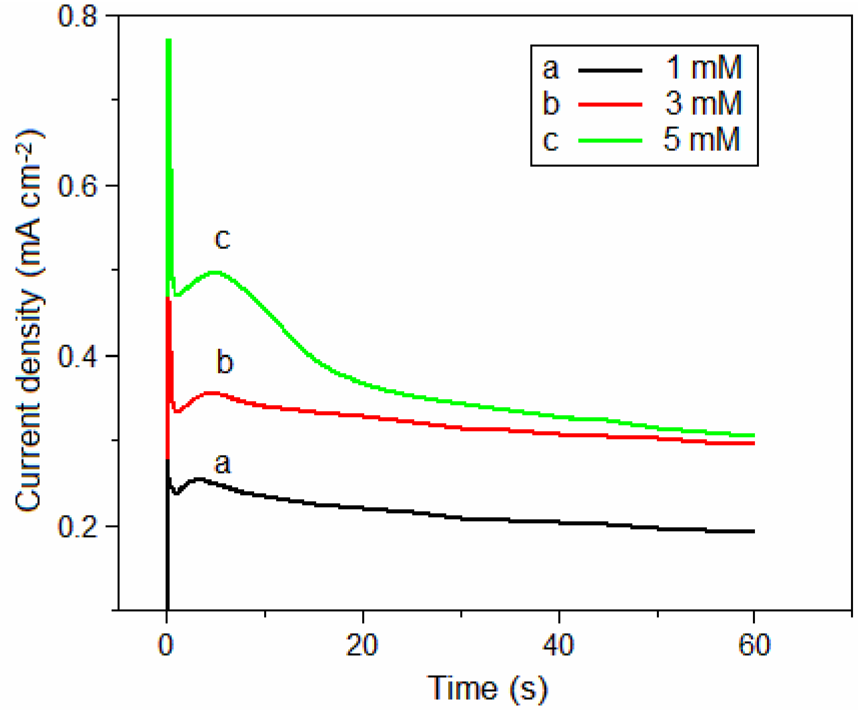

Figure 7-2. The current density-time transients for the polymerization of thiophene under the constant potential of 1.3 V. Curves a, b and c corresponding to 1, 3 and 5 mM thiophene in BFEE solution.

During the electropolymerization of thiophene, the dissolved species of monomer or short oligomers are first transferred to radical cations and two radical cations can combine to form an unstable dehydrogenated dication, which then release protons to form a longer oligomer chain (see Scheme 7-1). In this case, the electrodeposition of polythiophene is similar to that of the metal deposition mentioned above, in which it proceeds through a nucleation and growth pathway. This mechanism has been confirmed by Hillman's group (1987) using potentiostatic steps. Their data indicated that a bulk film was formed by the instantaneous nucleation and three-dimensional growth of polymer on top of this monolayer. Rate constants for growth parallel to the surface on substrate and the covering polymer layer were very close. Within a narrow potential range, the observation of maxima and minima in current-time transients was interpreted in terms of the “death” and “rebirth” of growing centres. Through layer-by-layer deposition, therefore, it is possible to manufacture films with a thickness of limited number of monolayers, which may find important and useful technology.

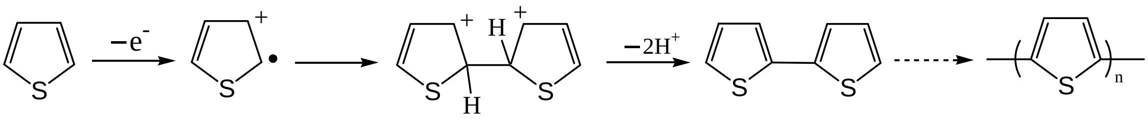

Scheme 7-1. Mechanism of thiophene electropolymerization.

EDX analysis revealed the chemical composition of the three PTh/TNT composites (PTh1/TNT, PTh3/TNT, and PTh5/TNT) as shown in Figure 7-1 (b2, c2 and d2), respectively. Similar to the TNT sample, the three composites exhibit the strong K diffraction peaks at 4.51, 4.92 and 0.52 keV, corresponding to the elemental Ti and O, respectively. At the same time, two new diffraction peaks at 0.28 and 2.31 keV also appeared in their EDX spectra, corresponding to the elemental C and S. An approximate ratio of S/Ti was estimated for each sample, according to the integral areas of the characteristic peaks for both elements. The spectra indicate that the ratios of S/Ti in the three PTh/TNT composites are approximately 0.1, 0.8 and 13.3 wt%, respectively. These results therefore reflect the feasibility of the chemical modification of polythiophene molecules for nanotubular TiO_2 films, and the amount of polythiophene coated is significantly dependent on the concentration of monomer used in the electrolyte solution.

7.2.2 XRD and XPS Characterization

The XRD patterns of the Ti foil, TNT, PTh1/TNT, PTh3/TNT and PTh5/TNT samples are shown in Figure 7-3. The pure TNT calcined at 500 ^{o}C had characteristic peaks at 25.35^{o} (101), 27.5^{o} (110), 36.1^{o} (101), 48.1^{o} (200), 54.3^{o} (211) and 69.8^{o} (220). According to the indexation of peaks, the TNT film calcined at 500 ^{o}C mainly contains anatase and rutile phases. These results have been presented in Chapters 4 and 5. For the PTh1/TNT composite, it can be seen that the peak intensity of rutile quickly decreases and the anatase peak at 2θ = 25.35^{o} becomes smaller and broader compared to that of the TNT film. A more critical trend can be confirmed for the two samples of PTh3/TNT and PTh5/TNT as with the increased amount of polythiophene: the diffraction peak of anatase (101) became smaller and broader, and peaks attributed to rutile phase (110) disappeared completely. This was most likely because the amorphous state of the polythiophene polymer deposited on/in TNT attenuated the characteristic diffraction of TNT, thus affecting the detection of the crystal diffraction of TNT film. As a result, it should be noted that the presence of polythiophene has a significant effect on the TiO_2 crystalline structure observed in the pure TNT film.

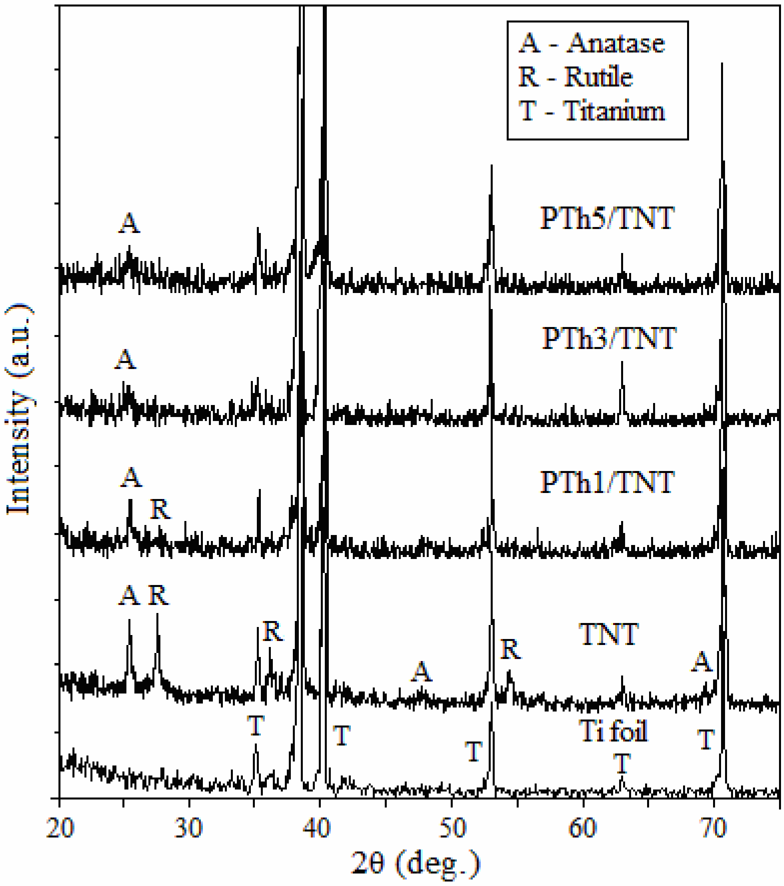

Figure 7-3. XRD patterns of Ti foil, pure TNT and PTh/TNT composite films.

Table 7-1 shows the binding energies of S 2p and Ti 2p obtained from their high resolution XPS spectra. Obviously, the binding energies of S 2p for the pure polythiophene film (peeled off from the PTh/ITO samples) can be deconvoluted into three peaks (Figure 7-4a) centred at 163.32, 164.41 and 167.57 eV. The first two peaks are assigned to the neutral S $2p_{3/2}$, and the oxidized S $2p_{1/2}$. With these results it is possible to quantitatively separate the oxidized thiophene sulfur species from total thiophene sulfur species according to the areas of two sulfur peaks. In the pure PTh sample, about 45% fraction of thiophene contains the oxidized sulfur. The third peak (at 167.57 eV) is associated with the formation of positively charged sulfur ($S^{\delta+}$) (Takemura et al., 1999). This positive charge is consistent with the formation and transport of polarons and bipolarons in the conductive grafted polythiophene chains.

Table 7-1. Binding energy of Ti and S elements in obtained samples.

Sample	Ti $2p_{3/2}$ [eV]	Ti $2p_{1/2}$ [eV]	S $2p_{3/2}$ [eV]	S $2p_{1/2}$ [eV]
TNT	459.48	465.17	–	–
PTh	–	–	163.32, 167.57	164.41
PTh3/TNT	459.15	464.83	163.69, 168.28	164.89
PTh5/TNT	458.88	464.56	163.58, 167.82	164.74

However, its content in total thiophene sulfur species is only about 6%, much less when compared to the first two peaks. This result indicates that the neutral and oxidized sulfur species were mainly produced in the polymer backbone when thiophene monomer was electropolymerized at 1.3 V for 1 min. The XPS peaks of S 2p in PTh3/TNT (Figure 7-4b) can also be deconvoluted into three peaks as well as that of the polythiophene film, while the higher binding energy (163.69, 164.89 and 168.28 eV) is observed. This result indicates the strong interaction between polythiophene and titania through electron transfer from polythiophene to titania, or the formation of bonding between sulfur and oxygen (Takemura et al., 1999). While the PTh3/TNT and PTh5/TNT composites showed a similar pattern of their composition, the PTh5/TNT composite showed a higher ratio of S/Ti and also a higher level of the positively charged sulfur. In contrast, a small shift to the lower value of the Ti 2p binding energies of three composites occurs as compared to that of the TNT sample. This also reflects the strong interaction between S sites of polymer backbone and TiO_2 nanotubes, in which electron transfer from polythiophene to titania takes place. From the results of FESEM, XRD and XPS analyses, it can be confirmed that the PTh/TNT composites were successfully formed by this two-step electrochemical process.

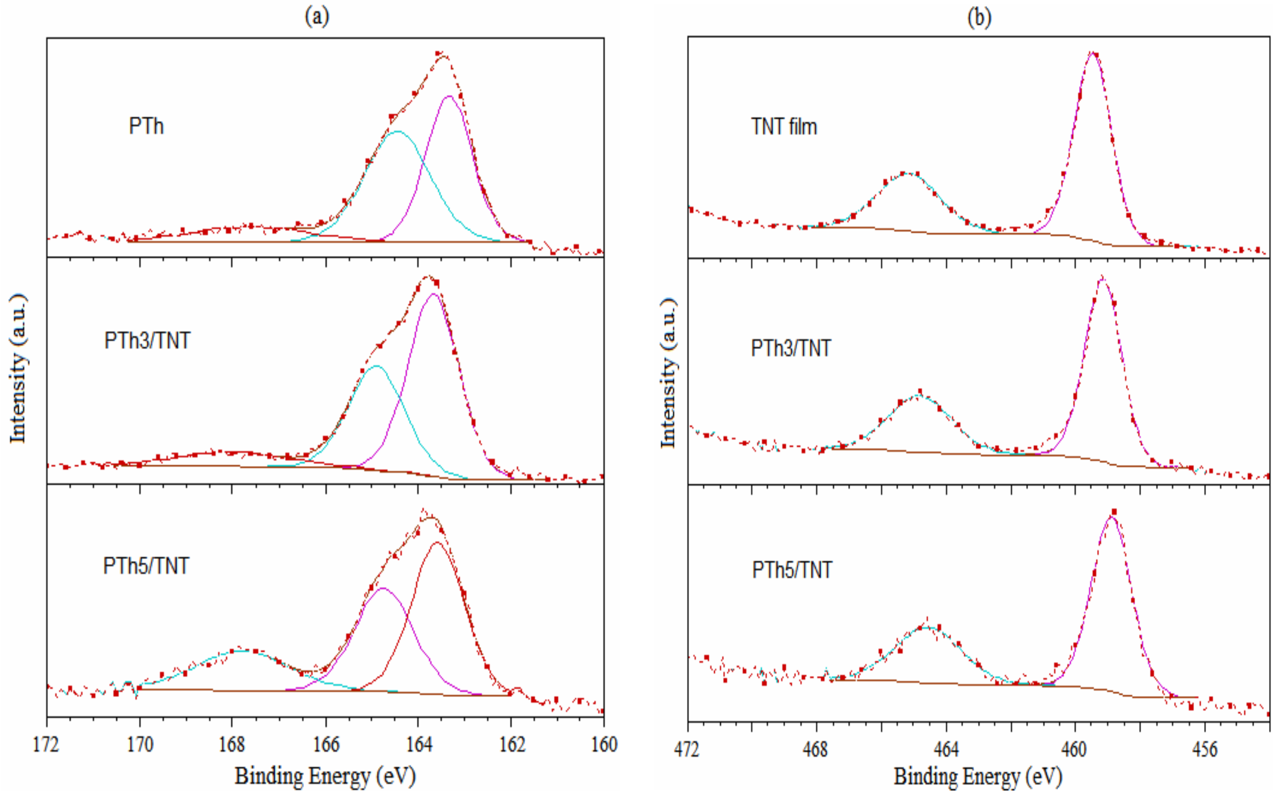

Figure 7-4. (a) XPS S 2p spectra of pure PTh and PTh/TNT composites; (b) XPS Ti 2p spectra of pure TNT film and PTh/TNT composites. Dot line: experimental curve; Solid line: deconvolution curve (the XPS spectrum of PTh1/TNT is not listed here due to the insufficient amount of S/Ti, which could result in inaccurate data).

7.2.3 Optical Properties

The optical properties of the as-prepared samples were studied by measuring their UV-Vis absorption. Figure 7-5 shows the UV-Vis absorption spectra of PTh, TNT and PTh/TNT composites where the as-prepared PTh/ITO sample was placed in the reference beam to measure the UV-Vis absorption of PTh film. The spectrum of

PTh/ITO (curve a) shows a broad absorption band from 350 to 650 nm with its maximum absorption at ~500 nm, which is attributed to π-π* (HOMO-LUMO) transition of the polythiophene backbones. It has been reported that the large π-conjugated systems of polythiophene can create small π-π* energy gaps within the visible spectrum (Vu et al., 2005). The width of absorption band indicates the coexistence of both long and short effective conjugation lengths in the polythiophene chains.

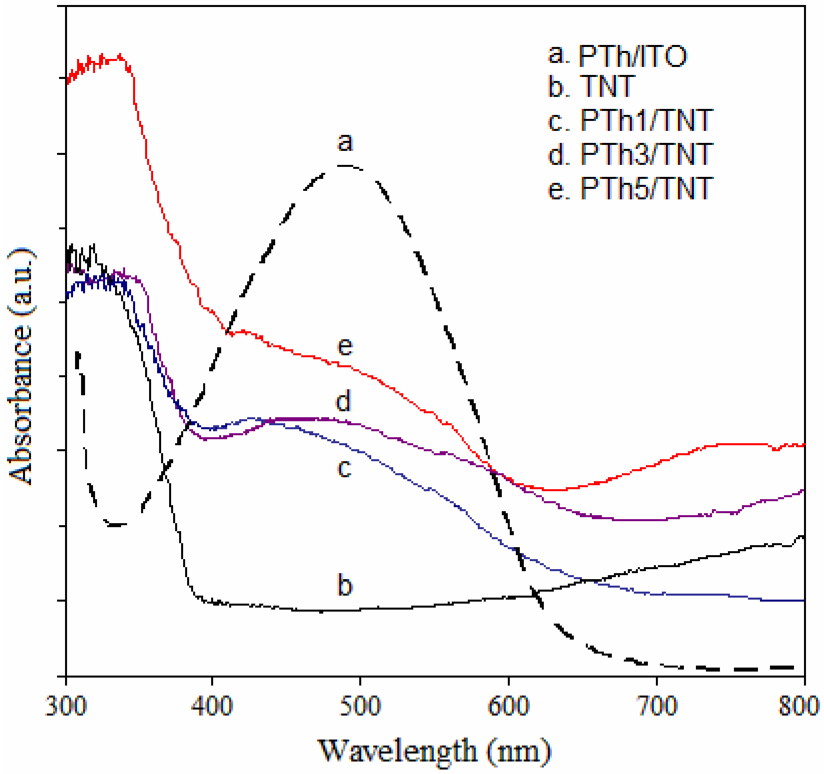

Figure 7-5. (1) UV-Vis absorption spectrum of PTh/ITO (curve a); (2) the diffuse reflectance spectra of a pure TNT and polythiophene modified TNT samples (curves b, c, d and e represent the spectra of TNT, PTh1/TNT, PTh3/TNT and PTh5/TNT, respectively).

The TNT sample (curve b) in Figure 7-5 shows very weak absorption in the visible region with its band gap transition starting from ~395 nm. This is attributed to the unique tubular structures of TiO_2. Unlike TNT, the PTh/TNT composites (curves c-e) exhibit a new and broad absorption band in the range of 400–600 nm with a main shoulder at 540 nm. These results further imply the existence of the interaction between polymer and nanotubular TiO_2, as identified by the XPS spectra. Moreover, this pattern becomes more prominent with an increased amount of polythiophene layers (curves c-e). Obviously, the TNT film functionalized with polythiophene causes a strong red shift in its light absorption as a result of the strong electronic interaction between polythiophene and titania, and a direct charge transfer from polythiophene to the semiconductor surface that takes place during the photoexcitation. A transition of energy levels between this polymer orbital and TiO_2 orbital, as shown in Figure 2-2, would be a key step to result in such as a significant red shift.

7.3 PTh/TNT Photocatalysis with Different Light Sources

7.3.1 PTh/TNT Photocatalysis under Visible Light Irradiation

The photocatalytic activities of PTh/TNT composites were evaluated in terms of the

2,3-DCP degradation in aqueous solution under visible light irradiation and the TNT sample was also tested for comparison, as shown in Figure 7-6. It is found that only a minor removal of 2,3-DCP either under visible illumination alone or with TNT under visible illumination after 420 min reaction. These results therefore indicate that the direct photolysis and the TNT photocatalysis did not demonstrate any significant photoactivities under visible illumination. In contrast, the 2,3-DCP was significantly degraded by 51% using the PTh3/TNT composite under visible illumination after 420 min reaction and, at least four different intermediates from 2,3-DCP degradation were detected by HPLC. In a polymer-TiO_2/visible light system, some positive carbon radicals in polymer chains are formed, as well as in a dye sensitized-TiO_2 system, when the photoexcited electrons of polythiophene are injected into the conduction band of TiO_2. These positive carbon radicals undergo delocalization along the conjugated π-orbital on polymer chains until being attacked by an electronegative group. When the electronegative group is water or oxygen, the resulting molecule may be called a hydrogen radical or triplet/singlet oxygen (Gou et al., 2004), respectively, which is an active oxidizer and capable of attacking organic pollutants to the ultimate products. Hence, 2,3-DCP may be degraded through one or more pathways, as shown in Chapter 4.

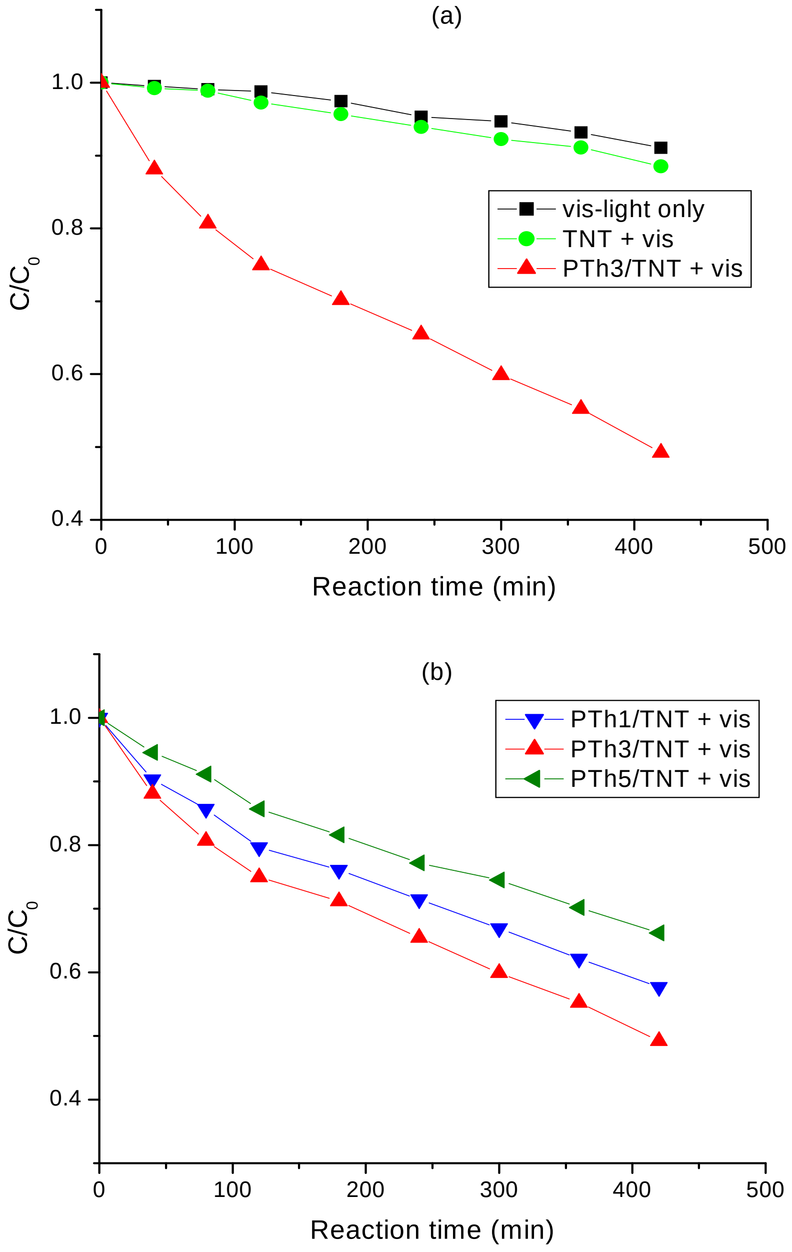

Figure 7-6. 2,3-DCP degradation in aqueous solution under visible light irradiation. Here, C_0 = 20 mg L^{-1} and the fraction of 2,3-DCP loss during reaction due to evaporation has been deducted according to the results of a blank experiment without catalysts.

Figure 7-6b shows the visible photoactivities of three PTh/TNT composites in our experiment. It can be seen that the PTh3/TNT sample exhibits the highest photocatalytic activities by 51% of 2,3-DCP removal after 420 min irradiation, while the PTh1/TNT and PTh5/TNT degraded 2,3-DCP by 42% and 34%, respectively under the same experimental condition. This result indicates there is an optimal amount of the polythiophene deposition to achieve the best photocatalytic performance. In fact, the optical properties of PTh/TNT composites depend on the growth mechanism of the polythiophene layer during electrochemical synthesis. When a very low concentration of thiophene monomer (e.g., less than 1 mM) was applied, the detached polymer clusters were yielded on the TNT substrate, as shown in Figure 7-1b1. As a result, only a small fraction of photons were absorbed by the detached polymer clusters to sensitize TiO_2 nanotubes crystal, leading to the limited photocatalytic activities. In contrast, with an increased concentration of thiophene monomers in the electrolyte solution, more polymer chains were aggregated and a well-connected polythiophene layer was formed on the TNT substrate surface (see Figure 7-1c1 and d1). These well-connected polythiophene films can absorb more photons to carry out the charge transfer on the PTh/TNT interface, resulting in the higher photocatalytic activities. However, the fact is that the photoactivities of PTh/TNT with an excessively thick polythiophene layer, such as PTh5/TNT, declined in the experiments, which might be attributed to the combination of three factors, including (1) the reduced active surface area of TNT films, (2) the poor pore structure (see the SEM images in Figure 7-1) and (3) the occurrence of profuse defects (such as the formation of positively charged sulfur) in the deposited polymer chain.

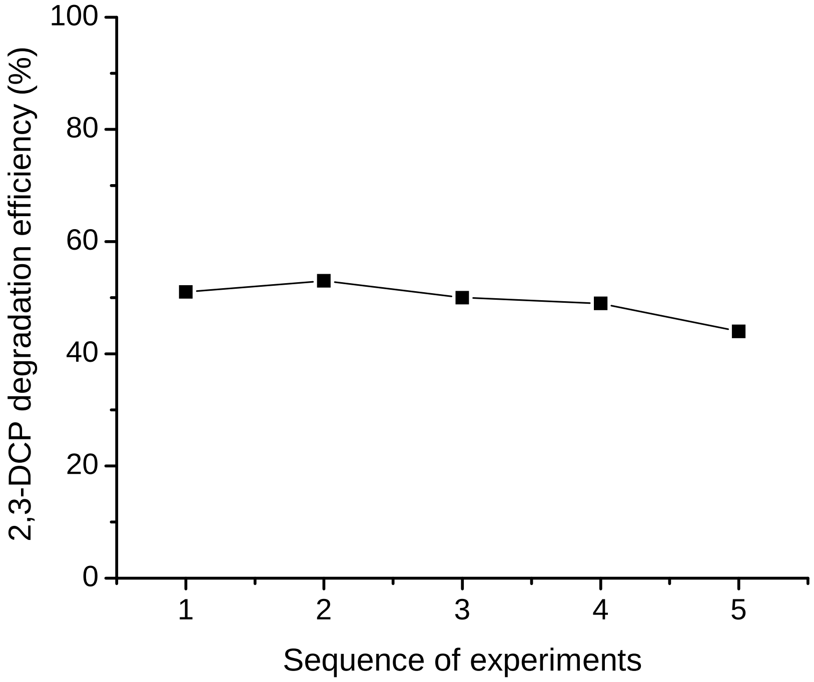

Figure 7-7. Efficiency of 2,3-DCP degradation with the PTh/TNT catalyst under visible light irradiation in 5 repeated experiments (C_0 = 20 mg L^{-1}).

To evaluate the reusability of the PTh/TNT films, the PTh3/TNT film was repeatedly used in several experimental runs, in which each run lasted for 420 min. After the first photocatalytic reaction, the catalyst was rinsed by DDW, dried at 103

^{o}C and re-used immediately without any treatment. The experimental results showed that after 5 runs the activities of PTh3/TNT film only decreased slightly to be ~86% of the photocatalytic efficiency in the first run, as shown in Figure 7-7, which indicates that the PTh3/TNT films can maintain relatively high activities.

7.3.2 PTh/TNT Photocatalysis under UV Light Irradiation

One set of experiments for 2,3-DCP degradation under UV light irradiation was performed and the results are presented in Figure 7-8. It is observed that the 2,3-DCP with an initial concentration of 20 mg L^{-1} was degraded by 78% under UV light irradiation for 300 min with the TNT sample, and by ~62% with the PTh3/TNT sample. It is easy to understand that for the PTh3/TNT sample, both the polythiophene and TiO_2 can be excited by UV light irradiation. The excited electrons on the CB of TiO_2 will accumulate and resist any electrons transfer from the photoexcited states of polythiophene. Consequently, the electrons on the CB of TiO_2 either delocalize inside TiO_2 bulk or eventually find its way to transfer into the ground state of polymer (Duncan and Prezhdo, 2007). Moreover, the coating of polythiophene not only lowers the extent of TNT crystallinity (see XRD spectrum in Figure 7-3) but also reduces the active surface area of TNT. Hence, the overall photocatalytic efficiency of PTh/TNT was lower than that of TNT under UV illumination. This observation is similar to the general fact that the modification of TiO_2 to achieve visible photoactivities always loses its photocatalytic activities under UV light to a certain extent as reported by earlier studies (Demeestere et al., 2005; Park and Choi, 2005).

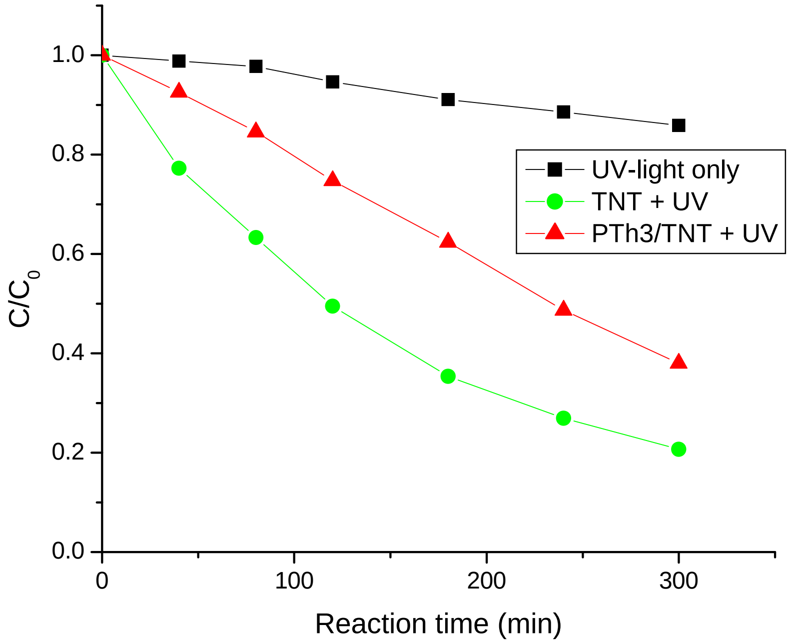

Figure 7-8. 2,3-DCP degradation under UV light irradiation (a 8W-UV lamp with 365 nm) in different systems. Here C_0 = 20 mg L^{-1} and the fraction of 2,3-DCP loss during reaction due to evaporation has been deducted according to the results of a blank experiment without catalysts.

7.3.3 PTh/TNT Photocatalysis under Sunlight Irradiation

As utilizing sunlight is always the most economical option to conduct photoreaction (Bandala et al., 2002; Kuo and Ho, 2006), this composite PTh/TNT film should be photocatalytically active under sunlight irradiation with a broad wavelength range from near UV to visible region. It is worthwhile to conduct the above experiments outdoor under sunlight irradiation to further revaluate the photocatalytic activities of the PTh/TNT catalyst.

Figure 7-9 shows the degradation of 2,3-DCP by TNT and PTh3/TNT films under sunlight irradiation. It can be found that the 2,3-DCP degradation with the PTh3/TNT film was achieved by about 88% after 420 min reaction, while that with TNT film was only by 70%. To explain these results, the optical behaviour of the composite materials under solar illumination must be considered. It is well known that sunlight not only contains visible light but even UV light (< 5% of the total radiation) passing through the atmosphere to the earth. The experimental results in Figure 7-9 show that 2,3-DCP degradation with the TNT film under sunlight irradiation was slower than that with the PTh/TNT film, since sunlight has only a small fraction of UV light. These results indicate that the PTh/TNT catalyst can effectively absorb both UV and visible lights to promote the electronic excitation

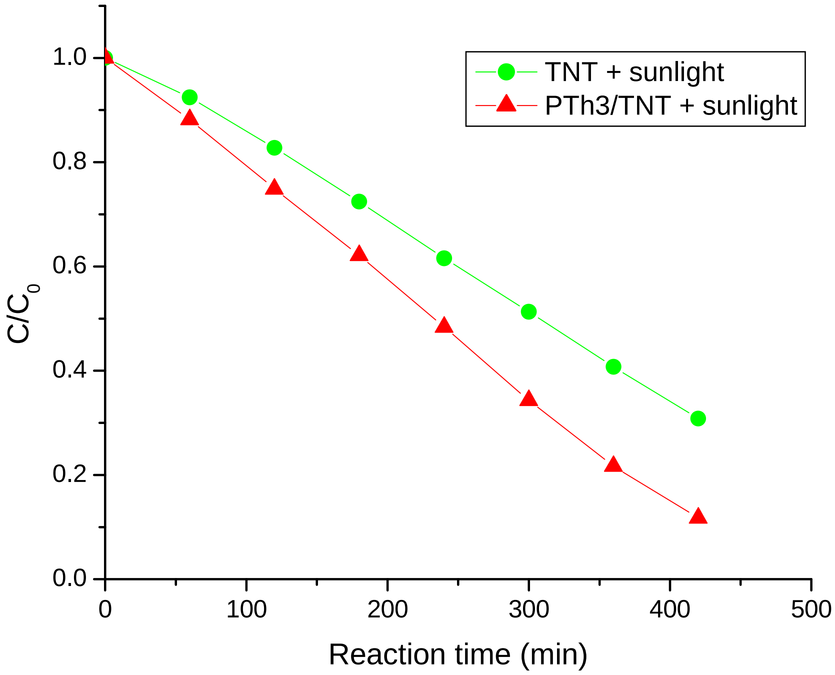

Figure 7-9. 2,3-DCP degradation under sunlight irradiation with TNT and PTh3/TNT. Here, C_0 = 20 mg L^{-1} and the fraction of 2,3-DCP loss during reaction due to evaporation has been deducted according to the results of a blank experiment without catalysts.

between the valence and conduction bands, where the fraction of UV light is responsible for the well-known direct excitation of TiO_2 and visible light responds to the sensitized excitation. The two approaches can promote the generation of electro-hole pairs and also charge transfer through the interaction between PTh and TiO_2 nanotubes. It is generally accepted that if the electrons and holes created do not recombine rapidly, they need to either be trapped in metastable states or migrate to the semiconductor surface separately, in which the amount of surface-trapped carriers is responsive for determining the overall activities of the TiO_2 films (Hao et al., 2005). Consequently, the sunlight experiments reveal the major contribution of the sensitization mechanism under UV-Vis light rather than the direct excitation of TNT.

To further evaluate the efficiency of various catalysts irradiated by different light sources, the reaction rates in different experiments can be compared on a basis of photonic efficiency or quantum yield (Serpone et al., 1993 and 1997). Here, the photonic efficiency of reaction (ζ) is defined below:

$$\zeta = \frac{R}{\mathrm{I}_0}$$

where R is the initial rate of 2,3-DCP degradation (mol L^{-1} min^{-1}) and I_0 is the incident photon flux (Einstein m^{-2} s^{-1}).

According to the conversion factors among radiation intensity, photon (energy) intensity and lumination intensity (Thimijan and Heins, 1983), the values of ζ for different systems were calculated based on the above equation and are summarized in Table 7-2. In addition, a relative photonic efficiency (ζ_r) is also determined for easy comparison as listed in Table 7-2. It can be seen that the TNT film demonstrated the highest ζ value of 0.4037 (ζ_r = 1.0) under UV light irradiation, whereas it revealed much lower ζ value of 0.003 (ζ_r = 0.0074) under sunlight and had almost no activities under visible light irradiation.

Table 7-2. Comparison of rate constants, photonic efficiency and relative photonic efficiency for 2,3-DCP degradation in different systems.

Studied system[a]	2,3-DCP degradation[b] (C_0 = 0.123 mmol L^{-1})			
	k (× 10^{-3} min^{-1})	R (× 10^{-5} mmol L^{-1} min^{-1})	ζ (mol $Einstein^{-1}$ m^{-1})	ζ_r
TNT + UV	5.4	66.42	0.4037	1.0000
PTh3/TNT + UV	3.0	36.90	0.2243	0.5560
TNT + vis	--[c]	--	--	--
PTh3/TNT + vis	1.7	20.91	0.0036	0.0089
TNT + sun	2.7	33.21	0.0030	0.0074
PTh3/TNT + sun	4.1	50.43	0.0046	0.0114

[a] In the studied systems, the light intensity of UV, visible and sunlight is 27.42, 978.07 and 1832.57 μ Einstein m^{-2} s^{-1}, respectively.

[b] The 2,3-DCP degradation is suggested to follow the pseudo-first order reaction and the reaction rate can be calculated from the equation: $R = k C_0$.

[c] -- is nearly zero.

Meanwhile, the photonic efficiency of PTh3/TNT under UV, sunlight and visible irradiation was determined to be 0.2243 (ζ_r = 0.556), 0.0046 (ζ_r = 0.0114) and 0.0036 (ζ_r = 0.0089), respectively. From the above data, the photonic efficiency of all systems can be ranked as UV/TNT > UV/PTh3/TNT > sun/PTh3/TNT > vis/PTh3/TNT > sun/TNT > vis/TNT. These results confirmed that the PTh/TNT catalyst demonstrated higher photonic efficiency ($\zeta_r = 0.0114$) than the TNT catalyst under sunlight irradiation ($\zeta_r = 0.0074$) due to its overall light absorption in a broad range of near UV and also visible region. It may imply that such composite catalysts could better utilize sunlight energy for its practical application in water and wastewater treatment.

7.4 Effect of the Side-Chain Substitution of Polythiophene on Photoactivities

Substitution patterns are strong features of polythiophenes and their derivatives, and significantly influence their physical, optical and electronical properties (Vamvounis et al., 2004; Li et al., 2007). In principle, optimal polymer substitution should lead to an effective charge transfer without unwanted conformational changes, leading to good optical efficiency. In this study, three polythiophene derivatives with different side-chains, poly3-methylthiophene (P3Meth), poly3-hexylthiophene (P3Hexth) and poly3-thiophenecarboxylic acid (P3ThCA), were electropolymerized on the TNT substrate and the effect of the side-groups on the 2,3-DCP degradation under visible light irradiation was investigated. The experimental results listed in Table 7-3 show that the 2,3-DCP degradation with the P3Meth/TNT film was achieved by 52%, close to that with PTh3/TNT by 51%. In the meantime, the similar DOC removals in both experiments were achieved by > 26%. When compared to PTh3/TNT and P3Meth/TNT, the P3ThCA/TNT and P3Hexth/TNT catalysts exhibited lower photocatalytic activities under the same experimental condition in terms of 2,3-DCP degradation and DOC removal significantly. It can be understood that the visible photoactivities of polymer/TNT composites are significantly dependent on the efficiency of light absorption by polymer as well as the electron transfer on the interface of polymer/TNT composites.

Table 7-3. 2,3-DCP degradation and DOC removal with different polymer/TNT composites (C_0 = 20 mg L^{-1}).

Sample	2,3-DCP degradation [%]	DOC removal [%]
PTh3/TNT	52	26.6
P3Meth/TNT	51	26.5
P3Hexth/TNT	34	9.6
P3ThCA/TNT	41	16.8

To increase the light harvest by catalysts, the strong and broad absorbance of light are both needed. Li and co-workers (Hou et al., 2006; Tan et al., 2007) have reported that thiophene polymers as electron-donor substituents with some side-chains, such as the methoxy group, can benefit the light absorption with a red shift but the polymers with other side chains, such as styryl and hexyl groups, due to their large steric hindrance, may weaken the absorbance in the visible region (Somanathan and Radhakrishnan, 2005). In this study, the addition of methyl group in polymer backbone, due to its electron-donating ability, led to the red-shift absorption and enhanced its photoactivities as listed in Table 7-3. On the other hand, the steric hindrance of hexyl group weakened the interaction between the polymer chains and resulted in a less degree of 2,3-DCP degradation. A further reason is that the loading of P3Hexth onto TNT would reduce the pore volume and also surface area of the catalyst as supported by its FESEM result, as shown in Figure 7-10. This

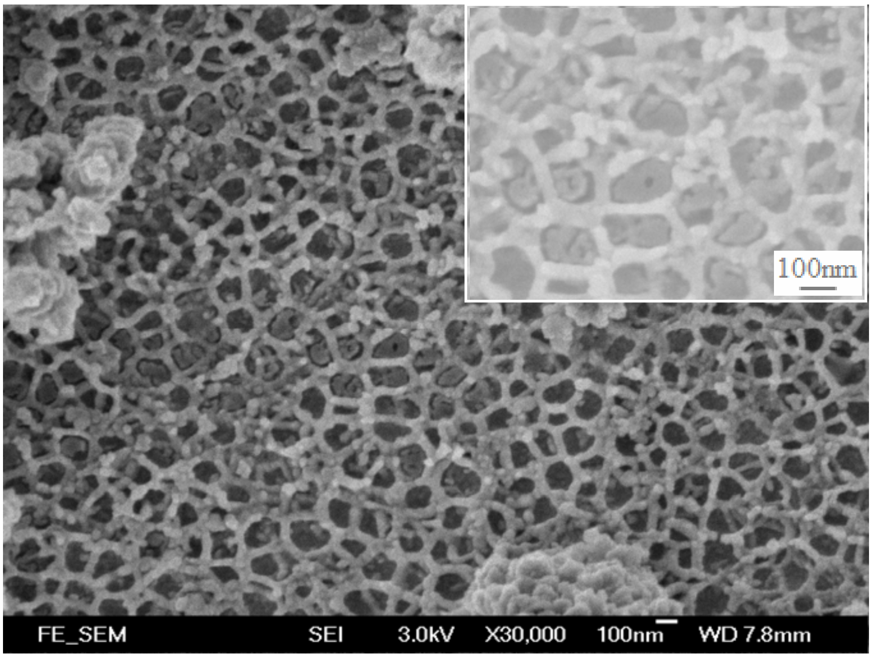

Figure 7-10. FESEM image of poly3-hexylthiophene electropolymerized on the TNT substrate.

phenomenon was not observed in the images of P3Meth/TNT and P3ThCA/TNT. For the addition of the carboxyl group, an electron-withdrawing subunit, the opposite trend in comparison to the methyl group should be expected, as mentioned above. While the positive effect may be compensated by the formation of coordination bands between polymer and TiO_2 nanotubes, which results from the esterification of carboxylic acid with hydroxylic groups on titania surface. There are a number of literature precedents suggesting that carboxylic acid and hydroxylic groups on oxide surface form chelates or coordinative bonds (Frei et al., 1990; Moser et al., 1991). Taking into account these results, the possible coordinations can be found in Scheme 7-2. In this way, a dramatic acceleration of the interfacial electron transfer from the conduction band of the polymer to TiO_2 acceptors is achieved. Therefore, it can be inferred that the side-chain structures of conjugated polymer have obvious influence on the photocatalytic activities of the polymer/TNT composites.

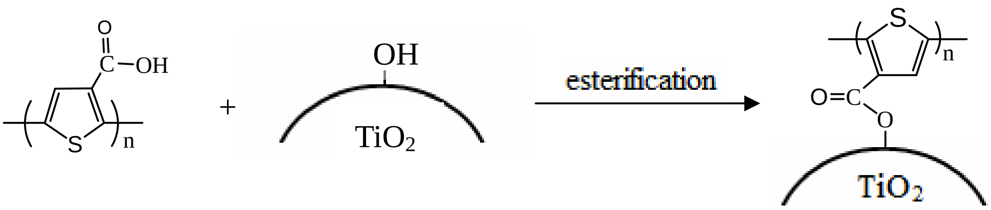

Scheme 7-2. Esterification of poly3-thiophenecarboxylic acid on the TiO_2 surface.

7.5 Summary

In this study, polythiophene was successfully deposited on the TiO_2 nanotube films by a two-step electrochemical method. XPS spectra of PTh/TNT composites indicate the strong interaction between S sites of polymer backbone and TiO_2 nanotubes, in which electron transfer from polythiophene to titania takes place. UV-Vis DRS analysis shows that these composites have a strong photoresponse in the visible region at 500 nm. The prepared PTh/TNT films revealed significant activities for 2,3-DCP degradation under visible light irradiation and also sunlight irradiation, in which the PTh3/TNT film achieved the best performance. The experiments also confirmed that the side-chains of polythiophene could influence its photocatalytic activities significantly with an order of P3Meth/TNT ≈ PTh3/TNT > P3ThCA/TNT > P3Hexth/TNT. Further work is required to evaluate the effectiveness of this catalyst in degrading other common pollutants and the reaction pathways under UV and visible illumination, respectively.

Chapter 8 – Conclusion and Recommendation

8.1 Conclusion

In this study, TNT films were successfully prepared by an anodic oxidation process with post-calcination. The results indicate that all of the anodic TNT films exhibited better photocatalytic activities for 2,3-DCP degradation in aqueous solution than that of the traditional TiO_2 film prepared by the sol-gel method. Such higher photocatalytic performance might be attributed to the large specific surface area, high pore volume, thin tube wall and optimal tube length. Moreover, the TNT films calcined at 500 ^{o}C for 1 h with a higher degree of crystallinity exhibited higher photocatalytic activities than other TNT films calcined at 300 and 800 ^{o}C. Consequently, these results indicate that the optimization of TNT structures is critical to achieving the high performance of photocatalytic reaction.

In the second phase of this study, the effects of DO, pH and the presence of anions on the photocatalytic activities of TNT films were investigated. The results show that the role of DO in the 2,3-DCP degradation with the TNT film is significant for enhancing photoefficiency of TNT films. Regarding the pH effect, 2,3-DCP in alkaline solution was degraded and dechlorinated faster than that in acidic solution whereas DOC removal presented an opposite order in dependence of pH. Meanwhile, major intermediate products from 2,3-DCP degradation were identified by a ^{1}H-NMR technique to explore a possible degradation pathway. Among these identified intermediates, 2-chlororesorcinol, with the highest concentration, was found as a new species when compared to the previous reports in the photodegradation of 2,3-DCP. For the effect of individual anions (NO_3^-, Cl^-, SO_4^{2-}, and $H_2PO_4^-$), the inhibition degree of photocatalytic degradation of 2,3-DCP caused by these anions could be ranked from high to low as $SO_4^{2-} > Cl^- > H_2PO_4^- > NO_3^-$. The observed inhibition effect can be attributed to the competitive adsorption and the formation of less reactive radicals during the photocatalytic reaction.

In the third phase, mechanism and pathways of diphenaimd degradation in aqueous solution by UVC-photolysis and TNT/UVA-photocatalysis were investigated. It was found that at neutral pH, photolysis system with UVC (254 nm) irradiation alone could be quite efficient in degrading DPA (100% removal after 360 min), but poor in reducing DOC (only 8% removal after 360 min). In contrast, photocatalysis system with TNT/UVA (350 nm) showed 51% of DPA removal and 11% of DOC removal, respectively after 360 min. These results indicate that although the DPA degradation by the photocatalysis with TNT/UVA was much slower than that by the photolysis with UVC, the DOC removal by the photocatalysis was higher than that of photolysis. These results might reveal that the photocatalysis process had relatively poor selectivity in degrading different compounds, such as various intermediates from the DPA degradation, which is more conducive to DPA mineralization. In addition, over 20 intermediates were identified by LC-MS and ^{1}H-NMR techniques. In terms of these intermediates a detailed pathway for the DPA degradation by photolysis and photocatalysis respectively was proposed as the first time.

Finally, a visible-induced photocatalyst based on the polythiophene-sensitized TiO_2 nanotube films (PTh/TNT) were successfully prepared by a two-step electrochemical process of anodizaton and electropolymerization. XPS spectra of PTh/TNT composites indicate the strong interaction between S sites of polymer backbone and TiO_2 nanotubes, in which electron transfer from polythiophene to titania takes place. UV-Vis DRS analysis shows that these composites have a strong photoresponse in the visible region at 500 nm. The prepared PTh/TNT films revealed significant activities for 2,3-DCP degradation under visible light irradiation and also sunlight irradiation, in which the PTh3/TNT film achieved the best performance. On the other hand, this study also confirmed that the side-chains of polythiophene could influence its photocatalytic activities significantly in an order from high to low as poly3-methylthiophene ≈ polythiophene > poly3-thiophenecarboxylic acid > poly3-hexylthiophene. The results may provide useful information to further develop effective polymer-semiconductor catalysts for pollutant degradation under sunlight irradiation for water and wastewater treatment.

8.2 Limitation and Recommendation

In this study, all photochemical reactions were carried out in a batch reactor with a focus on the destruction of sole target organics in aqueous solution. For practical application, it is suggested to design a continuous flow photoreactor system (see Figure 8-1) using TiO_2 nanotube films, and also to examine the effect of photocatalysis in the presence of multiple organics. In addition, effects of key operating parameters such as light intensity, catalyst dosage, water retention time,

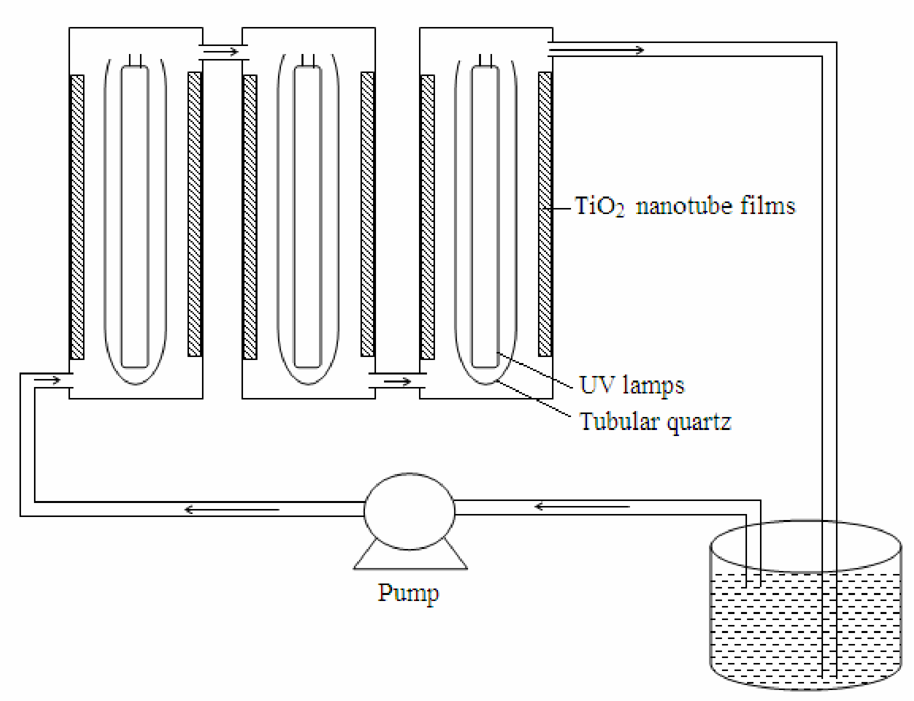

Figure 8-1. Schematic diagram of continuous flow photoreactor with TiO_2 nanotube films for the degradation of organic pollutants in water.

removal efficiency, organic loading and so on must be evaluated in order to optimize the performance of the photoreactor system. On the other hand, the UV light cannot be fully utilized by the TiO_2 nanotube film due its limited area (3 cm^2) in this study, which significantly limited its photocatalytic capacity, larger TiO_2 films therefore should be developed. However, the cost for fabricating such films should also be estimated.

According to the comparison between UVC-photolysis and TNT-photocatalysis for the degradation of DPA in Chapter 6, it was found that they have different advantages in terms of DPA degradation and mineralization and the coupling of two reaction mechanisms in design would be a beneficial option. Therefore, the development of a photolysis-photocatalysis system is recommended for the degradation of different other recalcitrant organic pollutants in water and its operating cost could be evaluated by comparing with either UVC-photolysis or TNT-photocatalysis system.

As suggested by the focused study on dissolved oxygen, it is recommended that alternative electron acceptors, such as H_2O_2, $KBrO_3$ and $(NH_4)_2S_2O_8$, may be used in the photocatalytic reactions, where they can (i) increase the number of trapped electrons and consequently avoid electron-hole recombination, (ii) generate more •OH radicals and other oxidizing species, and (iii) increase the oxidation rate of intermediates. Actually, some pollutants with high oxidative potential, such as Cr^{6+} and azo dye in wastewater, may also be utilized as electron acceptors. Further optimization of the operating conditions is needed if these electron acceptors are added in the TNT/UV system.

The type of polymer sensitized-TNT catalyst has a vital role in visible-induced photocatalytic oxidation but its photocatalytic ability is not high enough for the practical application. There are still vast areas in which to improve the utilization efficiency or quantity of visible sunlight by exploring other polymer/TNT systems for the visible oxidation treatment of pollutants in water. As well as the application in water treatment, the immobilized TiO_2 nanotube films can be expanded to other applications, such as in gas-phase reactions, solar cells and water-splitting to produce hydrogen gas, especially under sunlight irradiation.

REFERENCES

Abdullah, M., Low, K.C., Mattheus, R.W., 1990. Effects of common inorganic anions on rates of photocatalytic oxidation of organic carbon over illuminated titanium dioxide. J. Phys. Chem. 94, 6820-6825.

Aceituno, M., Stalikas, C.D., Lunar, L., Rubio, S., Pérez-Bendito, D., 2002. H_2O_2/TiO_2 photocatalytic oxidation of metol. Identification of intermediates and reaction pathways. Water Res. 36, 3582-3592.

Almquist, C.B., Biswas, P., 2001. A mechanistic approach to modeling the effect of dissolved oxygen in photo-oxidation reactions on titanium dioxide in aqueous systems. Chem. Eng. Sci. 56, 3421-3430.

Amine-Khodja, A., Lavédrine, B., Richard, C., Sehili, T., 2002. Photocatalytic degradation of metoxuron in aqueous suspensions of TiO_2: analytical and kinetic studies. Int. J. Photoenergy. 4, 147-151.

Antonaraki, S., Androulaki, E., Dimotikali, D., Hiskia, A., Papaconstantinou, E., 2002. Photolytic degradation of all chlorophenols with polyoxometallates and H_2O_2. J. Photochem. Photobiol. A 148, 191-197.

Arsov, L.D., Efremova, A.T., 1992. In situ determination of the optical constants of titanium surface films in higher voltage anodization. Electrochim. Acta 37, 2099-2100.

Asahi, R., Morikawa, T., Ohwaki, T., Aoki, K., Taga, Y., 2001. Visible-light photocatalysis in nitrogen-doped titanium oxides. Science 293, 269-271.

Auriol, M., Meknassi, Y.F., Tyagi, R.D., Adams, C.D., Surampalli, R.Y., 2006. Endocrine disrupting compounds removal from wastewater, a new challenge. Process Biochem. 41, 525-539.

Bandala, E.R., Gelover, S., Leal, M.T., Bulnes, C.A., Jimenez, A., Estrada, C.A., 2002. Solar photocatalytic degradation of Aldrin. Catal. Today 76, 189-199.

Baran, W., Makowski, A., Wardas, W., 2005. The separation of catalyst after photocatalytic reactions conducted in the presence of $TiO_2/FeCl_3$/UV. Chemosphere 59, 853-859.

Barbier, J., Oliviero, L., Renard, B., Duprez, D., 2002. Catalytic wet air oxidation of ammonia over M/CeO_2 catalysts in the treatment of nitrogen-containing pollutants. Catal. Today 75, 29-34.

Bargon, J., Mohmand, S., Waltman, R.J., 1983. Electrochemical synthesis of electrically conducting polymers from aromatic compounds. IBM J. Res. Develop. 27, 330-341.

Bayarri, B., Giménez, J., Curcó, D., Esplugas, S., 2005. Photocatalytic degradation of 2,4-dichlorophenol by TiO_2/UV: kinetics, actinometries and models. Catal. Today 101, 227–236.

Beek, W.J.E., Wienk, M.M., Kemerink, M., Yang, X., Janssen, R.A.J., 2005. Hybrid zinc oxide conjugated polymer bulk heterojunction solar cells. J. Phys. Chem. B 109, 9505-9516.

Bekbölet, M., Boyacioglu, Z., Özkaraova, B., 1998. The influence of solution matrix on the photocatalytic removal of color from natural waters. Water Sci. Technol. 38 (6), 155-162.

Bellar, J.A., Lichtenberg, J.J., Kroner, R.C., 1974. The occurrence of organohalides in chlorinated drinking waters. J. Am. Water Works Ass. 66 (22), 703-706.

Bhargava, R.N., Gallaghr, D., Hong, X., Nurmikko, A., 1994. Optical properties of manganese-doped nanocrystals of ZnS. Phys. Rev. Lett. 72, 416-419.

Bickley, R.I., Slater, M.J., Wang, W.J., 2005. Engineering development of a photocatalytic reactor for wastewater treatment. Process Saf. Environ. 83, 205–216.

Bideau, M., Claudel, B., Dubien, C., Faure, L., Kazouan, H., 1995. On the immobilization of titanium dioxide in the photocatalytic oxidation of spent waters. J. Photochem. Photobiol. A 91, 137-144.

Boer, K W., 1990. Survey of semiconductor physics; Van Nostrand Reinhold: New York, p 249.

Brezova, V., Blazkova, A., Breznan, M., Kottas, P., Ceppan, M.,1995. Phenol degradation on glass fibers with immobilized titanium dioxide particles. Collect. Czech. Chem. Commun. 60, 788-794.

Brudnik, A., Czternastek, H., Zakrzewska, K., Jachimowski, M., 1991. Plasma-emission-controlled dc magnetron sputtering of TiO_{2-x} thin films. Thin Solid Films 199, 45-58.

Brune, B.J., Koehler, J.A., Smith, P.J., Payne, G.F., 1999. Correlation between adsorption and small molecule hydrogen bonding. Langmuir 15, 3987-3992.

Byrne, J.A., Eggins, B.R., Brown, N.M.D., McKinney, B., Rouse, M., 1998. Immobilisation of TiO_2 powder for the treatment of polluted water. Appl. Catal. B-Environ. 17, 25-36.

Cai, Q.Y., Paulose, M., Varghese, O.K., Grimes, C.A., 2005. The effect of electrolyte composition on the fabrication of self-organized titanium oxide nanotube arrays by anodic oxidation. J. Mater. Res. 20, 230-234.

Cámara, O.R., De Pauli, C.P., Vaschetto, M.E., Retamal, B., Aquirre, M.J., Zagal, J.H., Biaggio, S.R., 1995. Semiconducting properties of TiO_2 films thermally formed at 400 °C. J. Appl. Electrochem. 25, 247-251.

Caruso, R.A., Schattka, J.H., Greiner, A., 2001. Titanium dioxide tubes from sol-gel coating of electrospun polymer fibers. Adv. Mater. 13, 1577-1579.

Chang, H.T., Wu, N., Zhu, F., 2000. A kinetic model for photocatalytic degradation of organic contaminants in a thin film TiO_2 catalyst. Water Res. 34, 407-416.

Chen, H.Y., Zahraa, O., Bouchy, M., 1997. Inhibition of the adsorption and photocatalytic degradation of an organic contaminant in an aqueous suspension of TiO_2 by inorganic ions. J. Photochem. Photobiol. A 108, 37-44.

Chen, Q., Du, G. H., Zhang, S., Peng, L.M., 2002. The structure of trititanate nanotubes. Acta Crystallogr. Sect. B 58, 587-593.

Chen, R.F., Zhang, L., Wei, Y., Hou, D.L., 2007. Preparation of rutile (TiO_2) nanostructured materials at low temperature from $TiCl_4$ aqueous solution. J. Mater. Sci. 42, 714-7146.

Chen, S., Paulose, M., Ruan, C., Mor, G.K., Varghese, O.K., Kouzoudis, D., Grimes, C.A., 2006. Electrochemically synthesized CdS nanoparticle-modified TiO_2 nanotube-array photoelectrodes: Preparation, characterization, and application to photoelectrochemical cells. J. Photochem. Photobiol. A 177, 177-184.

Chen, W., Wang, Z.G., Lin, Z.J., Lin, L.Y., 1997. Absorption and luminescence of the surface states in ZnS nanoparticles. J. Appl. Phys. 82, 3111-3115.

Chen, W., Xue, G., 2005. Low potential electrochemical syntheses of heteroaromatic conducting polymers in a novel solvent system based on trifluroborate–ethyl ether. Prog. Polym. Sci. 30, 783–811.

Chen, Y.J., Dionysiou, D.D., 2006. Correlation of structural properties and film thickness to photocatalytic activity of thick TiO_2 films coated on stainless steel. Appl. Catal. B-Environ. 69, 24-33.

Chen, Y.S., Crittenden, J.C., Hackney, S., Sutter, L., Hand, D.W., 2005. Preparation of a novel TiO_2-based p-n junction nanotube photocatalyst. Environ. Sci. Technol. 39, 1201-1208.

Chester, G., Anderson, M., Read, H., 1993. A jacketed annular membrane photocatalytic reactor for wastewater treatment: degradation of formic acid and atrazine. J. Photochem. Photobiol. A 71, 291-297.

Choi, H., Stathatos, E., Dionysiou, D.D., 2007. Photocatalytic TiO_2 films and membranes for the development of efficient wastewater treatment and reuse systems. Desalination 202, 199-206.

Choo, K.H., Tao, R., Kim, M.J., 2008. Use of a photocatalytic membrane reactor for the removal of natural organic matter in water: effect of photoinduced desorption and ferrihydrite adsorption. J. membrane Sci. 322, 368-374.

Chung, Y.S., Park, S.B., Kang, D.W., 2004. Magnetically separable titania-coated nickel ferrite photocatalyst. Mater. Chem. Phys. 86, 375–381.

Costa, F.A.P., Reis, E.M., Azevedo, J.C.R., Nozaki, J., 2004. Bleaching and photodegradation of textile dyes by H_2O_2 and solar or ultraviolet radiation. Sol. Energy 77, 29–35.

Crittenden. J.C., Liu. J., Hand, D.W., Perram, D.L., 1997. Photocatafytic oxidation of chlorinated hydrocarbons in water. Water Res. 31, 429-438.

D’Oliveira, J.C., Minerob, C., Pelizzettib, E., Pichat, P., 1993. Photodegradation of dichlorophenols and trichlorophenols in TiO_2 aqueous suspensions: kinetic effects of the positions of the Cl atoms and identification of the intermediates. J. Photochem. Photobiol. A 72, 261–267.

Datye, A.K., Riegel, G., Bolton, J.R., Huang, M., Prairie, M.R., 1995. Microstructural characterization of a fumed titanium dioxide photocatalyst. J.

Solid State Chem. 115, 236–239.

Dechakiatkrai, C., Chen, J., Lynam, C., Phanichphant, S., Wallace, G.G., 2007. Photocatalytic oxidation of methanol using titanium dioxide/single-walled carbon nanotube composite. J. Electrochem. Soc. 154, A 407-411.

Deki, S., Aoi, Y., Hiroi, O., Kahinami, A., 1996. Titanium (IV) oxide thin films prepared from aqueous solution. Chem. Lett. 25, 433-434.

Delplancke, J.L., Winand, R., 1988. Galvanostatic anodization of titanium-I. Structures and compositions of the anodic films. Electrochim. Acta 33, 1539-1549.

Demeestere, K., Dewulf, J., Ohno, T., Salgado, P.H., Langenhove, H.V., 2005. Visible light mediated photocatalytic degradation of gaseous trichloroethylene and dimethyl sulfide on modified titanium dioxide. Appl. Catal. B-Environ. 61, 140-149.

Dionysiou, D.D., Burbano, A.A., Suidan, M.T., Baudin, I., Laîné, J.M., 2002. Effect of oxygen in a thin-film rotating disk photocatalytic reactor. Environ. Sci. Technol. 36, 3834-3843.

Domínguez, J.R., Beltrán, J., Rodríguez, O., 2005. Vis and UV photocatalytic detoxification methods (using TiO_2, TiO_2/H_2O_2, TiO_2/O_3, $TiO_2/S_2O_8^{2-}$, O_3, H_2O_2, $S_2O_8^{2-}$, Fe^{3+}/H_2O_2 and $Fe^{3+}/H_2O_2/C_2O_4^{2-}$) for dyes treatment. Catal. Today 101, 389-395.

Doong, R.A., Chen, C.H., Maithreepala, R.A., Chang, S.M., 2001. The influence of pH and cadmium sulfide on the photocatalytic degradation of 2-chlorophenol in titanium dioxide suspensions. Water Res. 35, 2873-2880.

Du, G.H., Chen, Q., Che, R.C., Yuan, Z.Y., Peng, L.M., 2001. Preparation and structure analysis of titanium oxide nanotubes. Appl. Phys. Lett. 79, 3702-3704.

Duncan, W.R., Prezhdo. O.V., 2007. Theoretical studies of photoinduced electron transfer in dye-sensitized TiO_2. Annu. Rev. Phys. Chem. 58, 143-184.

Eder, D., Kinloch, I.A., Windle, A.H., 2006. Pure rutile nanotubes. Chem. Commun. 13, 1448–1450.

Eley, D.D., 1963. Chemistry Cationic Polymerization; Plesch, P.H. Ed., Macmillan, New York.

Erdei, L., Arecrachakul, N., Vigneswaran, S., 2008. A combined photocatalytic slurry reactor-immersed membrane module system for advanced wastewater treatment. Sep. Purif. Technol. 62, 382-388.

Es-Safi, N.E., Guernevé, C.L., Cheynier, V., Moutounet, M., 2000. New phenolic compounds obtained by evolution of (+)-catechin and glyoxylic acid in hydroalcoholic medium. Tetrahedron Lett. 41 (12), 1917–1921.

Fabiyi, M.E., Skelton, R.L., 2000. Photocatalytic mineralization of methylene blue using buoyant TiO_2-coated polystyrene beads. J. Photochem. Photobiol. A 132, 121-128.

Fernandez, A., Lassaletta, G., Jimenez, V.M., Justo, A., Gonalez-Elipe, A.R., Herrmann, J.M., Tahiri, H., Ait-Ichou, Y., 1995. Preparation and characterization of TiO_2 photocatalysts supported on various rigid supports (glass, quartz and stainless steel). Comparative studies of photocatalytic activity in water purification. Appl. Catal. B-Environ. 7, 49-63.

Filipiak, P., Hug, G.L., Marciniak, B., 2006. Photochemistry of carboxylic acids containing the phenyl and thioether groups: steady-state and laser flash photolysis studies. J. Photochem. Photobiol. A 177, 295–306.

Foladori, P., Laura, B., Gianni, A., Giuliano, Z., 2007. Effects of sonication on bacteria viability in wastewater treatment plants evaluated by flow cytometry—Fecal indicators, wastewater and activated sludge. Water Res. 41, 235-243.

Folmar, L.C., Denslow, N.D., Rao, V., Chow, M., Crain, D.A., Enblom, J., Marcino, J., Guillette, J.R.L.J., 1996. Vitellogenin induction and reduced serum testosterone concentrations in feral male carp (Cyprinus carpio) captured near a major metropolitan sewage treatment plant. Envron. Health. Persp. 104, 1096-1101.

Frei, H., Fitzmaurice, D.J., Grätzel, M., 1990. Surface chelation of semiconductors and interfacial electron transfer. Langmuir 6, 198-206.

Fry, D.M., 1995. Reproductive effects in birds exposed to pesticides and industrial chemicals. Environ. Health. Persp. 31, 165-171.

Fujishima, A., Honda, K., 1972. Electrochemical photolysis of water at a semiconductor electrode. Nature 238, 37-38.

Fujishima, A., Zhang, X.T., 2006. Titanium dioxide photocatalysis: present situation and future approaches. C. R. Chimie. 9, 750-760.

Gerischer, H., Heller, A., 1991. The role of oxygen in photooxidation of organic molecules on semiconductor particles. J. Phys. Chem. 95, 5261-5267.

Ghicov, A., Macak, J.M., Tsuchiya, H., Kunze, J., Haeublein, V., Kleber, S., Schmuki, P., 2006. TiO_2 nanotube layers: Dose effects during nitrogen doping by ion implantation. Chem. Phys. Lett. 419, 426–429.

Ghicov, A., Schmidt, B., Kunze, J., Schmuki, P., 2007. Photoresponse in the visible range from Cr doped TiO_2 nanotubes. Chem. Phys. Lett. 433, 323–326.

Gogate, P.R., Pandit, A.B., 2004. A review of imperative technologies for wastewater treatment I: oxidation technologies at ambient conditions. Adv. Environ. Res. 8, 501-551.

Goi, A., Trapido, M., 2002. Hydrogen peroxide photolysis, Fenton reagent and photo-Fenton for the degradation of nitrophenols: a comparative study. Chemosphere 46, 913-922.

Goldstein, S., Aschengrau, D., Diamant, Y., Rabani, J., 2007. Photolysis of aqueous H_2O_2: quantum yield and applications for polychromatic UV actinometry in photoreactors. Environ. Sci. Technol. 41, 7486-7490.

Gong, D.W., Grimes, C.A., Varghese, O.K., Hu, W.C., Singh, R.S., Chen, Z., Dickey, E.C., 2001. Titanium oxide nanotube arrays prepared by anodic oxidation. J. Mater. Res. 16, 3331-3334.

Gou, Y.Q., Chen, D.Y., Su, Z.X., 2004. Photocatalyst of nanometer TiO_2/conjugated polymer complex employed for depigmentation of methyl orange. Appl. Catal. A 261, 15-18.

Grätzel, M., 1989. Heterogeneous photochemical electron transfer; CRC Press: Boca Raton, FL.

Grätzel, M., 2001. Photoelectrochemical cells. Nature 414, 338-344.

Grätzel, M., 2003. Dye-sensitized solar cells. J. Photochem. Photobiol. C 4, 145-153.

Gryta, M., Tomaszewska, M., Grzechulska, J., Morawski, A.W., 2001. Membrane distillation of NaCl solution containing natural organic matter. J. Membrane Sci. 181, 279–287.

Guillard, C., Lachheb, H., Houas, A., Ksibi, M., Elaloui, E., Herrmann, J.M., 2003. Influence of chemical structure of dyes, of pH and of inorganic salts on their photocatalytic degradation by TiO_2 comparison of the efficiency of powder and supported TiO_2. J. Photochem. Photobiol. A 158, 27-36.

Guo, B., Liu, Z.L., Hong, L., Jiang, H.X., 2005. Sol gel derived photocatalytic porous TiO_2 thin films. Surf. Coat. Technol. 198, 24-29.

Guo, T., Bai, Z.P., Wu, C., Zhu, T., 2008. Influence of relative humidity on the photocatalytic oxidation (PCO) of toluene by TiO_2 loaded on activated carbon fibers: PCO rate and intermediates accumulation. Appl. Catal. B-Environ. 79, 171-178.

Hagfeld, A., Grätzel, M., 1995. Light-induced redox reactions in nanocrystalline systems. Chem. Rev. 95, 49-68.

Hahn, R., Ghicov, A., Salonen, J., Lehto, V.P., Schmuki, P., 2007. Carbon doping of self-organized TiO_2 nanotube layers by thermal acetylene treatment. Nanotechnology 18, 105604.

Hamnett, A., 1980. Porous-electrodes for water oxidation. Faraday Discuss. Chem. Soc. 70, 127-134.

Hanprasopwattana, A., Srinivasan, S., Sault, A. G., Datye, A. K., 1996. Titania coatings on monodisperse silica spheres (characterization using 2-propanol dehydration and TEM). Langmuir 12, 3173-3179.

Hao, W.C., Pan, F., Wang, T.M., 2005. Photocatalytic activity TiO_2 granular films prepared by layer-by-layer self-assembly method. J. Mater. Sci. 40, 1251-1253.

He, M.Q., Mohammad, S.N., 2006. Novel chemical-vapor deposition technique for the synthesis of high-quality single-crystal nanowires and nanotubes. J. Chem. Phys. 124, 064714.

Hillman, A.R., Mallen, E.F., 1987. Nucleation and growth of polythiophene films on gold electrodes. J. Electroanal. Chem. 220, 351-367.

Hitchman, M.L., Tian, F., 2002. Studies of TiO_2 thin films prepared by chemical vapour deposition for photocatalytic and photoelectrocatalytic degradation of 4-chlorophenol. J. Electroanal. Chem. 538, 165-172.

Ho, W.K., Yu, J.C., Lee, S.C., 2006. Low-temperature hydrothermal synthesis of S-doped TiO_2 with visible light photocatalytic activity. J. Solid State Chem. 179, 1171–1176.

Hoffmann, M.R., Martin, S.T., Choi, W.Y., Bahnemannt, D.W., 1995. Environmental applications of semiconductor photocatalysis. Chem. Rev. 95, 69-96.

Hofstadler, K., Bauer, R., Novalic, S., Heisler, G., 1994. New reactor design for photocatalytic wastewater treatment with TiO_2 immobilized on fused-silica glass fibers: photomineralization of 4-chlorophenol. Environ. Sci. Technol. 28, 670-674.

Hou, J.H., Huo, L.H., He, C., Yang, C.H., Li, Y.F., 2006. Synthesis and absorption spectra of poly(3-(phenylenevinyl)thiophene)s with conjugated side chains. Macromolecules 39, 594-603.

Hou, L.R., Yuan, C.Z., Peng, Y., 2007. Synthesis and photocatalytic property of SnO_2/TiO_2 nanotubes composites. J. Hazard. Mater. 139, 310–315.

Hoyer, P., 1996a. Formation of a titanium dioxide nanotube array. Langmuir 12, 1411-1413.

Hoyer, P., 1996b. Semiconductor nanotube formation by a two-step template process. Adv. Mater. 8, 857-859.

Hsien, Y.H., Chang, C.F., Chen, Y.H., Cheng, S., 2001. Photodegradation of aromatic pollutants in water over TiO_2 supported on molecular sieves. Appl. Catal. B 31, 241–249.

Hu, C., Wang, Y.Z., Tang, H.X., 2001. Influence of adsorption on the photodegradation of various dyes using surface bond-conjugated TiO_2/SiO_2 photocatalyst. Appl. Catal. B-Environ. 35, 95-105.

Hu, C., Yu, J.C., Hao, Z., Wong, P.K., 2003. Effects of acidity and inorganic ions on the photocatalytic degradation of different azo dyes. Appl. Catal. B-Environ. 46, 35-47.

Hwang, B.J., Hwang, J.R., 1993. Kinetic model of anodic oxidation of titanium in sulphuric acid. J. Appl. Electrochem. 23, 1056-1062.

Ilisz, I., László, Z., Dombi, A., 1999. Investigation of the photodecomposition of phenol in near-UV irradiated aqueous TiO_2 suspensions. I: effect of charge-trapping species on the degradation kinetics. Appl. Catal. A 180, 25-33.

Ince, N.H., Apikyan, I.G., 2000. Combination of activated carbon adsorption with light-enhanced chemical oxidation via hydrogen peroxide. Water Res. 34, 4169-4176.

Janda, V., Vasek, P., Bizova, J., Belohlav, Z., 2004. Kinetic models for volatile chlorinated hydrocarbons removal by zero-valent iron. Chemosphere 54, 917-925.

Jiang, D.L., Zhao, H.J., Zhang, S.Q., John, R., 2003. Characterization of photoelectrocatalytic processes at nanoporous TiO_2 film electrodes: photocatalytic oxidation of glucose. J. Phys. Chem. B 107, 12774-12780.

Jin, F., Leitich, J., Sonntag, C.V., 1995. The photolysis ($\lambda = 254$ nm) of tyrosine in aqueous solutions in the absence and presence of oxygen: the reaction of tyrosine with singlet oxygen. J. Photochem. Photobiol. A 92, 147-153.

Jirkovský, J., Faure, V., Boule, P., 1997. Photolysis of diuron. Pestic. Sci. 50 (1), 42-52.

Johnson, A.C., Sumpter, J.P., 2001. Removal of endocrine-disrupting chemicals in activated sludge treatment works. Environ. Sci. Technol. 35, 4697-4703.

Kabra, K., Chaudhary, R., Sawhney, R.L., 2004. Treatment of hazardous organic and inorganic compounds through aqueous-phase photocatalysis: a review. Ind. Eng. Chem. Res. 43, 7683-7696.

Kagaya, S., Shimizu, K., Arai, R., Hasegawa, K., 1999. Separation of titanium dioxide photocatalyst in its aqueous suspensions by coagulation with basic aluminium chloride. Water Res. 33, 1753-1755.

Kalyanasundaram, K., 1982. Photophysics, photochemistry and solar energy conversion with tris(bipyridyl)ruthenium(II) and its analogues. Coord. Chem. Rev. 46, 159-244.

Kang, S.F., Liao, C.H., Po, S.T., 2000. Decolorization of textile wastewater by photo-fenton oxidation technology. Chemosphere 41, 1287-1294.

Kasuga, T., Hiramatsu, M., Hoson, A., Sekino, T., Niihara, K., 1998. Formation of titanium oxide nanotube. Langmuir 14, 3160-3163.

Kasuga, T., Hiramatsu, M., Hoson, A., Sekino, T., Niihara, K., 1999. Titania nanotubes prepared by chemical processing. Adv. Mater. 11, 1307-1311.

Katsoyiannis, A., Samara, C., 2004. Persistent organic pollutants (POPs) in the sewage treatment plant of Thessaloniki, northern Greece: occurrence and removal. Water Res. 38, 2685-2698.

Kavan, L., O'Regan, B., Kay, A., Grätzel, M., 1993. Preparation of TiO_2 (anatase) films on electrodes by anodic oxidative hydrolysis of $TiCl_3$. J. Electroanal. Chem. 346, 291-307.

Kawai, S., Ueda, R., 1975. Magnetic properties of anodic oxide coatings on aluminum containing electrodeposited Co and Co-Ni. J. Electrochem. Soc. 122, 32-36.

Kemell, M., Pore, V., Tupala, J., Ritala, M., Leskelä, M., 2007. Atomic layer deposition of nanostructured TiO_2 photocatalysts via template approach. Chem. Mater. 19, 1816 -1820.

Khan, M.A., Jung, H.T., Yang, O.B., 2006. Synthesis and characterization of ultrahigh crystalline TiO_2 nanotubes. J. Phys. Chem. B 110, 6626-6630.

Khodja, A.A., Lavedrine, B., Richard, C., Sehill, T., 2002. Photocatalytic degradation of metoxuron in aqueous suspension of TiO_2. Analytical and kinetic studies. Int. J. Photoenergy 4, 147-151.

Kim, D.H., Anderson, M.A., 1994. Photoelectrocatalytic degradation of formic acid using a porous TiO_2 thin- film electrode. Environ. Sci. Technol. 28, 479-483.

Kim, Y.J., Francis, L.F., 1993. Processing and characterization of porous TiO_2 coatings. J. Am. Ceram. Soc. 76, 737-742.

Kinzell, L.H., McKenzie, R.M., Olson, B.A., Kirsch, D.G., Shull, L.R., 1979. Priority pollutants, I: a perspective view. Environ. Sci. Technol. 13, 416-423.

Kochany, J., Maguire, R., 1994. Sunlight photodegradation of metolachlor in water. J. Agric. Food Chem. 42, 406-412.

Kolla, A., Parasukb, V., Parasukc, W., Karpfend, A., Wolschann, P., 2004.

Theoretical study on the intramolecular hydrogen bond in chloro-substituted N,N-dimethylaminomethylphenols. I. Structural effects. J. Mol. Struct. 690, 165-174.

Konstantinou, I.K., Sakkas, V.A., Albanis, T.A., 2001. Photocatalytic degradation of the herbicides propanil and molinate over aqueous TiO_2 suspensions: identification of intermediates and the reaction pathway. Appl. Catal. B-Environ. 34, 227-239.

Kositzi, M., Poulios, I., Malato, S., Caceres, J., Campos, A., 2004. Solar photocatalytic treatment of synthetic municipal wastewater. Water Res. 38, 1147-1154.

Krautler, B., Bard, A.J., 1978. Heterogeneous photocatalytic synthesis of methane from acetic acid - new Kolbe reaction pathway. J. Am. Chem. Soc. 100, 2239-2240.

Krýsová, H., Krýsa, J., Macounová, K., Jirkovský, J., 1998. Photocatalytic degradation of diuron [3-(3,4-dichlorophenyl)-1,1-dimethylurea] on the layer of TiO_2 particles in the batch mode plate film reactor. J. Chem. Technol. Biotechnol. 72, 169-175.

Krzeminski, L.F., Cox, B.L., Neff, A.W., 1966. Separation and identification of carbon-14 diphenamid metabolites using chromatographic techniques. J. Agr. Food Chem. 14, 126-130.

Ku, Y., Leu, R.M., Lee, K.C., 1996. Decomposition of 2-chlorophenol in aqueous solution by UV irradiation with the presence of titanium dioxide. Water Res. 30, 2569-2578.

Kudo, A., Steinberg, M., Bard, A.J., Campion, A., Fox, M.A., Mallouk, T.E., Webber, S.E., White, J.M., 1990. Photoelectrochemical properties of titanium dioxide electrodes prepared from a titanium-aluminum alloy. J. Electrochem. Soc. 137, 3846-3849.

Kuo, W.G., 1992. Decolorizing dye wastewater with Fenton's reagent. Water Res. 26, 881-886.

Kuo, W.S., Ho, P.H., 2006. Solar photocatalytic decolorization of dyes in solution with TiO_2 film. Dyes Pigments 71, 212-217.

Kurinobu, S., Tsurusaki, K., Natui, Y., Kimata, M., Hasegawa, M., 2007. Decomposition of pollutants in wastewater using magnetic photocatalyst particles. J. Magn. Magn. Mater. 310, E1025-1027.

Lai, Y.K., Sun, L., Chen, Y.C., Zhuang, H.F., Lin, C.J., Chin, J.W., 2006. Effects of the structure of TiO_2 nanotube array on Ti substrate on its photocatalytic activity. J. Electrochem. Soc, 153, D123-127.

Lai, Y.K., Sun, L., Chen, Y.C., Zhuang, H.F., Lin, C.J., Chin, J.W., 2006. Effects of the structure of TiO_2 nanotube array on Ti substrate on its photocatalytic activity. J. Electrochem. Soc. 153, D123-127.

Lakshmi, B.B., Patrissi, C.J., Martin, C.R., 1997. Sol-gel template synthesis of semiconductor oxide micro- and nanostructures. Chem. Mater. 9, 2544-2550.

Langlais, B., Reckhow, D.A., Brink, R.B. (Eds.), 1991. Ozone in water treatment—Application and engineering. Lewis Publishers, Chelsea, USA, pp. 43-45.

Lee, C.H., Yoon, J.Y., 2008. UV direct photolysis of 2,2’-azino-bis(3-ethylbenzothiazoline-6-sulfonate) (ABTS) in aqueous solution: kinetics and mechanism. J. Photochem. Photobiol. A 197, 232–238.

Lee, J.C., Kim, M.S., Kim, C.K., Chung, C.H., Cho, S.M., Han, G.Y., Yoon, K.J., Kim, B.W., 2003. Removal of paraquat in aqueous suspension of TiO_2 in an immersed UV photoreactor. Korean J. Chem. Eng. 20, 862-868.

Lee, J.Y., Park, J., Cho, J.H., 2005. Electronic properties of N- and C-doped TiO_2. Appl. Phys. Lett. 87, 11904.

Lee, P.F., Zhang, X.W., Sun, D.D., Du, J.H., Leckie, J.O., 2008. Synthesis of bimodal porous structured TiO_2 microsphere with high photocatalytic activity for water treatment. Colloid. Surface A 324, 202-207.

Lee, S.A., Choo, K.H., Lee, C.H., Lee, H.I., Hyeon, T., Choi, W.Y., Kwon, H.H., 2001. Use of ultrafiltration membranes for the separation of TiO_2 photocatalysts in drinking water treatment. Ind. Eng. Chem. Res. 40, 1712-1719.

Legrini, O., Oliveros, E., Braun, A.M., 1993. Photochemical processes for water treatment. Chem. Rev. 93, 671-698.

Lei, L.C., Su, Y.L., Zhou, M.H., Zhang, X.W., Chen, X.Q., 2007. Fabrication of multi-non-metal-doped TiO_2 nanotubes by anodization in mixed acid electrolyte. Mater. Res. Bull. 42, 2230-2236.

Leyva, E., Moctezuma, E., Ruíz, M.G., Martínez, L., 1998. Photodegradation of phenol and 4-chlorophenol by $BaO–Li_2O–TiO_2$ catalysts. Catal. Today 40, 367-376.

Li, H.Y., Sundararaman, A., Venkatasubbaiah, K., Jäkle, F., 2007. Organoborane acceptor-substituted polythiophene via side-group borylation. J. Am. Chem. Soc. 129, 5792-5793.

Li, X.Q., Elliott, D.W., Zhang, W.X., 2006. Zero–valent iron nanoparticles for abatement of environmental pollutants: materials and engineering aspects. Crit. Rev. Solid State Mater. Sci. 31, 111-122.

Li, X.Z., Li, F.B., Yang, C.L., Ge, W.K., 2001. The photo-catalytic activity of WO_x-TiO_2 under visible light irradiation. J. Photochem. Photobiol. A 141, 209-217.

Li, X.Z., Liu, H., Cheng, L.F., Tong, H.J., 2003. Photocatalytic oxidation using a new catalyst-TiO_2 microsphere-for water and wastewater treatment. Environ. Sci. Technol. 37, 3989-3994.

Li, X.Z., Liu, H.L., Yue, P.T., Sun, Y.P., 2000. Photoelectrocatalytic oxidation of rose bengal in aqueous solution using a Ti/TiO_2 mesh electrode. Environ. Sci. Technol. 34, 4401–4406.

Li, X.Z., Liu, H.S., 2005. Development of an E-H_2O_2/TiO_2 photoelectrocatalytic oxidation system for water and wastewater treatment. Environ. Sci. Technol. 39, 4614-4620.

Li, X.Z., Zhao, Q.L., Hao, X.D., 1999a. Ammonium removal from landfill leachate by chemical precipitation. Waste Manage. 19, 409-415.

Li, X.J., Cubbage, J.W., Jenks, W.S., 1999b. Photocatalytic degradation of 4-chlorophenol. 2. The 4-chlorocatechol pathway. J. Org. Chem. 64, 8525-8536.

Limiroli, R., Consonni, R., Ranalli, A., Bianchi, G., Zetta, L., 1996. ^{1}H NMR study of phenolics in the vegetation water of three cultivars of *olea europaea*: similarities and differences. J. Agric. Food Chem. 44, 2040-2048.

Lin, L., Lin, W., Zhu, Y.X., Zhao, B.Y., Xie, Y.C., 2005. Phosphor-doped titania: a novel photocatalyst active in visible light. Chem. Lett. 34, 284-285.

Linsebigler, A.L., Lu, G., Yates, J.T., 1995. Photocatalysis on TiO_2 surfaces: principles, mechanisms, and selected results. Chem. Rev. 95, 735–758.

Litter, M.I., 2005. Introduction to photochemical advanced oxidation processes for water treatment. Hdb. Environ. Chem. 2, 325–366.

Lu, N., Quan, X., Li, J.Y., Chen, S., Yu, H.T., Chen, G.H., 2007. Fabrication of boron-doped TiO_2 nanotube array electrode and investigation of its hotoelectrochemical capability. J. Phys. Chem. C 111, 11836-11842.

Lubberhuizen, W.H., Vanmaekelbergh, D., Van Faassen, E., 2000. Recombination of photogenerated charge carriers in nanoporous gallium phosphide. J. Porous Mater. 7, 147-152.

Ma, R., Bando, Y., Sasaki, T., 2003. Nanotubes of lepidocrocite titanates. Chem. Phys. Lett. 380, 577-582.

Macák, J.M., Tsuchiya, H., Ghicov, A., Schmuki, P., 2005. Dye-sensitized anodic TiO_2 nanotubes. Electrochem. Commun. 7, 1133–1137.

Macák, J.M., Zlamal, M., Krysa, J., Schmuki, P., 2007. Self-organized TiO_2 nanotube layers as highly efficient photocatalysts. Small 3, 300-304.

Macdonald, D.D., 1993. On the formation of voids in anodic oxide films on aluminum. J. Electrochem. Soc. 140, L27-30.

Mars, J.A., Gihwala, D., Przybyowicz, W.J., Bladergroen, B., Linkov, V., 2004. μ-IBA analysis of Al_2O_3-ZrO_2 tubes to be used in wastewater purification. Radiat. Phys. Chem. 71, 799-800.

Martin, C.R., 1991. Template synthesis of polymeric and metal microtubules. Adv. Mater. 3, 457-459.

Martin, C.R., 1996. Membrane-based synthesis of nanomaterials. Chem. Mater. 8, 1739-1746.

Martin, S.T., Herrmann, H., Choi, W., Hoffmann, M.R., 1994. Time-resolved microwave conductivity. Trans. Faraday Soc. 90, 3315-3323.

Matthews, R.W., 1987. Solar-electric water-purification using photocatalytic oxidation with TiO_2 as a stationary phase. Sol. Energy 38, 405-413.

Matthews, R.W., 1988. Kinetics of photocatalytic oxidation of organic solutes over titanium dioxide. J. Catal. 111, 264-272.

Matthews, R.W., 1991. Photooxidative degradation of coloured organics in water using supported catalysts TiO_2 on sand. Water Res. 25, 1169-1176.

Matthews, R.W., McEvoy, S.R., 1992. Photocatalytic degradation of phenol in the presence of near-UV illuminated titanium dioxide. J. Photochem. Photobiol. A 64, 231-246.

McMurraya, T.A., Byrne, J.A., Dunlop, P.S.M., Winkelman, J.G.M., Eggins, B.R., McAdams, E.T., 2004. Intrinsic kinetics of photocatalytic oxidation of formic and oxalic acid on immobilised TiO_2 films. Appl. Catal. A 262, 105-110.

Mei, Y.F., Wu, X.L., Shao, X.F., Huang, G.S., Siu. G.G., 2003. Formation mechanism of alumina nanotube array. Phys. Lett. A 309, 109-113.

Miller, L.L., Zinger, B., Zhou, Q.X., 1987. Electrically controlled release of hexacyanoferrate(4-) from polypyrrole. J. Am. Chem. Soc. 109, 2267-2272.

Mills, A., Hunte, S.L., 1997. An overview of semiconductor photocatalysis. J. Photochem. Photobiol. A 108, 1-35.

Mills, G., Hoffmann, M.R., 1993. Photocatalytic degradation of pentachlorophenol on titanium dioxide particles: identification of intermediates and mechanism of reaction. Environ. Sci. Technol. 27, 1681-1689.

Min, S.X., Wang, F., Han, Y.Q., 2007. An investigation on synthesis and photocatalytic activity of polyaniline sensitized nanocrystalline TiO_2 composites. J.

Mater. Sci. 42, 9966-9972.

Mmurraya, T.A., Byrne, J.A., Dunlop, P.S.M., Winkelman, J.G.M., Eggins, B.R., Adams, E.T., 2004. Intrinsic kinetics of photocatalytic oxidation of formic and oxalic acid on immobilised TiO_2 films. Appl. Catal. A 262, 105–110.

Mohapatra, S.K., Misra, M., Mahajan, V.K., Raja. K.S., 2007. Design of a highly efficient photoelectrolytic cell for hydrogen generation by water splitting: application of $TiO_{2-x}C_x$ nanotubes as a photoanode and Pt/TiO_2 nanotubes as a cathode. J. Phys. Chem. C 111, 8677-8685.

Molinari, R., Mungari, M., Drioli, E., Paola, A.D., Loddo, V., Palmisanob, L., Schiavello, M., 2000. Study on a photocatalytic membrane reactor for water purification. Catal. Today 55, 71–78.

Molinari, R., Palmisano, L., Drioli, E., Schiavello, M., 2002. Studies on various reactor configurations for coupling photocatalysis and membrane processes in water purification. J. Membrane Sci. 206, 399-415.

Mor, G.K., Shankar, K., Paulose, M., Varghese, O.K., Grimes, C.A., 2005a. Enhanced photocleavage of water using titania nanotube arrays. Nano Lett. 5, 191-195.

Mor, G.K., Varghese, O.K., Paulose, M., Grimes, C.A., 2005b. Transparent highly ordered TiO_2 nanotube arrays via anodization of titanium thin films. Adv. Funct. Mater. 15, 1291-1296.

Mor, G.K., Varghese, O.K., Paulose, M., Shankar, K., Grimes,C.A., 2006a. A review on highly ordered, vertically oriented TiO_2 nanotube arrays: fabrication, material properties, and solar energy applications. Sol. Energy Mater. Sol. Cells 90, 2011-2075.

Mor, G.K., Shankar, K., Paulose, M., Varghese, O.K., Grimes, C.A., 2006b. Use of highly-ordered TiO_2 nanotube arrays in dye-sensitized solar cells. Nano Lett. 6, 215-218.

Mor, G.K., Varghese, O.K., Paulose, M., Ong, K.G., Grimes, C.A., 2006c. Fabrication of hydrogen sensors with transparent titanium oxide nanotube-array thin films as sensing elements. Thin Solid Films 496, 42-48.

Morikawa, T., Asahi, R., Ohwaki, T., Aoki, K., Taga, Y., 2001. Band-gap narrowing of titanium dioxide by nitrogen doping. J. Appl. Phys. Lett. 40, L561-563.

Moser, J., Punchihewa, S., Infelta, P.P., Grätzel, M., 1991. Surface complexation of colloidal semiconductors strongly enhances interfacial electron-transfer rates. Langmuir 7, 3012-3018.

Mozia, S., Morawski, A.W., 2006. Hybridization of photocatalysis and membrane distillation for purification of wastewater. Catal. Today 118, 181–188.

Mozia, S., Morawski, A.W., Toyoda, M., Inagaki, M., 2008. Effectiveness of photodecomposition of an azo dye on a novel anatase-phase TiO_2 and two commercial photocatalysts in a photocatalytic membrane reactor (PMR). Sep. Purif. Technol. 63, 386–391.

Muktha, B., Mahanta, D., Patil, S., Madras, G., 2007. Synthesis and photocatalytic activity of poly(3-hexylthiophene)TiO_2 composites. J. Solid State Chem. 180, 2986-2989.

Nagaoka, S., Hamasaki, Y., Ishihara, S., Nagata, M., IiO, K., Nagasawa, C., Ihara, H., 2002. Preparation of carbon/TiO_2 microsphere composites from cellulose/TiO_2 microsphere composites and their evaluation. J. Molecular Catal. 177, 255-263.

Nair, M., Luo, Z., Heller, A., 1993. Rates of photocatalytic oxidation of crude oil on salt water on buoyant cenosphere-attached titanium dioxide. Ind. Eng. Chem. Res. 32, 2318-2323.

Nakade, S., Saito, Y., Kubo, W., Kanzaki, T., Kitamura, T., Wada, Y., Yanagida, S., 2003. Enhancement of electron transport in nano-porous TiO_2 electrodes by dye adsorption. Electrochem. Commun. 5, 804-808.

Nakahira, A., Kato, W., Tamai, M., Isshiki, T., Nishio, K., 2004. Synthesis of nanotube from a layered $H_2Ti_4O_9{\cdot}H_2O$ in a hydrothermal treatment using various titania sources. J. Mater. Sci. 39, 4239-4245.

Naskar, S., Pillay, S.A., Chanda, M., 1998. Photocatalytic degradation of organic dyes in aqueous solution with TiO_2 nanoparticles immobilized on foamed polyethylene sheet. J. Photochem. Photobiol. A 113, 257-264.

Nazeeruddin, M.K., Kay, A., Rodicio, I., Baker, R., Müller, E., Liska, P., Vlachopoulos, N., Grätzel, M., 1993. Conversion of light to electricity by cis-X2bis(2,2'-bipyridyl-4,4'-dicarboxylate)ruthenium(II) charge-transfer sensitizers (X = Cl^-, Br^-, I-, CN^-, and SCN^-) on nanocrystalline titanium dioxide electrodes. J. Am. Chem. Soc. 115, 6382-6390.

Neale, N.R., Kopidakis, N., Lagemaat, J., Grätzel, M., Frank, A.J., 2005. Effect of a coadsorbent on the performance of dye-sensitized TiO_2 solar cells: shielding versus band-edge movement. J. Phys. Chem. B 109, 23183-23189.

O’Regan, B., Grätzel, M., 1991. A low-cost, high-efficiency solar cell based on dye-sensitized colloidal TiO_2 films. Nature (London) 353, 737-740.

Pagga, U., Taeger, K., 1994. Development of a method for adsorption of dyestuffs on activated sludge. Water Res. 28, 1051-1057.

Pan, L.M., Ji, M., Wang, M.M., Zhang, X., Lu, B., 2007. Preparation of titanium dioxide nanotube and its catalytic activity for ozonation. (Chinese) J. Chem. Ind. Eng. 11, 2787-2792.

Park, H., Choi, W., 2005. Photocatalytic reactivities of nafion-coated TiO_2 for the degradation of charged organic compounds under UV or visible light. J. Phys. Chem. B 109, 11667-11674.

Park, J., Kim, S., Bard, A.J., 2006. Novel carbon-doped TiO_2 nanotube arrays with high aspect ratios for efficient solar water splitting. Nano Lett. 6, 24-28.

Parkhutik, V.P., Shershulsky, V.I., 1992. Theoretical modeling of porous oxide growth on aluminum. J. Phys. D Appl. Phys. 25, 1258-1263.

Patermarakis, G., Karayannis, H.S., 1995. The mechanism of growth of porous anodic Al_2O_3 films on aluminium at high film thicknesses. Electrochim. Acta 40, 2647-2656.

Paulose, M., Mor, G.K., Varghese, O.K., Shankar, K., Grimes, C.A., 2006. Visible light photoelectrochemical and water-photoelectrolysis properties of titania nanotube arrays. J. Photochem. Photobiol. A 178, 8-15.

Pavia, D.L., Lampman, G.M., Kriz, G.S., 2001. Introduction to spectroscopy: a guide for students of organic chemistry. Brooks/Cole. 3rd ed. Singapore.

Peng, T.Y., Hasegawa, A., Qiu, J.R., Hirao, K., 2003. Fabrication of titania tubules with high surface area and well-developed mesostructural walls by surfactant-mediated templating method. Chem. Mater. 15, 2011-2016.

Peterson, C.E., Reneau, R.B., Hagedorn, C., 1994. Use of mine fills for biological renovation of domestic wastewater. J. Environ. Qual. 23, 592-596.

Piao, Y.Z., Lim, H.C., Chang, J.Y., Lee, W.Y., Kim, H., 2005. Nanostructured materials prepared by use of ordered porous alumina membranes. Electrochim. Acta 50, 2997-3013.

Pocchiari, F., Silano, V., 1982. Contingency planning for and response to emergencies and accidents involving toxic chemicals. Third international symposium on chlorinated dioxins and related compounds, Saltzburg, Austria, 12-14.

Polo, A.S., Itokazu, M.K., Iha, N.Y.M., 2004. Metal complex sensitizers in dye-sensitized solar cells. Coord. Chem. Rev. 248, 1343-1361.

Prieto, O., Fermoso, J., Nuěez, Y., Del Valle, J.L., Irusta, R., 2005. Decolouration of textile dyes in wastewaters by photocatalysis with TiO_2. Sol. Energy 79, 376-383.

Pron, A., Rannou, P., 2002. Processible conjugated polymers from organic semiconductors to organic metals and superconductors. Prog. Polym. Sci. 27, 135-190.

Qamar, M., Yoon, C.R., Oh, H.J., Lee, N.H., Park, K., Kim, D.H., Lee, K.S., Lee, W.J., Kim, S.J., 2008. Preparation and photocatalytic activity of nanotubes obtained from titanium dioxide. Catal. Today 131, 3-14.

Quan, X., Ruan, X.L., Zhao, H.M., Chen, S., Zhao, Y.Z., 2007. Photoelectrocatalytic degradation of pentachlorophenol in aqueous solution using a TiO_2 nanotube film electrode. Environ. Pollut. 147, 409-414.

Quan, X., Yang, S.G., Ruan, X.L., Zhao, D.M., 2005. Preparation of titania nanotubes and their environmental applications as electrode. Environ. Sci. Technol. 39, 3770-3775.

Rachel, A., Subrahmanyam, M., Boule, P., 2002. Comparison of photocatalytic efficiencies of TiO_2 in suspended and immobilised form for the photocatalytic degradation of nitrobenzenesulfonic acids. Appl. Catal. B-Environ. 37, 301-308.

Rahman, M.A., Muneer, M., Bahnemann, D., 2003. Photocatalysed degradation of a herbicide derivatives, diphenamid in aqueous suspension of titanium dioxide. J. Adv. Oxid. Technol. 6, 100–108.

Rao, C.N.R., Govindaraj, A., Deepak, F.L., Gunari, N.A., 2001. Surfactant-assisted synthesis of semiconductor nanotubes and nanowires. Appl. Phys. Lett. 78, 1853-1855.

Rensmo, H., Westermark, K., Södergren, S., Kohle, O., Perssona, P., Lunell, S., Siegbahn, H., 1999. XPS studies of Ru-polypyridine complexes for solar cell applications. J. Chem. Phys. 111, 2744-2750.

Reuterglrdh, L.B., Iangphasuk. M., 1997. Photocatalytic decolourization of reactive azo dye: a comparison between TiO_2 and CdS photocatalysis. Chemosphere 35, 585-596.

Rincón, A.G., Pulgarin, C., 2004. Effect of pH, inorganic ions, organic matter and H_2O_2 on E. coli K12 photocatalytic inactivation by TiO_2 implications in solar water disinfection. Appl. Catal. B-Environ. 51, 283-302.

Roberson, L.B., Poggi, M.A., Kowalik, J., Smestad, G.P., Bottomley, L.A., Tolbert, L.M., 2004. Correlation of morphology and device performance in inorganic-organic TiO_2-polythiophene hybrid solid-state solar cells. Coordin. Chem. Rev. 248, 1491-1499.

Rosen, J.D., 1967. The photolysis of diphenamid. B. Environ. Contam. Tox. 2, 349-354.

Ruan, C., Paulose, M., Varghese, O.K., Mor, G.K., Grimes, C.A., 2005. Fabrication of highly ordered TiO_2 nanotube arrays using an organic electrolyte. J. Phys. Chem. B 109, 15754-15759.

Salzner, U., Lagowski, J.B., Pickup, P.G., Poirier, R.A., 1998. Comparison of electronic structures of polycylopentadiene, polypyrrole, polyfuran, polysilole, polyphosphole, polythiophene, polyselenophene, and polytellurophene. Synth. Met. 96, 177-189.

Schultz, D.P., Tweedy, B.G., 1972. The effect of light and humidity on absorption and degradation of diphenamid in tomatoes. J. Agric. Food Chem. 20, 10-13.

Schulz, D.L., Marks, T.J., 1994. MOCVD routes to thin metal oxide films for superconducting electronics. Adv. Mater. 6, 719-730.

Seo, D.S., Lee, J.K., Kim, H., 2001. Preparation of nanotube-shaped TiO_2 powder. J. Cryst. Growth 229, 428-432.

Serpone, N., 1997. Relative photonic efficiencies and quantum yields in heterogeneous photocatalysis. J. Photochem. Photobiol. A 104, 1-12.

Serpone, N., Lawless, D., Disdier, J., Herrmann, J.M., 1994. Spectroscopic, photoconductivity, and photocatalytic studies of TiO_2 colloids: naked and with the lattice doped with Cr^{3+}, Fe^{3+}, and V^{5+} cations. Langmuir 10, 643-652.

Serpone, N., Maruthamuthu, P., Pichat, P., Pelizzetti, E., Hidaka, H., 1995. Exploiting the interparticle electron transfer process in the photocatalyzed oxidation of phenol, 2-chlorophenol and pentachlorophenol: chemical evidence for electron and hole transfer between coupled semiconductors. J. Photochem. Photobiol. A 85, 247-255.

Serpone, N., Terzian, R., Lawless, D., Kennepohl, P., Sauve, G., 1993. On the usage of turnover numbers and quantum yields in heterogeneous photocatalysis. J.

Photochem. Photobiol. A 73, 11-16.

Shaheen, S.E., Brabec, C.J., Padinger, F., Fromherz, T., Hummelen, J.C., Sariciftci, N.S., 2001. 2.5 % efficient organic plastic solar cell. Appl. Phys. Lett. 78, 841-843.

Shephard, G.S., Stochenstrom, S., De-Villiers, D., Engelbrech, W.J., Wessels, G.F.S., 2002. Degradation of microcystin toxins in a falling film photocatalytic reactor with immobilized titanium dioxide catalyst. Water Res. 36, 140-146.

Shiny, K.J., Remani, K.N., Nirmala, E., Jalaja, T.K., Sasidharan, V.K., 2005. Biotreatment of wastewater using aquatic invertebrates, Daphnia magna and Paramecium caudatum. Bioresource Technol. 96, 55-58.

Shon, H.K., Phuntsho, S., Vigneswaran, S., 2008. Effect of photocatalysis on the membrane hybrid system for wastewater treatment. Desalination 225, 235–248.

Snook, J.H., Samuelson, L.A., Kumar, J., Kim, Y.G., Whitten, J.E., 2005. Ultraviolet photoelectron spectroscopy of nanocrystalline titanium dioxide films sensitized with (2,2'-bipyridyl)ruthenium(II) dyes for photovoltaic applications. Org. Electron. 6, 55-64.

Somanathan, N., Radhakrishnan, S., 2005. Optical properties of functionalized polythiophenes. Int. J. Mod. Phys. B 19 (32) 4645-4676.

Song, L., Qiu, R.L., Mo, Y.Q., Zhang, D.D., Wei, H., Xiong, Y., 2007. Photodegradation of phenol in a polymer-modified TiO_2 semiconductor particulate system under the irradiation of visible light. Catal. Commun. 8, 429-433.

Stafford, U., Gray, K.A., Kamat, P.V., 1994. Radiolytic and TiO_2-assisted photocatalytic degradation of 4-chlorophenol. A comparative study. J. Phys. Chem. 98, 6343-6351.

Su, Y.L., Zhang, X.W., Zhou, M.H., Han, S., Lei, L.C., 2008. Preparation of high efficient photoelectrode of N-F-codoped TiO_2 nanotubes. J. Photochem. Photobiol. A 194, 152–160.

Suri, R.P.S., Liu, J.B., Crittenden, J.C., Hand, D.W., 1999. Removal and destruction of organic contaminants in water using adsorption, steam regeneration, and photocatalytic oxidation: a pilot-scale study. J. Air. Waste Manage. 49, 951-958.

Tada, H., Honda, H., 1995. Photocatalytic activity of TiO_2 film coated on internal lightguide. J. Electrochem. Soc. 142, 3438-3443.

Tahiri, H., Ichou, Y.A., Herrmann, J.M., 1998. Photocatalytic degradation of chlorobenzoic isomers in aqueous suspensions of neat and modified titania. J. Photochem. Photobiol. A 114, 219-226.

Takemura, S., Kato, H., Nakajima, Y., 1999. Photoelectron studies of electrochemical diffusion of conducting polymer/transparent conductive metal oxide film interfaces. Appl. Surf. Sci. 144-145, 360-365.

Takeuchi, M., Yamashita, H., Matsuoka, M., Anpo, M., Hirao, T., Itoh, N., Iwamoto, N., 2000. Photocatalytic decomposition of NO under visible light irradiation on the Cr-ion-implanted TiO_2 thin film photocatalyst. Catal. Lett. 67, 135-137.

Tallec, G., Garnier, J., Billen, G., Gousailles, M., 2006. Nitrous oxide emissions from secondary activated sludge in nitrifying conditions of urban wastewater treatment plants: effect of oxygenation level. Water Res. 40, 2972-2980.

Tan, Z.A., Zhou, E.J., Yang, Y., He, Y.J., Yang, C.H., Li, Y.F., 2007. Synthesis, characterization and photovoltaic properties of thiophene copolymers containing conjugated side-chain. Eur. Polym. J. 43, 855-861.

Tang, H., Prasad, K., Sanjinès, R., Schmid, P.E., Lévy, F., 1994. Electrical and optical properties of TiO_2 anatase thin films. J. Appl. Phys. 75, 2042-2047.

Tang, W.Z., Huang, C.P., 1995. The effect of chlorine position of chlorinated phenols on their dechlorination kinetics by Fenton’s reagent. Waste Manage. 15, 615-622.

Tang, X.H., Li. D.Y., 2008. Sulfur-doped highly ordered TiO_2 nanotubular arrays with visible light response. J. Phys. Chem. C 112, 5405-5409.

Tehan, B.G., Lloyd, E.J., Wong, M.G., Pitt, W.R., Montana, J.G., Manallack, D.T., Gancia, E., 2002. Estimation of pK_a using semiempirical molecular orbital methods. Part 1: Application to phenols and carboxylic acids. Quant. Struct-Act. Rel. 21, 457-472.

The Southampton Electrochemistry Group, Instrumental Methods in Electrochemistry, Ellis Horwood, Chichester, 1985, p. 283.

Thimijan, R.W., Heins, R.D., 1983. A review of conversion constants and procedures for photometric, radiometric, and quantum light units of measure. Hortscience 18, 818-822.

Thiruvenkatachari, R., Vigneswaran, S., Moon, S., 2008. A review on TiO_2/UV photocatalytic oxidation process. Korean J. Chem. Eng. 25, 64-72.

Thorne, A., Kruth, A., Tunstall, D., Irvine, J.T.S., Zhou, W., 2005. Formation, structure, and stability of titanate nanotubes and their proton conductivity. J. Phys. Chem. B 109, 5439-5444.

Trejo-Tzab, R., Alvarado-Gil, J.J., Quintana, P., López, T., 2008. Study of the photoactivation of titania Degussa P25 in ethanol–methanol suspensions using a piezoelectric sensor. J. Mol. Catal. A 281, 113–118.

Tsai, C.C., Teng, H., 2006. Structural features of nanotubes synthesized from NaOH treatment on TiO_2 with different post-treatments. Chem. Mater. 18, 367-373.

Tsuchiya, H., Macak,J.M., Taveira, L., Balaur, E., Ghicov, A., Sirotna, K., Schmuki. P., 2005. Self-organized TiO_2 nanotubes prepared in ammonium fluoride containing acetic acid electrolytes. Electrochem. Commun. 7, 576–580.

Turchi, C. S., Ollis, D.F., 1990. Photocatalytic degradation of organic water contaminants: mechanisms involving hydroxyl radical attack. J. Catal. 122, 178-192.

Uchikoshi, T., Suzuki, T.S., Tang, F., Okuyama, H., Sakka, Y., 2004. Crystalline-oriented TiO_2 fabricated by the electrophoretic deposition in a strong magnetic field. Ceramic Inter. 30, 1975-1978.

Vamvounis, G., Yu, J.F., Holdcroft, S., 2004. Photo-physical and electro-optical properties of polythiophenes bearing tetrahydropyran side groups. Eur. Polym. J. 40, 2659-2664.

Varghese, O.K., Gong, D., Paulose, M., Grimes, C.A., Dickey, E.C., 2003. Crystallization and high temperature structural stability of titanium oxide nanotube arrays. J. Mater. Res. 18, 156-165.

Varghese, O.K., Mor, G.K., Grimes, C.A., Paulose, M., Mukherjeeb, N., 2004. A titania nanotube-array room-temperature sensor for selective detection of hydrogen at low concnetrations. J. Nanosci. Nanotechnol. 4, 733-737.

Varghese, O.K., Paulose, M., Shankar, K., Mor, G.K., Grimes. C.A., 2005. Water-photolysis properties of micron-length highly-ordered titania nanotube-arrays. J. Nanosci. Nanotechnol. 5, 1158–1165.

Vinodgopal, K., Stafford, U., Gray, K.A., Kamat, P.V., 1994. Electrochemically assisted photocatalysis. 2. The role of oxygen and reaction intermediates in the degradation of 4-chlorophenol on immobilized TiO_2 particulate films. J. Phys. Chem. 98, 6797-6803.

Vitiello, R.P., Macak, J.M., Ghicov, A., Tsuchiya, H., Dick, L.F.P., Schmuki, P., 2006. N-doping of anodic TiO_2 nanotubes using heat treatment in ammonia. Electrochem. Commun. 8, 544–548.

Vu, Q.T., Pavlik, M., Hebestreit, N., Pfleger, J., Rammelt, U., Plieth, W., 2005. Electrophoretic deposition of nanocomposites formed from polythiophene and metal oxides. Electrochim. Acta 51, 1117-1124.

Wang, N., Lin, H., Li, J.B., Yang, X.Z., Chi, B., 2006. Electrophoretic deposition and optical property of titania nanotubes films. Thin Solid Films 496, 649-652.

Wang, Y.B., Hong, C.S., 1999. Effect of hydrogen peroxide, periodate and persulfate on photocatalysis of 2-chlorobiphenyl in aqueous TiO_2 suspensions. Water Res. 33, 2031-2036.

Watanabe, N., Horikoshi, S., Kawabe, H., Sugie, Y., Zhao, J., Hidaka, H., 2003. Photodegradation mechanism for Bisphenol A at the TiO_2/H_2O interfaces. Chemosphere 52, 851-859.

Weed Science Society of America, Herbicide Handbook Committee, Herbicide Handbook of the Weed Science Society of America, 5th ed., Weed Science Society of America, Champaign, IL, 1983, p 515.

Wei, T.Y., Wan, C.C., 1991. Heterogeneous photocatalytic oxidation of phenol with titanium dioxide powders. Ind. Eng. Chem. Res. 30, 1293-1300.

Wen, C., Hasegawa, K., Kanbara, T., Kagaya, S., Yamamoto. T., 2000. Visible light-induced catalytic degradation of iprobenfos fungicide by poly(3-octylthiophene-25-diyl) film. J. Photochem. Photobiol. A 133, 59-66.

Wu, M.M., Long, J.B., Huang, A.H., Luo, Y.J., 1999. Microemulsion-mediated hydrothermal synthesis and characterization of nanosize rutile and anatase particles. Langmuir 15, 8822-8825.

Xie, Y.B., 2006. Photoelectrochemical application of nanotubular titania photoanode. Electrochim. Acta 51, 3399-3406.

Xu, Y.L., He, Y., Cao, X.D., Zhong, D.J., Jia, J.P., 2008. TiO_2/Ti rotating disk photoelectrocatalytic (PEC) reactor: a combination of highly effective thin-film PEC and conventional PEC processes on a single electrode. Environ. Sci. Technol. 42, 2612-2617.

Xue, X.D., Fu, J.F., Zhu, W.F., Guo, X.C., 2008. Separation of ultrafine TiO_2 from aqueous suspension and its reuse using cross-flow ultrafiltration (CFU). Desalination 225, 29-40.

Yanagida, S., Senadeera, G.K.R., Nakamura, K., Kitamura, T., Wada, Y., 2004. Polythiophene-sensitized TiO_2 solar cells. J. Photochem. Photobiol. A 166, 75-80.

Yang, J., Chen, C.C., Ji, H.W., Ma, W.H., Zhao, J.C., 2005. Mechanism of TiO_2-assisted photocatalytic degradation of dyes under visible irradiation: photoelectrocatalytic study by TiO_2-film electrodes. J. Phys. Chem. B 109, 21900–21907.

Yang, J., Jin, Z., Wang, X., Li, W., Zhang, J., Zhang, S., Guo, X., Zhang, Z., 2003. Study on composition, structure and formation process of nanotube $Na_2Ti_2O_4(OH)_2$. J. Chem. Soc., Dalton Trans. 20, 3898-3901.

Ye, F.X., Shen, D.S., 2004. Acclimation of anaerobic sludge degrading chlorophenols and the biodegradation kinetics during acclimation period. Chemosphere 54, 1573-1580.

Yoon, Y., Westerhoff, P., Snyder, S.A., Wert, E.C., Yoon, J., 2007. Removal of endocrine disrupting compounds and pharmaceuticals by nanofiltration and ultrafiltration membranes. Desalination 202, 16-23.

Yu, H.G., Yu, J.G., Cheng, B., Liu, S.W., 2007. Novel preparation and photocatalytic activity of one-dimensional TiO_2 hollow structures. Nanotechnology 18, 065604.

Yu, J.G., Yu, H.G., Cheng, B., Trapalis, C., 2006. Effects of calcination temperature on the microstructures and photocatalytic activity of titanate nanotubes. J. Mol. Catal. A 249, 135-142.

Yu, J.G., Zhao, X.J., Zhao, Q.N., 2000. Effect of surface structure on photocatalytic activity of TiO_2 thin films prepared by sol-gel method. Thin Solid Films 379, 7-14.

Yu, J.G., Zhao, X.J., Zhao, Q.N., 2001. Photocatalytic activity of nanometer TiO_2 thin films prepared by the sol-gel method. Mater. Chem. Phys. 69, 25-29.

Yuan, Z.Y., Su, B.L., 2004. Titanium oxide nanotubes, nanofibers and nanowires. Colloids Surf. A 241, 173-183.

Zafer, C., Karapire, C., Sariciftci, N.S., Icli, S., 2005. Characterization of N, N′-bis-2-(1-hydoxy-4-methylpentyl)-3, 4, 9, 10-perylene bis (dicarboximide) sensitized nanocrystalline TiO_2 solar cells with polythiophene hole conductors. Sol. Energ. Mater. Sol. Cells 88, 11-23.

Zhang, H.M., Quan, X., Chen, S., Zhao, H.M., Zhao, Y.Z., 2006. The removal of sodium dodecylbenzene sulfonate surfactant from water using silica/titania nanorods/nanotubes composite membrane with photocatalytic capability. Appl. Surf. Sci. 252, 8598-8604.

Zhang, L., Zhu, Y.F., He, Y., Sun, H.B., 2003a. Preparation and performances of mesoporous TiO_2 film photocatalyst supported on stainless steel. Appl. Catal. B-Environ. 40, 287-292.

Zhang, S., Peng, L.M., Chen, Q., Du, G.H., Dawson, G., Zhou, W.Z., 2003b. Formation mechanism of $H_2Ti_3O_7$ nanotubes. Phys. Rev. Lett. 91, 256103.

Zhang, M., Jin, Z.S., Zhang, J.W., Guo, X.Y., Yang, J.J., Li, W., Wang, X.D., Zhang, Z.J., 2004a. Effect of annealing temperature on morphology, structure and photocatalytic behavior of nanotubed $H_2Ti_2O_4(OH)_2$. J. Mol. Catal. A 217, 203-210.

Zhang, H., Ma, X., Xu, J., Yang, D., 2004b. Synthesis of CdS nanotubes by chemical bath deposition. J. Cryst. Growth 263, 372-376.

Zhang, Q., Gao, L., Sun, J., Zheng, S., 2002. Preparation of long TiO_2 nanotubes from ultrafine rutile nanocrystals. Chem. Lett. 2, 226-228.

Zhang, W.X., 2003. Nanoscale iron particles for environmental remediation: an overview. J. Nanopart. Res. 5, 323-332.

Zhang, Y., Crittenden, J.C., Hand, D.W., Perram, D.L., 1994. Fixed-bed photocatalysts for solar decontamination of water. Environ. Sci. Technol. 28, 435-442.

Zhang, Z.H., Yuan, Y., Liang, L.H., Fang, Y.J., Cheng, Y.X., Ding, H.C., Shi, G.Y., Jin, L.T., 2008. Sonophotoelectrocatalytic degradation of azo dye on TiO_2 nanotube electrode. Ultrason. Sonochem. 15, 370-375.

Zhao, Y., Zhang, X.T., Zhai, J., He, J.L., Jiang, L., Liu, Z.Y., Nishimoto, S., Murakami, T., Fujishima, A., Zhu, D., 2008. Enhanced photocatalytic activity of hierarchically micro-/nano-porous TiO_2 films. Appl. Catal. B-Environ. 83, 24-29.

Zheng, S.K., Yang, Z.F., Job, D.H., Yun Hee Park, Y.H., 2004. Removal of chlorophenols from groundwater by chitosan sorption. Water Res. 38, 2315-2322.

Zhou, S.M., Feng, Y.S., Zhang, L.D., 2003. A two-step route to self-assembly of CdS nanotubes via electrodeposition and dissolution. Eur. J. Inorg. Chem. 9, 1794-1797.

Zhu, H.Y., Gao, X.P., Lan, Y., Song, D.Y., Xi, Y.X., Zhao, J.C., 2004. Hydrogen titanate nanofibers covered with anatase nanocrystals: a delicate structure achieved by the wet chemistry reaction of the titanate nanofibers. J. Am. Chem. Soc. 126, 8380-8381.

Zhu, K., Neale, N.R., Miedaner, A., Frank, A.J., 2007. Enhanced charge-collection efficiencies and light scattering in dye-sensitized solar cells using oriented TiO_2 nanotubes arrays. Nano Lett. 7, 69-74.

Zhu, Y.C., Li, H.L., Koltypin, Y., Hacohen, Y.R., Gedanken. A., 2001. Sonochemical synthesis of titania whiskers and nanotubes. Chem. Commun. 24, 2616-2617.

Zhuang, H.F., Lin, C.J., Lai, Y.K., Sun, L., Li, J., 2007. Some critical structure factors of titanium oxide nanotube array in its photocatalytic activity. Environ. Sci. Technol. 41, 4735-4740.

Zou, Z.G., Ye, J.H., Sayama, K., Arakawa, H., 2001. Direct splitting of water under visible light irradiation with an oxide semiconductor photocatalyst. Nature 414, 625-627.

Zwilling, V., Ceretti, E., Forveille, A.B., David, D., Perrin1, M.Y., Aucouturier, M., 1999. Structure and physicochemistry of anodic oxide films on titanium and TA6V alloy. Surf. Interface Anal. 27, 629-637.